A study of the groundwater travel time distribution at a rural watershed in Iowa: A systems theory approach to groundwater flow analysis

by

Priyanka Jindal

A dissertation submitted to the graduate faculty

in partial fulfillment of the requirements for the degree of

DOCTOR OF PHILOSOPHY

Major: Environmental Science

Program of Study Committee:
Eugene S. Takle, Major Professor
Matthew J. Helmers
Kristie J. Franz
Manoj K. Jha
Catherine L. Kling
Keith E. Schilling
Nandita Basu

Iowa State University

Ames, Iowa

2010

Table of contents

List of figures

List of tables

Abstract

This dissertation is a study of groundwater-surface water interaction in terms of the travel time distribution framework applied to a tile-drained, agricultural landscape at the watershed scale. Specifically, we examined the two dimensional, steady state groundwater flow characterizing a shallow, unconfined aquifer at a representative watershed. A groundwater flow model of the aquifer was constructed using MODFLOW (Harbaugh et al., 2000). Hypothetical particles were then tracked through the simulated groundwater flow field using MODPATH (Pollock, 1994) to determine travel times associated with advective solute transport. The resultant distribution of travel times was represented by an exponential decay function with a mean travel time of 20.51 years. We further examined the impact of various control variables on groundwater travel times. First, the influence of the model selection on the travel time distribution results was examined by comparing results obtained from three models – analytic, GIS-based, and MODFLOW. Distributions obtained from all three models were represented by exponential decays, with the mean travel time varying between 16.22 and 20.51 years. The agreement between the MODFLOW and GIS models was probed by analyzing their flowpath length and velocity distributions. The spatial distributions of travel times obtained from the two models were analyzed, and conclusions of the impact of model selection on travel times were drawn. We also examined the impact of depth of flow on groundwater travel times. The analysis, conducted using the sink strength threshold parameter as a surrogate to depth showed that travel times, and structure of the effective sink network, are significantly impacted by depth. We examined the impact of variable tile drainage density and incision depth on travel times and baseflow. The marginal impact of tile drainage density on travel times and baseflow volumes was observed to diminish with

increasing density, while the impact of tile incision depth on the two variables was observed to be linear. Overall, tile drainage density was observed to have a stronger impact on travel times than baseflow, while tile incision depth impacted baseflow more than travel times. The impact of aquifer recharge on travel times was observed to vary based on landscape position.

I. Introduction

1.1. Motivation for present research

The groundwater travel time distribution of a watershed is defined as the probability density function of the time a tracer particle takes to travel inside the aquifer, from its entry point at the water table to the exit point. This single function condenses in it the complex interaction of all the myriad variables governing groundwater flow, namely, topography, geomorphology; climate (primarily, precipitation); land use patterns; soil structure and properties; geology; and physical boundaries comprising sources, sinks, and groundwatershed divides. The combined influence of all these factors produces a unique, three dimensional hydraulic head configuration and flow field that vary as a function of space and time. For most real world systems, the distributions of these two variables over space and time are not only difficult to obtain, but also difficult to analyze and extract meaningful information from.

Fortunately, there exists a scheme by which this distributed information can be distilled into one function: the watershed's groundwater travel time distribution. The structure of this distribution captures the essence of all information regarding hydraulic head gradients, flow path lengths, and aquifer properties such as hydraulic conductivity, storage, porosity and aquifer recharge at the watershed scale. Indeed, the travel time distribution constitutes the system response function of a watershed. According to the systems theory approach, the system's output is a convolution of the input signal and the system response function that characterizes the system. For a watershed system, the groundwater travel time distribution is

its characteristic response function, that when convolved with the input signal (here, aquifer recharge) produces the output signal (here, baseflow) (Maloszewski and Zuber, 1982).

The value of using the travel time distribution as a representative of the entire groundwater hydrology of a system is even more obvious in light of its wide-ranging applications. Subsurface travel time (also called residence or transit time) is a primary measure of the aquifer-solute contact time, that in turn affects the extent to which the solute is subjected to various physical and biogeochemical processes such as diffusion, dispersion, sorption, and reaction, as the solute advects through the system. Thus, travel time determines contaminant concentrations in aquifers, and ultimately stream water quality (Burns et al., 2003; Molenat and Gascuel-Odoux, 2002; Wriedt and Rode, 2006). In this way, we can use a watershed's travel time distribution to evaluate the extent to which land use practices, both past and present, are affecting current streamwater quality (Schilling and Wolter, 2007; Pijanowski et al., 2007; Wayland et al., 2002). Indeed, Turner (et al. (2006) have identified the existence of a close link between the travel time distribution, contaminant degradation rates, and the problem of contaminant persistence and concluded that quantifying travel times in different hydrologic setting (surface and subsurface) would be vital for predicting the transport and fate of diffuse contaminants. This would better equip watershed managers to identify contaminants of concern, detrimental land use practices and human activities, and assess various possible conservation and remediation scenarios.

Besides streamwater chemistry, the groundwater travel time distribution also influences other streamflow characteristics, and serves as a link between streamflow behavior and watershed-wide distributed inputs like recharge and evapotranspiration. For example, Wondzell et al. (2007) observed an interesting correlation between watershed-wide

distributed inputs such as evapotranspiration and the diel fluctuations in baseflow (timing and amplitude) at the outlet of a 100-ha watershed in the central western Cascade Mountains in Oregon. Furthermore, the contact time between rainwater and soils, as determined by the characteristic time scales of travel and storage in the watershed, also gives us a means to determine the extent of change in rainwater chemistry (Burns et al., 1998).

Additionally, the extreme complexity of flow in domains such as karst aquifers and other fractured media make analysis using the travel time distribution a much preferred and practical approach compared to distributed parameter modeling, that requires extensive data to determine the parameters and boundary conditions designating the system. A number of researchers (example, Long and Derickson, 1999; Ozyurt, 2008) have employed simple, lumped parameter models to produce a single function (the travel time distribution), that has made it possible for them to extract significant information about such complex aquifers. This is particularly useful to assess the groundwater vulnerability of sensitive aquifers (Ozyurt, 2008), and also to estimate the extent of well capture zones that are critical to delineate wellhead protection areas (Riva et al., 2006; Buxton et al., 1991; Clarke and West, 1998).

Finally, the travel time distribution approach is a step towards advancing the overall theoretical framework of the field of hydrology. The scalability of travel time distributions makes it a useful approach to link the hydrologic response across the hierarchy of spatial scales, from plot and hillslope, to watershed scales. In this way, it creates a more generalized hydrologic modeling framework that has wider applicability (Sivapalan, 2003).

Given the essential role that travel time distributions play in capturing flow dynamics, there is a great need to develop effective models that accurately determine the travel time

distribution that is unique to each landscape. In most natural, uncontrolled settings it is widely known that experimental estimations of the travel time distribution are highly impractical (McGuire and McDonnell, 2006). Instead, the travel time distributions are usually inferred from lumped parameter models characterizing the movement of a specific tracer through the flow system. Interpretation of natural variations observed in environmental isotopes groundwater can be used to supplement research efforts to understand various subsurface hydrologic mechanisms at the watershed scale. Indeed, the study of environmental tracers has been applied to analyze streamflow components and hydrograph separation – specifically the estimation of origin and magnitudes of the various streamflow components (Dinçer et al., 1970; Mook et al., 1974). It has also been used to enhance the calibration and validation of other hydrologic models (Reilly et al., 1994), and in the determination of the characteristic travel time distribution (Niemi, 1978; Yurtsever, 1983; Maloszewski and Zuber, 1993).

The utility of tracer data in hydrologic research coupled with the inability to experimentally estimate the travel time distribution has led to the development of various modeling techniques that analyze the isotopic response of the groundwater flow in the watershed. Mathematical models of tracer movement attempt to link measured tracer concentrations to other variables defining the flow system. A variety of modeling techniques – ranging from conceptual, physically based, distributed, and those based on time series analysis, have been developed to achieve this purpose. The two most common environmental tracers are oxygen-18 and deuterium. However, tracer analysis is limited due to the fact that tracer concentrations are impacted by additional solute mechanisms such as mixing, dilution, and other tracer-specific processes, such as denitrification in the case of nitrates.

Note that the application of isotopic data is only of as much value as the model that is used to analyze it. An over- or incorrectly-parameterized model would only serve to increase the constraints and degree of uncertainty in the system, and not aid the solution process. Moreover, it has been found that the same observations can be matched to a variety of models. Thus, measurements of tracer concentrations obtained from field studies must be incorporated into the research with caution, keeping in mind the problem of non-uniqueness and subjectivity inherent in the process of environmental tracer modeling.

In summary, travel time distributions are uniquely placed to improve our understanding of the hydrology of a system, assess the impacts of current natural and anthropogenic environmental changes on water quality and quantity, predict the hydrologic responses to future environmental changes, evaluate the hydrologic impact of various alternative conservation and restoration strategies, and facilitate the development of scientifically grounded environmental policy guidelines. Therefore, the motivation and over-arching goal of this research was to harness the potential of the travel time distribution formulation more deeply, and gain access to its full spectrum of applications discussed above by developing our knowledge of the concept within the domain of subsurface flow in tile-drained agricultural watersheds.

1.2. Overall objectives and research significance

1.2.1. Prediction of surface water quality response time

As shown in the previous section, the power of the travel time distribution approach lies in the versatility of its application, ease of use and interpretation, and its remarkable evaluative and predictive capabilities. Yet, its use in groundwater hydrology, and more so in

the field of groundwater-surface water interaction, has been fairly limited in comparison with other conventional approaches such as grid-based numerical modeling. Furthermore, the use of travel time distributions to understand the groundwater-surface water interaction within the environment of artificially drained agricultural landscapes at the watershed scale is even more uncommon.

Thus, our first overall objective is to address this gap in the field of hydrology by demonstrating the utility of travel times at the watershed scale. This was done by predicting the turnover time of streamwater quality in response to changes in land use practices at a representative agricultural watershed in Iowa using a distributed hydrologic model.

This objective is particularly significant in light of the key issues of nonpoint source pollution that many watersheds in Iowa are currently facing (Goolsby and Battaglin, 2000). High contaminant concentrations in the Upper Mississippi River Basin (UMRB) region have caused water quality degradation of several streams and rivers. This effect has travelled downstream and been linked to the prevalence of hypoxia (oxygen depletion that adversely affects the aquatic ecosystem) in the Gulf of Mexico, the second-largest human-caused zone of hypoxia in the world (Rabalais et al., 2002).

With row crops comprising the dominant land use category in the state, excessive nutrient losses from agricultural watersheds, in the form of widespread use of fertilizers, application of livestock manure, legume fixation, and in-soil mineralization, is of prime concern (Burkart and James, 1999; Goolsby and Battaglin, 2000). Transfer of nonpoint source pollutants to surface water bodes typically occurs via leaching and transport in shallow groundwater. For many streams in Iowa, groundwater discharge, in the form of baseflow and outflow from artificial subsurface drainage channels, is the major pathway of contaminant transport

(Hallberg, 1987; Schilling, 2002). Thus, determination of subsurface travel times is one of the most effective ways of studying the impact of reductions in contaminant concentrations at the land surface on streamwater quality (Meals et al., 2010; Schilling and Wolter, 2007).

We selected the Walnut Creek watershed, located in Jasper county, Iowa, as our case study. The Walnut Creek watershed has been the focus of extensive watershed habitat restoration and agricultural management changes as a part of the Walnut Creek Watershed Restoration and Water Quality Monitoring Project, that was implemented by the U.S. Fish and Wildlife Service (USFWS) at the Neal Smith National Wildlife Refuge (NSNWR). Established in 1995, the ten year project was a part of the U.S. Environmental Protection Agency's Nonpoint Source National Monitoring Program. Before restoration, the dominant land use in the watershed was agriculture, with row crops (corn and soybeans) comprising nearly 70% of the land area (Schilling and Spooner, 2006). They reported that by 2005, native prairie restoration conducted by the USFWS at the NSNWR accounted for 23.5% of the watershed area, and led to a reduction in the row crop land cover from 69.4% in 1990 to 54.5% in 2005. To obtain a quantitative measure of how changes in water quality at the land surface are conveyed to the stream, it is necessary to estimate groundwater travel times in the watershed. By using the travel time distribution framework to address this question, our research will demonstrate the immense potential of this tool to advance our understanding of contaminant transport at the watershed scale.

1.2.2. Assessment of travel time control variables

The Walnut Creek watershed is unique in that, besides offering an ideal platform to study how change in water quality propagates from ground to surface water, it has also, as part of the abovementioned project, been a hub of extensive monitoring and field data collection

over the past 16 years. This has allowed us to employ a data-intensive, distributed hydrologic model to compute the groundwater travel time distribution of the watershed. There exist a number of other schemes to estimate travel time distributions at the catchment scale, such as analytical, lumped parameter, and GIS-based methods. Distributed hydrologic modeling is less common, mainly because many catchments lack the extensive field data that is required to construct such models (see review by McGuire and McDonnell, 2006).

In the same review the authors also report that many of the common methods are not designed to account for various physical factors that can potentially influence travel time distributions, such as a spatially varying flow field, heterogeneous hydraulic conductivity, dual porosities, spatially varying recharge, etc. The distributed hydrologic modeling framework is designed to incorporate spatially detailed descriptions of various aquifer parameters and aquifer boundaries. Thus, the use of a distributed hydrologic model gives us an opportunity to examine the control that various physical variables exercise on watershed groundwater travel times.

Furthermore, many methods (like certain lumped parameter and analytic methods) select the travel time distribution from a set of standard distributions, and use data to only compute the assumed distribution's best-fit parameters. On the other hand, distributed hydrologic models derive a travel time distribution more directly, starting from the basic groundwater flow equation. There is no specific distribution assumed beforehand, and the travel times are derived "empirically" from the numerical solution of groundwater flow and solute transport. Therefore, the results can be taken to be very reliable, particularly the results of integrated measures such as the cumulative travel time along groundwater flow paths. This consequent reliability of results though comes at the cost of added complexity in constructing the model.

By constructing an alternative groundwater travel time distribution using a distributed modeling scheme, we are in a unique position of comparing results across a range of different modeling choices, from the simplest to the most complex. This enables us to ascertain the control that the choice of a model has on the desired results, in this case, the watershed groundwater travel time distribution.

Hence, our combination of a watershed that has extensive field data, a model that accounts for spatial variations in aquifer boundaries and properties, and derives a travel time distribution , gives us a rare opportunity to analyze the impact of various control variables on groundwater travel times costs vis-à-vis (a) model selection and (b) aquifer characteristics (physical boundaries and aquifer properties). Thus, the second overall objective of this research is to examine the sensitivity of the travel time distribution of a watershed to the abovementioned factors. In the long run, a deeper understanding of the relative impact of these control variables will enable us to identify factors that do not exercise significant influence on groundwater travel times. This identification will serve three purposes :

(1) It will assist elimination of the redundant factors and enhance the utility of travel time distributions, by enabling the user to study a wider variety of systems (including those that might lack extensive data) in a more efficient way.

(2) It will help the user to choose the method for evaluating the travel time distribution more judiciously.

(3) It will facilitate the development of simpler techniques to compute travel time distributions.

The second overall objective is particularly significant in light of the comments made by McGuire and McDonnell in their review article (McGuire and McDonnell, 2006). With

regard to the estimation of travel times using models, they state that "… there is little guidance on the assumptions and limitations of different modeling approaches applied to catchment systems". By comparing the three abovementioned models, that span the range of model complexity, we shall be able to gain some insight into the assumptions and limitations of each. This shall serve to guide the user in model selection (the second sub-objective listed above).

In the same review article, the authors also state that "… while there have been numerous recent publications using tracers to estimate transit times, relatively little advancement in transit time estimation methodology has been made at the catchment scale". Our objective (specifically, the third sub-objective) directly addresses this concern by seeking to identify superfluities in the modeled variables, and the modeling approach itself, that will facilitate advancement in the area of transit time estimation methods.

Finally, the authors state that "… very little guidance exists for catchment hydrologists on the use and interpretation of transit time modeling approaches for complex catchment systems". Our first sub-objective listed above addresses this challenge by seeking to remove the redundant physical variables that possibly define a complex catchment, thereby rendering the system more accessible to the modeler.

1.3. Specific objectives

We addressed the overall goals outlined above by delineating a set of specific objectives as listed below :

1. Quantify the lag time that meditates the impact of shallow groundwater quality on stream water quality at the watershed scale in a tile-drained, agricultural environment. This

was done by building a travel time distribution using a MODFLOW-MODPATH coupled distributed hydrologic model (Harbaugh et al., 2000; Pollock, 1994) that simulates the steady state dynamics of groundwater flow and advective solute transport in the Walnut Creek watershed in Jasper county, Iowa.

2. Examine the sensitivity of travel times to model selection by comparing and contrasting three alternative modeling schemes that span the range of model complexity. Specifically, we compared the subsurface travel time distribution of the watershed that was obtained in the first part of the research using a distributed hydrologic modeling that lies at the higher end of complexity, to those obtained using (a) an analytic model proposed by Haitjema (1995), that lies at the lower end of complexity, and (b) a GIS-based model proposed by Schilling and Wolter (2007), that lies in the intermediate range of model complexity.

3. Examine the sensitivity of the groundwater travel time distribution to various physical control variables at the watershed scale. This was done by ascertaining the sensitivity of the distribution of groundwater travel times to –

(a) The depth of flow in the aquifer.

(b) Aquifer boundary conditions, namely, the spatial distribution and incision depth of the subsurface artificial tile drainage network.

(c) Aquifer parameters, namely, net aquifer recharge.

1.4. Thesis organization

The dissertation is organized in six chapters and its outline is described as given below.

*** Chapter one**: “Introduction”

The concept of the travel time distribution is introduced. The motivation of this work is presented in light of the importance of this formulation and its multiple applications, specifically with regard to groundwater flow at the watershed scale. An outline of the overall objectives of this research follows. This leads to the definition of our specific research objectives that are addressed in the following chapters.

*** Chapter two**: "Background and methods"

The case study area is introduced. This is followed by an introduction of the theoretical foundations of MODFLOW and MODPATH, the two models used in this research. We then describe the conceptual design and construction of the groundwater flow model, followed by a description of the model calibration procedure and final results. A discussion of the assumptions and limitations of the model follows. Finally, we describe the Kolmogorov-Smirnov statistical test that is used in the analysis of results presented in chapters three and four.

*** Chapter three**: "A comparison of three different models for estimation of the steady-state groundwater travel time distribution at the Walnut Creek watershed, Iowa"

This chapter is adapted from an article to be submitted to a journal. The chapter presents the study area's groundwater travel time distribution constructed using the distributed hydrologic modeling scheme of MODFLOW and MODPATH, which is then compared to the distributions obtained from two other approaches, an analytic and GIS-based model.

*** Chapter four**: "Groundwater sink strength as a means to link watershed travel times and drainage network structure to depth of flow"

This chapter is adapted from an article to be submitted to a journal. The chapter analyzes the impact of depth of flow on groundwater travel times at the watershed scale and the

properties of the corresponding sink network via the medium of the MODPATH model variable termed the sink strength threshold parameter.

*** Chapter five**: “Impact of artificial subsurface drainage network density and incision depth on groundwater travel times and baseflow at the watershed scale“

This chapter is adapted from an article to be submitted to a journal. The chapter examines the impact of the spatial distribution (in terms of drainage density) and incision depth of the artificial subsurface drainage network on the distribution of groundwater travel times and the tile contribution to baseflow. A conceptual analysis for the relation between groundwater travel times and incision depth is presented and shown to agree with simulated results.

*** Chapter six**: “General conclusions”

The concluding chapter includes a brief overview of the results presented in chapters three to five, and links them to goals of our research stated in chapter one. Some results presented in an appendix that have the potential to be examined further are also accounted for in this discussion. Finally, recommendations for future work close this chapter.

II. Background and methods

2.1. Site description

2.1.1. Location and climate

The Walnut Creek watershed in Jasper county, Iowa, is a HUC 12 watershed covering an area of 51.94 km^2 (Fig. 1). The watershed lies inside the Lake Red Rock watershed, a HUC 8 watershed located in the Upper Mississippi River Basin. The watershed is located in the Southern Iowa Drift Plain landscape region of South Central Iowa, that is characterized by steeply rolling hills and well-developed drainage (Prior, 1991). The climate of the area is humid and continental. Temperatures in the region vary widely, ranging from average maximum values over 20°C between June and September to less than 0°C in December and January. Annual precipitation averages around 850 mm. Maximum rainfall typically occurs in the months of May and June, though large convective storms can deliver heavy rainfall in relatively short periods of time anytime in the summer.

The hydrologic response of the watershed to rainfall is very fast, that is indicated by the presence of a natural relief of 51.07 m across a basin length of 12.51 km. Moreover, the stream channel is deeply incised, being eroded from depths of starting around 1 m at the tributary headwaters and steadily increase in the downstream direction to depths of around 3 m, which also represents the incision depth along the main channel. High channel incision has a significant impact on the hydrology of the watershed (Schilling et al., 2004; Schilling et al., 2006b; Schilling and Jacobson, 2008), and is associated with the flashy discharge of the stream in response to storm events.

The watershed is drained by a system of artificial subsurface tile drains incised to a depth of around 1.2 m below the land surface. Unlike the common patterned tile network, the current tile network at the Walnut Creek watershed is primarily branched along the first order drainageways, and underlies the grassed waterways in the watershed. This is a recommended design practice for grassed waterways to prevent the buildup of excessive wetness, so as to maintain the vegetative cover, prevent formation of further gullies, and facilitate accessibility to farm equipment (Stone and McKague, 2009; Green and Haney, 2005; NRCS, 2004).

2.1.2. Stratigraphy

The stratigraphy of the watershed is similar to Quarternary stratigraphy that is found across much of the Southern Iowa Drift Plain. Fig. 2 shows the stratigraphic cross section of a representative well transect whose location is shown in Fig. 5. The upland divide areas of the watershed comprise mantles of Wisconsinan-age Peoria loess overlying pre-Illinoian oxidized till. The thickness of the loess units has been observed to vary depending on the landscape position, with thickness as high as 4-6 m being reported in the uplands (Schilling et al., 2007) to ranges of 2-3 m nearer to the floodplain (Schilling and Thompson, 1999). The side slope areas are lined with intermittent outcrops of pre-Illinoian till (primarily oxidized), Late Sangamon gray and red paleosols, and rare occurrences of Pennsylvanian shale. Holocene age alluvium, consisting of stratified sands, silts, clays, and occasional peat deposits, constitutes the main channel floodplain and higher order tributaries, and has been observed to penetrate the aquifer up to depths of around 10 m (Schilling and Thompson, 1999).

The texture of the floodplain alluvium is similar to that of the loess mantles in the uplands. This is because erosion of the loess provided the source material for the alluvial

deposits. Therefore, although deposited by different processes, the surficial deposits for the upland and floodplain areas are very similar and predominantly composed of silt. One might therefore expect the hydrologic characteristics of the two soil types to match. Weisbrod (2005), through a series of slug tests whose results were analyzed using the Hvorslev method (Hvorslev, 1951), determined the hydraulic conductivities of the loess and alluvial deposits at one site within the watershed to vary in the range of 1.2-5.5 x 10^{-6} m/s. These values agreed well with the hydraulic conductivity measurements of silty alluvium at another site located in the Walnut Creek floodplain, which were determined, through an analysis of slug test results using the methods of Bouwer and Rice (1976), to range from 1.7-4.9 x 10^{-6} m/s (Schilling et al., 2004). Moreover, the hydraulic conductivities of the oxidized till and paleosol outcrops occurring at locations along the watershed side slopes and valley walls have been measured by Schilling and Wolter (2001) using slug tests, the results of which were analyzed using the Hvorslev method. These values have been found to be similar and lying in the range of 1.6 to 4.7 x 10^{-7} m/s. Due to lack of field evidence to the contrary, we assumed the vertical and horizontal hydraulic conductivities of all units to be equal.

Pre-Illinoian unoxidized till underlies most of the watershed at estimated depths of around 10-11 m. This unit is characterized by poor hydraulic conductivity that is around two orders of magnitude (10^{-8} m/s, Schilling and Wolter, 2001) less than that of the alluvium samples obtained at other locations in the watershed (10^{-6} m/s) (Schilling et al., 2004; Weisbrod et al., 2005). This suggests that the unoxidized till unit acts as confining layer to the overlying loess-alluvial aquifer.

Bedrock, underlies the unoxidized till unit, and comprises shale, limestone, sandstone, and coal from the Pennsylvanian Cherokee Group. Stray outcrops of shale and sandstone are

visible in a few areas towards the southern end of the watershed and at stray spots along the Walnut Creek main channel.

2.1.3. Land use

In 1990, the land cover in the watershed was predominantly agricultural, with 69.4% of the area comprising row crops. From 1990 to 2005, vast tracts of row crop lands were converted to native prairie as part of habitat restoration and agricultural management changes implemented by the United States Fish and Wildlife Service (USFWS) at the Neal Smith National Wildlife Refuge (NSNWR) and Prairie Learning Center. This caused the row crop cover at the watershed to decrease from 69.4% to 54.5%. As of 2005, native prairie constituted around 23.5% of the watershed area. Most of the conversion has been concentrated in the central portion of the watershed. In 1995, the Walnut Creek Watershed Monitoring Project was established to monitor the progress of the land use changes and prairie restoration vis-à-vis changes in the groundwater and stream sediment, nutrient and pesticide concentrations for ten water years up to 2005. The results of the monitoring studies showed a decrease of up to 3.4 mg/l over the ten years, suggesting that conversion of row crop land to prairie can reduce nitrate concentrations in the stream and improve surface water quality (Schilling et al., 2006a).

2.2. Model description: MODFLOW

MODFLOW is a Fortran program developed by the United States Geological Survey (USGS) to numerically solve the three dimensional groundwater flow equation using the finite difference method (Harbaugh et al., 2000).

The equation governing groundwater flow through saturated porous media in three dimension is derived from Darcy's law and the continuity equation, and is given as:

$$\frac{\partial}{\partial x}\left(K_{xx}\frac{\partial h}{\partial x}\right)+\frac{\partial}{\partial y}\left(K_{yy}\frac{\partial h}{\partial y}\right)+\frac{\partial}{\partial z}\left(K_{zz}\frac{\partial h}{\partial z}\right)+W=S_S\frac{\partial h}{\partial t} \quad (1)$$

where

* K_{xx}, K_{yy} and K_{zz} are the hydraulic conductivities (L/T) along the x, y, and z axes that are assumed to be parallel to the principal axes of the hydraulic conductivity tensor

* h is the hydraulic head (L)

* W is the volumetric flux per unit volume representing sources and/or sinks of water; W > 0 indicates recharge, or flow into the system and W < 0 indicates discharge, or flow out of the system (T^{-1})

* S_S is the specific storage of the material (L^{-1})

* t is time (T)

Here, K_{xx}, K_{yy} and K_{zz} are the functions of space (x,y,z) and W is a function of space and time (t).

This inhomogeneous, linear, second order partial differential equation represents non-equilibrium groundwater flow in a heterogeneous, anisotropic medium Together with the appropriate aquifer boundary conditions and initial conditions, the set constitutes a complete mathematical representation of the groundwater flow system, that can then be solved for hydraulic head as a function of space and time.

It is practically impossible to obtain an analytical solution for equation (1) except for highly simplified systems. Thus, various numerical methods are employed to obtain

approximate solutions. MODFLOW uses the finite difference method and the block centered approach, wherein a continuous system in replaced by a finite set of discrete points in space and time, located at the center of each discrete cell. The partial derivatives are replaced by terms calculated from the difference in hydraulic heads at these points. This yields a set of simultaneous linear algebraic equations that can be solved for the head at all the discrete points in the spatio-temporal grid.

To understand the implementation of boundary conditions in MODFLOW the concept of conductance needs to be introduced. This variable is obtained in the derivation of the finite-difference form of the groundwater flow equation (that is used by MODFLOW) directly from the continuity equation and Darcy's law, as shown below.

Consider a representative cell (i, j, k) in the model grid. The cell shares a common interface with 6 other cells as shown in Fig. 3. From the continuity equation for incompressible flow we know that the net rate of inflow of water into the cell must equal the rate of increase in the volume of water stored inside the cell. By definition, the specific storage (S_S) of the cell determines the rate of increase in this stored volume. Therefore the water balance equation can be expressed as,

$$\sum Q_{ijk} = S_s \frac{\Delta h}{\Delta t} \Delta V \qquad (2)$$

where

* Q_{ijk} is the inflow rate into the (i, j, k)-th cell (L^3/T)

* Δh is the change in head over time Δt

* ΔV is the volume of the cell (L^3) whose dimensions are Δx, Δy, and Δz

Furthermore, we can write the finite difference expression for Darcy's law for flow across the left face of the (i, j, k)-th cell, i.e. from cell (i, j-1, k) to cell (i, j, k) as :

$$Q_{j-} = -K_{j-}(\Delta x * \Delta z)\frac{(h - h_{j-})}{\Delta y}$$

or

$$Q_{j-} = -C_{j-}\left(h - h_{j-}\right) \tag{3}$$

where

* h is the head at the node (i, j, k)

* h_{j-} is the head at the node (i, j-1, k)

* Q_{j-} is the flow rate from (i, j-1, k) to (i, j, k)

* K_{j-} is the equivalent hydraulic conductivity between the nodes (i, j-1, k) and (i, j, k)

* $\left(\Delta x * \Delta z\right)$ is the cross-sectional area of the face between the cells (i, j-1, k) and (i, j, k)

* C_{j-} is the combined product of the grid dimensions and hydraulic conductivity, and is termed as the conductance between the nodes (i, j-1, k) and (i, j, k)

Similar expressions for inflow from cells across the remaining five faces can be written. Summation of these six individual flow rates gives us the net inflow rate that, by continuity equation, is also described by equation (2). This gives,

$$-\left(\Sigma C\right)h + C_{j-}h_{j-} + C_{j+}h_{j+} + C_{k-}h_{k-} + C_{k+}h_{k+} + C_{i-}h_{i-} + C_{i+}h_{i+} + W = S_S\frac{(h - h_{\Delta t-})}{\Delta t}\Delta V$$

where (4)

$$\Sigma C = C_{j-} + C_{j+} + C_{k-} + C_{k+} + C_{i-} + C_{i+} \tag{5}$$

is the sum of the conductances across all six faces. Here, all heads are computed at time t, except $h_{\Delta t-}$, which represents the hydraulic head in the cell (i, j, k) at a time $t - \Delta t$; where Δt is the time step in the simulation. For a steady-state simulation, the right hand side of equation (2) is zero. Thus, we obtain a set of simultaneous linear algebraic equations that can be solved for the steady state hydraulic heads as a function of space.

We observe that MODFLOW captures information about aquifer dimensions and hydraulic conductivity via the conductance parameter, C, computed between each pair of cells. C is given by,

$$C = \frac{KA}{L} \tag{6}$$

where

* K is the equivalent hydraulic conductivity between the two cells

* A is the cross-sectional area between the two cells

* L is the distance between the centers of the two cells

Thus, one can simplify the inter-cell flow rate (equation 3) into a product of the conductance times the head difference between the two cells.

The same concept is utilized in the implementation of boundary conditions. Boundary conditions such as a river or drain sink are first designated a spatial location in the model. The river sink is defined by the elevation of its stage, while the drain sink is defined by its boundary elevation. Flow to the sink is determined by the difference between the elevation characterizing the sink and the hydraulic head at the center of the cell associated with the

sink, times a conductance term characterizing the interface between the sink and the model cell (Fig. 3). Thus, flow from a model cell (i, j, k) associated with a sink that is characterized by a stage (for a river sink) or elevation (for a drain sink) given by h_s, is given as,

$$Q_{out} = -C_s \left(h_s - h_{cell} \right) \tag{7}$$

where

* Q_{out} is the outflow from cell to sink

* C_s is the conductance between the cell and sink

* h_{cell} is the hydraulic head at the cell (i, j, k)

* h_s is the stage or boundary elevation of the river or drain sink, respectively

Equation (7) is valid only for outflow, i.e. when $h_{cell} > h_s$. If the hydraulic head inside the cell drops below the stage or boundary elevation of the sink, then MODFLOW responds differently, based on whether the sink type is a river and drain. For a river sink, MODFLOW maintains a small infiltration rate from the river sink to the cell that is driven by the difference between the bottom elevation of the river streambed and its stage. On the other hand, for a drain sink, once head in the cell drops below the drain elevation, there is no further flow between the sink and cell (Q becomes equal to 0).

For a river sink, where flow is assumed to primarily occur across the streambed, the conductance term depends on the streambed conductance, and is given as

$$C_{RIV} = \frac{K(LW)}{M} \tag{8}$$

where

* K is the hydraulic conductivity of the streambed

* L is the length of the streambed layer that is associated with the cell

* W is the streambed width (the product of L and W gives the cross-sectional area across which the flow from cell to sink occurs)

* M is the thickness of the streambed ("distance" between the river sink and cell center)

The conductance between the drain sink and the cell is defined in a similar manner. Typically, river conductance can be estimated from the physical characteristics of the streambed, while drain conductance is harder to estimate due to the unavailability of the hydraulic parameters related to the drain-aquifer interaction. Therefore, drain conductance is typically estimated using values quoted in literature as initial values that are then calibrated during the stage of model calibration.

Thus, we obtain a set of simultaneous, linear algebraic equations that represent the interactions between all pairs of model cells, and between model cells and sinks. These are solved iteratively, until the solver convergence is reached. In this groundwater flow model, we used the PCG2 (Preconditioned Conjugate Gradient-2) solver. The computed inter-cell and cell-to-sink fluxes are then employed by MODPATH, a particle-tracking code, to obtain the advective travel times of tracer particles released at user-defined locations in the system. The description of this program follows below.

2.3. Model description: MODPATH

MODPATH is a particle tracking post-processing FORTRAN package that computes three-dimensional pathlines of advective transport based on the output of a MODFLOW simulation (Pollock, 1994). The package uses a semi-analytical approach wherein simulated

intercell flow rates from MODFLOW are used in an analytical expression of the flow path of a particle within grid cell. The package computes the spatial coordinates as well as the time of travel along the pathlines. This can be done for steady-state or transient simulations, as well in forward or reverse tracking modes. Forward tracking refers to the movement of the particle in the downgradient direction to the sink, whereas reverse tracking refers to the movement of the particle upgradient from the sink location. The latter option is useful for applications that involve an estimation of the area contributing to the flow reaching a sink, such as estimation of the capture zone of a well.

Implementation of the program involves determination of the groundwater flow velocities across the six faces of all model cells using the simulated values of flow rates across each cell face. The flow velocities inside all cells are then determined using linear interpolation from one cell face to opposite face. Individual particles are then released at user-specified locations within the model domain. The particle's velocity at the release point equals the flow velocity computed by MODFLOW at that point. Knowledge of the initial position and velocity of the particle at the time of release, along with the interpolated velocity field is sufficient to determine its position and velocity of the particle at all later times, until it reaches the terminal position, as demonstrated below.

For simplicity, we consider the derivation of the x-component of the velocity vector in a representative model cell with sides of length Δx, Δy, and Δz, in the x, y, and z, directions, respectively. The cell is shown in plan view in Fig. 4.

The results of the MODFLOW simulation provide the flow rate entering across the six faces of the cell. If Q_1 and Q_2 are the flow rates entering and leaving the cell from left and

right, respectively, then the x-components of the average linear velocity across the left and right faces, given as v_1 and v_2 respectively, are

$$v_1 = \frac{Q_1}{n\Delta y\Delta z} \quad \text{and} \quad v_2 = \frac{Q_2}{n\Delta y\Delta z} \tag{9}$$

where n is aquifer porosity, and ($\Delta y\Delta z$) is the cross-sectional area across each face.

By linear interpolation, we can estimate the x-component of velocity (v_x) at any intermediate location within the cell (x,y,z) as

$$v_x = A(x - x_1) + v_1 \tag{10}$$

where A is the velocity gradient within the cell in the x direction, whose value is known:

$$A = \frac{v_2 - v_1}{\Delta x} \tag{11}$$

Therefore, if one can determine the velocity component at a particular position, then equation (10) allows one to compute the spatial coordinate of that position. Furthermore, the velocity component of the particle at a particular position can be determined if one has knowledge of its velocity component (along the same coordinate direction) at an earlier time, t_0, within the cell. To see this we need to consider the movement of a particle through the cell. One can determine the rate of change in the particle's x-component of velocity within the cell as,

$$\left(\frac{dv_x}{dt}\right)_p = \left(\frac{dv_x}{dx}\right)\left(\frac{dx}{dt}\right)_p \tag{12}$$

Here the subscript "p" indicates that the term is evaluated at the location of the particle. Equation (12) states that the rate of change in the velocity component of the particle along a particular coordinate direction is a product of the rate at which the velocity changes along

that coordinate times the rate at which the particle moves along that coordinate. The latter term is simply the velocity component of the particle itself, while the former term is the velocity gradient along that coordinate axis (from equation 11) :

$$\left(\frac{dx}{dt}\right)_p = \left(v_x\right)_p \quad \text{and} \quad \frac{dv_x}{dx} = A \tag{13}$$

This reduces equation (12) to,

$$\left(\frac{dv_x}{dt}\right)_p = A(v_x)_p \tag{14}$$

This equation can be integrated by separation of variables. Knowing that at $t = t_0$, the velocity of the particle in the x-direction is v_0, we can determine the velocity of the particle at a position (α) that it reaches at a later time t_α as follows:

$$v_\alpha = v_0 * \exp(A\Delta t) \tag{15}$$

where Δt is the elapsed time interval, $t_\alpha - t_0$

Equation (15) now determines the velocity of the particle at any position within the cell in terms of the velocity component v_0, at an earlier time, t_0. Therefore, we can now use equation (10) to express the x-coordinate of the particle at time t_α in terms the particle's velocity at an earlier time as,

$$x_\alpha = x_1 + \left(\frac{1}{A}\right)\left(v_0 * \exp(A\Delta t) - v_1\right) \tag{16}$$

The analysis along the y and z direction produces similar equations in both directions. Equation (16), when inverted to solve for Δt in terms of x_α, is used to compute the time of travel from an initial x-coordinate x_0 at a time t_0 to final x-coordinate x_α. The exit location of the particle from a particular cell, and the travel time to the exit location, are also determined

using equation (16). In this way, particle pathlines computed in each cell are linked end to end, to generate the entire flow path under steady-state or transient conditions.

Thus we see that the estimation of the velocity field from flow rates across the faces of model cells enables MODPATH to track the position and travel time of a particle, given its initial release coordinates.

The termination of the path line of a particle typically occurs when the particle reaches an external boundary or an internal sink within the model (for the cases of exception, see Pollock, 1994). However, termination at a sink that does not capture all the flow entering the model cell is ambiguous. There is no analytic procedure to determine whether the particle should exit out of the sink or be a part of the flow that bypasses the sink, termed a weak sink. A strong sink on the other hand, that captures all the cell inflow, is sure to capture the particle. Hence the trace of a particle entering a strong sink is fully determined. To resolve the particle's pathline once it enters a weak sink, MODPATH provides the option of either passing all weak sinks and stopping only at strong sinks; stopping at all sinks, regardless of whether they are weak or strong; or stopping at sinks that capture a fraction of the total cell inflow that is larger than a user-defined threshold. The fraction of cell inflow captured by a sink is termed as the sink strength of the particular sink. Thus, in the third option, all sinks with a sink strength value that is higher than a user-defined threshold parameter will be treated as active, i.e. all particles entering sinks containing such sinks will be stopped. Sinks with strength lower than the user-defined threshold will be treated as inactive, and particles entering model cells containing such sinks will simply bypass the sink until they encounter an active sink further downgradient. In our work, we term this user-defined threshold as the sink strength threshold parameter (S*). Usually, the modeler has to settle for making an

arbitrary selection of one of the three options, since there are no physical indicators by which one can determine which option shall produce the "true" distribution of path lines and travel times. The model solution is highly sensitive to the option the user chooses. This issue is explored in greater detail in chapter 2.

2.4. Groundwater flow model: Conceptual design

A two-dimensional, steady-state MODFLOW-2000 model (Harbaugh et al., 2000) was constructed to simulate groundwater flow for the shallow, unconfined, alluvial-loess aquifer at the Walnut Creek watershed. The model required the use of the RIV and DRN packages. Particle tracking analysis using MODPATH (Pollock, 1994) was then performed to obtain the travel time distribution representing advective transport in the watershed. Both stages of model development were conducted through the medium of the graphical user interface (GUI) Groundwater Vistas, version 5.39 (Environmental Simulations Inc., Reinhold, PA). The conceptual design and steps involved in the model construction are described below.

2.4.1. Grid properties

We selected a grid resolution of 20 m based on the resolution of our input and calibration data, since the latter determines the resolution of known aquifer heterogeneity. For proper alignment of the watershed with the grid we rotated the watershed boundaries clock-wise by 21°, about the pivot with coordinate (475576.51, 4603858.80) (in meters, referenced relative to the coordinate system NAD 1983 UTM Zone 15N). Note that an alignment of the grid with the aquifer and the principal directions of flow is important for finite difference models such as MODFLOW, since the presence of diagonal flow across grid cells can result in water balance errors (Anderson and Woessner, 1992). Also, proper grid alignment minimizes the

total number of model cells by reducing the number of cells that fall outside the model domain. This in turn decreases model run time.

This alignment resulted in a grid dimension of 628 rows, 300 columns, and 1 layer. Of a total of 188400 cells, 129820 active cells covered the watershed area of 51.94 km^2, while the remaining 58580 cells were inactive, no-flow cells (Fig. 5). The stream and drain boundary conditions in the watershed were modeled using the RIV and DRN packages, respectively. Both boundary conditions were associated with 4012 and 6928 cells, respectively.

2.4.2. Spatial attributes

In general, the physical extent of a watershed can be very different from that of the underlying aquifer (Winter et al., 2003). However, in an old glaciated landscape, with low permeability and sloping lands, such as the landscape where Walnut Creek is located, there is strong coincidence of the watershed boundaries with the boundaries defining its shallow, unconfined aquifer. Thus, the shape of the watershed boundaries was used to delineate the horizontal extent of the aquifer. To obtain the vertical extent of the aquifer, we first defined the top elevation of the single layer model using a 20 meter resolution DEM that was obtained by aggregating a 1 meter resolution LIDAR (Light Detection and Ranging) DEM. The Pre-Illinoian unoxidized till unit, estimated to be located at depths of around 10-11 m, was estimated to be the confining layer for the overlying alluvial-loess aquifer (See section 2.1.2). Therefore, the bottom elevation of the single layer model was fixed at a depth of 11 meters relative to the top elevation of the layer. This resulted in a variable elevation, constant thickness, groundwater flow model that, unlike a traditional two dimensional planar model, could account for changes in the elevations of physical boundaries. All spatial data was

processed in GIS (ArcMap, version 9.3) and then imported into Groundwater Vistas, the MODFLOW GUI.

2.4.3. Aquifer parameters

(a) Hydraulic conductivity : Based on data presented in Schilling and Wolter (2001), Schilling et al. (2004), Weisbrod (2005), and Schilling et al. (2007) that has been reported in section 2.1.2, we delineated three primary zones of hydraulic conductivity: (a) loess overlying oxidized till in the uplands, (b) oxidized till and paleosol outcrops at certain areas along the side slopes, and (c) an alluvial floodplain. Different values for the thickness of loess that overlies the oxidized till in the upland areas, that was observed to range from 4-6 m by Schilling et al. (2007) were tested before selecting a value near 7 m that was observed to give the best model results. The similarity in the hydraulic properties of the oxidized till and paleosol enabled us to combine these into one zone that was assigned a common value of hydraulic conductivity. Similarly, the loess and the alluvium were assigned a common hydraulic conductivity, given the overlap in their measurements (reported in section 2.1.2).

The spatial distribution of these zones was determined using the composition of the soil parent material at each location, as identified by the ICSS (Iowa Cooperative Soil Survey) digital soil data for Jasper county. Soil mapping units with parent material described as alluvium, local alluvium, and sandy alluvium were located along the floodplain, and were therefore combined into an floodplain alluvial zone. Till, gray paleosol, and reddish paleosol units were combined to constitute the till zone. The remaining units were located in the uplands, and their parent material was defined pre-dominantly as loess (loess, loess-gray or gray mottles, loess-local alluvium). These were combined into loess zone. Stray spots of

weathered shale outcrops or undefined parent material were combined with the zone of their nearest neighbor.

The values of hydraulic conductivity were initially assigned based on the slug test measurements reported in section 2.1.2. However, these values consistently produced unrealistically high water table levels that exceeded the land surface elevation. This has been anticipated by a number of authors (Schulze-Makuch and Cherkauer, 1998; Rovey II, 1998) as reflective of the fact that groundwater flow is impacted by high-conductivity aquifer heterogeneities present at larger flow scales than the scale of flow created by localized slug tests. Estimates of saturated hydraulic conductivity obtained from the Soil Survey Geographic (SSURGO) database were approximately one order of magnitude higher than the values obtained from the slug tests. Moreover, using the SSURGO values caused a significant improvement in the simulated values of water table elevations. Thus, we chose to use the SSURGO data for our baseline values. The slug tests data was used to define limits of the hydraulic conductivity values that were considered reasonable during the stage of model calibration. To obtain the baseline SSURGO estimates of hydraulic conductivity we first extracted the average values of conductivity defining each unique combination of the MUKEY and slope class fields. This enabled us to assign floodplain alluvial zone a hydraulic conductivity of 9×10^{-6} m/s (0.7776 m/day). In case of the oxidized till zone, the SSURGO data gave three values of hydraulic conductivity, of which one value occurred far more commonly than the rest. Therefore, the till outcrops were assigned the hydraulic conductivity value of 3×10^{-6} m/s (0.2592 m/day), corresponding to the predominant till. As discussed earlier, the hydraulic conductivity of loess at the Walnut Creek watershed was found to be similar to that of the floodplain alluvium. Thus, initial estimates of the hydraulic conductivity

of the loess zone, comprising an estimated thickness of 7 m loess on top of 4 m oxidized till was determined by taking a thickness-weighted average of the hydraulic conductivities of alluvium and till (0.5891 m/day). Since these values were based on estimates, they were used as calibration parameters during the stage of model calibration. The final, calibrated hydraulic conductivity zones and their values (Fig. 6) are presented in the next section (section 2.5) dedicated to model calibration.

Besides hydraulic conductivity, estimates of porosity were required to simulate the steady-state, advective transport of particles in the watershed. We estimated aquifer porosity to be around 0.3, based on data reported for areas located in the regions of pre-Illinoian till in eastern Iowa (Helmke et al., 2005).

(b) Net areal recharge : Net areal recharge to the aquifer was initially selected as 129.5 mm/yr, based on the long-term average baseflow value at the Walnut Creek watershed (Schilling et al., 2006a). We then delineated three zones of aquifer recharge (Fig. 7) using the estimates of Schilling (2009). The author evaluated differential recharge to the aquifer based on the landscape position in the watershed. Net annual recharge in the flat floodplains, that occurs after the processes of surface runoff, interflow, and ET have taken place, was estimated to be around 44% of the annual precipitation. The sharper slopes defining the side slopes were characterized by a much smaller proportion of only 14% of total precipitation. Upland recharge lay in the intermediate range, and was estimated to be around 24% of total precipitation.

Thus, we distributed the total equivalent recharge of 129.5 mm/yr over the watershed such that the ratio of recharges at the floodplain to side slope to upland was 44:14:24. Based on the principle of water balance, the specific values of recharge in each zone were

calculated such that their area-weighted average turned out to be 129.5 mm. During the stage of model calibration, we varied zonal recharge values such that the ratio of recharge values remained unchanged. The final, calibrated net recharge that resulted was slightly lower than the initial value, and equal to 120.0 mm/yr. The calibrated zonal recharge values are presented in the next section (section 2.5) on model calibration.

Determination of the boundary and area of each recharge zone was done using the Iowa Cooperative Soil Survey (ICSS) soils database of Jasper County, IA. The soil mapping units located inside the Walnut Creek watershed were classified based on their slope class and type of parent material. Side slopes were characterized by the soil mapping units whose slope belonged to the classes C (5-9%), D (9-14%) and E (14-18%), and covered approximately 54% of the total watershed area. The remaining slope classes A (0-2%) and B (2-5%) were separated based on the soil parent material listed in the database. Alluvium units fell in the floodplain region and covered around 19% of the watershed area, while loess units comprised the uplands and covered the remaining 27% of the watershed area.

2.4.4. Boundary conditions

(a) Stream boundary condition : The Walnut Creek main channel and tributaries were defined using the RIV package and are shown in Fig. 5. The stream and its tributaries are classified as head-dependent boundaries, where flux between the model cell and the boundary is determined by the hydraulic head specified at the boundary (see equation 7 in section 2.2). Therefore, for a complete specification of this boundary type, one needs to define the hydraulic head (here, stream stage) and conductance associated with the boundary at each cell location, along with the physical extent of the stream network. We determined

the stream network extent, streambed conductance, and stream stage and bottom elevation as described below.

The extent of the stream network was determined by using a combination of the 2006 NAIP (National Agriculture Imagery Program) aerial photograph, 1 meter resolution LIDAR DEM, and the NWI (National Wetlands Inventory) remap stream network that was obtained from the 2002 CIR (Color Infrared) orthophotograph of Jasper county. The original stream network was digitized from the 2006 NAIP airphoto. This network did not contain a number of shorter tributaries that were visible in the NWI remap shapefile. On the other hand, the NWI remap shapefile contained a few discontinuous stream segments. Therefore, both networks were examined closely to generate an accurate stream network. The NWI remap lines were improved by digitizing stream segments in the regions of discontinuity based on the NAIP airphoto. The completed network was then compared with the theoretical stream network obtained from the LIDAR DEM. A verification of the digitized stream network using the DEM was considered necessary because DEM is the reference surface for the model. This is because during the stage of importing the stream network into the model, a possible assignment of a stream sink to a cell that is slightly misaligned (not running along the natural drainageway as determined by the land surface) could have a significant impact on the groundwater flow lines in that region. The model solver would be likely to attempt a convergence of the flow lines to a cell located higher than the place of natural depression. This would increase model error. Thus, a combination of the three data sources enabled us to arrive at a good representation of the stream network.

Definition of the stream conductance required estimates of streambed hydraulic conductivity, streambed thickness, and the length and width of stream segment associated

with the model cell. Streambed thickness along the Walnut Creek main channel was determined using field data presented in a paper by Schilling and Wolter (2000). The streambed thickness of most sampled stream segments fell in the range of 0-0.5 ft, while the thickness of a few segments was larger and fell in the range of 1-2.5 ft. Thus, we assigned a length-weighted average thickness of 0.1 m to the segments in the former range, and a length-weighted average thickness of 0.4 m to segments belonging to the latter range. The streambed thickness of tributary reaches was estimated to fall in the 0-0.5 ft range, and therefore assigned the average value of 0.1 m. Segments along the main channel with undefined thickness were assigned the overall length-weighted average of 0.13 m.

Streambed hydraulic conductivity was estimated using information presented in Schilling and Wolter (2000). They assessed streambed material to be mostly composed of silt, with some sand, sand and gravel, and pre-Illinoian till present. The composition was estimated to be similar to the recent, loose silt deposits belonging to the Camp Creek member of the DeForest formation that is present along the stream banks. Thus, we used the hydraulic conductivity estimate for the Camp Creek member (Schilling et al., 2004) to assign the streambed hydraulic conductivity a value of around 5×10^{-5} m/s, or 4.3 m/day. The few stream segments where the presence of till under the stream was known were assigned a hydraulic conductivity of 0.43 m/day that was one order smaller than the conductivity of the alluvial deposits.

The length of the stream segment associated with each model cell was estimated to be nearly equal to the length of the model cell, and therefore assigned a value of 20 m. To estimate the width of the stream segment associated with each cell, we first estimated the overall distribution of stream channel width. Channel width is estimated to range from 2-5 m

for the tributary reaches, and steadily increase in the downstream direction, to around 10 m along the main channel. The width of the stream segment is estimated to be around half of the channel width. Thus, the tributary reaches were assigned an initial width of 1 m at their start location and a width of 2.5 m at the location where they join the main channel. The width at all intermediate locations along the tributary reaches was determined by linear interpolation along the length of the tributary between these two end values. The width of the stream segments along the main channel was assigned a uniform value of 5 m (which was half the main channel width of 10 m).

The assignment of streambed conductance, thickness, and its length and width at each cell location along the stream network, enabled us to determine streambed conductance using equation 8 (section 2.2).

To determine the stream stage and bottom elevations at each cell location along the stream network we used the estimates of channel incision depth listed in section 2.1.1. Incision depths were estimated to be around 1 m at the tributary headwaters and steadily increase in the downstream direction to depths of around 3 m, which also represents the incision depth along the main channel. We determined incision depth at intermediate locations along the tributary reaches by linearly interpolating between the two end values (of 1 and 3 m) along the length of the tributary reach. Note that in the RIV package, the stream bottom elevation is defined as the bottom elevation of the stream, including the streambed layer. Thus, to determine the bottom elevation we subtracted the incision depth and the streambed thickness from the land surface elevation at each cell location along the stream. The steady-state stream stage relative to the top of the streambed was estimated to range from around 0.5 (0.15 m) to 1 ft (0.3 m) along the tributary reaches, increasing steadily in the

downstream direction. The steady-state stream stage along the main channel was estimated to be around 1 ft (0.3 m). Linear interpolation along the length of each tributary reach, between the end values of 0.15 m at the tributary initiation point and 0.3 m at its end where it joins the main channel, produced stream stage values along the entire stream network. These stage estimates were made relative to the top of the streambed. Thus, to obtain absolute stream stage elevations we first subtracted the incision depth from the land surface elevation. This gave us the absolute top elevation the streambed. Adding the previously obtained stage estimates to top elevation of the streambed provided estimates of the stage elevations along the entire stream network.

(b) Tile drain boundary condition : The subsurface tile drainage network at the Walnut Creek watershed was defined using the DRN package and is shown in Fig. 5. Tile drains are also classified as head-dependent boundaries, with flux between the model cell and the boundary being determined by the hydraulic head (here, drain elevation) specified at the boundary (equation 7 in section 2.2). In other words, MODFLOW simulates tile drains to remove water from the aquifer at a rate proportional to the difference in the local head in the cell and the drain elevation. The constant of proportionality is termed the drain conductance. Therefore, a complete definition of the tile drain requires specification of the drain elevation and drain conductance at each cell location, besides an outline of its spatial extent.

The current tile network at the Walnut Creek watershed is primarily branched along the first order drainageways, and underlies the grassed waterways in the watershed. This is a recommended design practice for grassed waterways to prevent the buildup of excessive wetness, so as to maintain the vegetative cover, prevent formation of further gullies, and facilitate accessibility to farm equipment (Stone and McKague, 2009; Green and Haney,

2005; NRCS, 2004). Therefore, a siting of the tile network was performed by mapping the grassed waterways in the watershed that were visible in the 2006 NAIP airphoto.

Elevation of the tile drains at each cell location was determined by subtracting an estimated incision depth of 1.2 m from the land surface elevation. Estimates of drain conductance were also required. A tile drain can be represented as a perforated, closed drain. For such a drain, the conductance is determined by the size and density of the perforations, the chemical precipitation around the drain, and the hydraulic conductivity and thickness of the backfill material around the drain (Ballaron, 1998). Generally, due to lack of knowledge of such design specifications for tile drains, their conductance values are usually estimated based on their impact on model results (Quinn et al., 2006; Goswami and Kalita, 2009). Our estimate of 8.7×10^{-4} m^2/s (75 m^2/day) produced reasonable model results, and was also very close to the value of 6.4×10^{-4} m^2/s used by Goswami and Kalita (2009) for a watershed in a similar landscape (the Big Ditch watershed, an agricultural watershed in Champaign county, Illinois).

2.5. Model calibration and results

Hydraulic head measurements at 84 calibration targets situated at different locations within the watershed were obtained from Dr. Schilling at the Iowa Department of Natural Resources (Iowa DNR), Iowa City, and Dr. Helmers at the Iowa State University, Ames, IA. The location of the calibration targets is shown in Fig. 5. Certain sites had multiple head measurements made in different years. These head values were averaged to obtain a mean head value to represent steady-state conditions at that location. On the other hand, for certain sites where measurements at multiple depths were available, the head measured at the well

which was screened closest to the estimated location of the water table was used as the representative head at that location. Hydraulic heads for wells where depths to water table were measured were evaluated by subtracting the depth to the water table from the land surface elevation at that location specified in the model.

Automated calibration procedures such as PEST (a nonlinear parameter estimation package developed by Watermark Numerical Computing, 2005), and the MODFLOW-2000 internal calibration algorithm were unsuccessful in generating good calibration results. Instead, the process of manual calibration, that involved testing the response of the model to gradual, incremental adjustments in the calibration parameters, seemed to produce the best results. We observed the model to be least sensitive to variations in tile drain conductance, stream stage, and streambed conductance. On the other hand, the model was most sensitive the value of total equivalent recharge and the zonal hydraulic conductivities, in particular, the value defining the till zone. This is because in the case of groundwater flow through units which are placed in series, and represented by different conductivities, the least conductive unit dominates the system and controls flow. Moreover, the model was found to be sensitive to location of the loess-till contact, across which flow exits the upland loess zone and enters the region of till outcrop.

Therefore, we calibrated the values of total equivalent recharge, hydraulic conductivity of the till zone, and the spatial location of the contact between the loess and till units. We first varied the hydraulic conductivity of the till areas on a cell-by-cell basis. To do so, we first determining the set of reasonable values to be used in the test runs. As discussed in section 2.4, the hydraulic conductivity estimates from the slug tests data were used to define the lower limit of the till conductivity values that would be considered reasonable. Based on the

measurements presented by Schilling and Wolter (2001), we selected an estimate of 0.02 m/day (2.3 x 10^{-7} m/s) as the lower value of the hydraulic conductivity of the till zone. The upper limit was set at the SSURGO value of 0.2592 m/day (3 x 10^{-6} m/s). A lowering of this upper limit to 0.1 m/day (1.16 x 10^{-6} m/s) was found to improve model results. Therefore, we selected the upper value of the hydraulic conductivity of the till zone to be 0.1 m/day. Selection of an intermediate value, between the SSURGO and slug test values, was considered reasonable, since the hydraulic conductivity aquifer parameter varies continuously, and would therefore also include values between the defined upper and lower ends (0.1 and 0.02 m/day, respectively). We selected a value of 0.05 m/day (5.8 x 10^{-7} m/s) as the intermediate hydraulic conductivity. Thus, three separate values of till conductivities, based on values obtained from SSURGO, slug tests, and an intermediate value, were used to alter the conductivity of individual model cells within the till zone.

Furthermore, model results responded to very small shifts of the boundary between the till and loess zones. Local hydraulic heads were impacted significantly when the identity of the zone to which the model cell at the transition line belonged was toggled between the loess and till zones. Therefore, we deduced that the hydraulic conductivity along the transition line might be an intermediate between the two zones. This would arise due to the increasing thickness of the till outcrop as it reaches the land surface, that cause the equivalent horizontal hydraulic conductivity at the contact line to transition over the length of a few model cells, instead of transitioning abruptly (across zero length). Physically, the placement of a transition zone with a conductivity value between that of the loess and till units seemed realistic. This led us to add a zone of transition characterized by a hydraulic conductivity of 0.2 m/day (2.32 x 10^{-6} m/s).

Finally, variation of the loess hydraulic conductivity and total equivalent recharge by a small magnitude, from 0.5891 m/day and 129.5 mm/yr to 0.5503 m/day (6.37×10^{-6} m/s) and 120.0 mm/yr, respectively, further improved model calibration. This was chosen as the best calibrated model, though in the future as new field measurements become available, further refinement is possible. The spatial distribution and values of the final calibrated hydraulic conductivity and recharge parameters are shown in Figs. 6 and 7, respectively.

The final calibrated model produced reasonable agreement between the simulated and observed hydraulic head values at the calibration targets (Fig. 8). The absolute residual mean (ARM, the average of the absolute values of the residuals, which are the difference between the simulated and observed heads) was 2.55 m, while the residual standard deviation was 2.29 m. The mass balance error for the model was 24.5 m^3/day, which corresponded to 0.12% of the total inflow (Fig. 9). The resultant distribution of water table elevations across the watershed is shown in Fig. 10.

For a model of this scale (covering an area of 51.94 km^2), an ARM of 2.55 m was considered reasonable. For example, a similar scale MODFLOW model presented in Christianson (2008), that covered an active model area of 27.20 km^2, and simulated the groundwater-lake interaction at the Ada Hayden Lake in Ames, Iowa, was associated with an ARM of 1.66 m. Therefore, an increase in the scale of the model is likely to increase the error associated with it.

However, for our specific project goals of evaluating the distribution of groundwater travel times, an error in hydraulic head generated at the scale of cell resolution is likely to not impact results significantly. This is because the travel time along the length of a flow path from its origin to the sink, is a cumulative measure. Thus, we can expect possible deviations

in hydraulic gradient along the length of the flow path to integrate out. Moreover, we generated the travel time distribution by aggregating the travel times of more than 120,000 particles and then studied the distribution as a whole. Thus, possible errors introduced by some particle traces are likely to have negligible impact on the shape and statistical properties of the overall travel time distribution that is generated from a large sample size. These two reasons indicated that the few stray spots of dry and flooded cells (Fig. 10) that remained were very unlikely to have any noticeable impact on the distribution of cumulative travel times obtained from a large sample of tracer particles.

Hints of the insensitivity of the distribution of cumulative travel times to localized model errors were evident in the earlier stages of model calibration when the distributions obtained for model runs with a higher number of dry and flooded cells were best-fit to the same theoretical distribution function (an exponential) as the final calibrated model. Comparing the final calibrated model to an earlier version, we observed that even though the number of dry cells in the latter were more than double of the final model (1171 cells versus 551 cells, respectively), and the number of flooded cells were nearly the same (1367 versus 1501 cells, respectively), both distributions were represented by an exponential decay function, with the characteristic mean travel time of the travel time distributions differing by 0.68% only (20.37 years in the earlier version versus 20.51 years for the final model). Therefore, we concluded that the distribution of cumulative travel times obtained by tracking a large number of particles (>120,000) was fairly robust and effective in integrating out deviations produced by error in hydraulic head of a small fraction of the total number of active cells (129,820). Thus, the simulated distribution of travel times was considered a valid representation of groundwater travel times at the Walnut Creek watershed.

Implementation of the MODPATH model involved the release of particles at the water table in every cell center of the active model domain. These particles were tracked in the forward direction (from the source location towards the sink). MODPATH used intercell flow rates computed by MODFLOW, and the estimated porosity of the aquifer, to determine the travel time of the particle along its flow path. In particle tracking codes like MODPATH, the trace of a particle that enters a cell where the sink captures only a partial amount of the inflow relation cannot be resolved analytically. To overcome this problem, MODPATH defines the strength of a sink as the fraction of cell inflow that is captured by the sink, and uses the value of that parameter to determine whether the particle will stop or bypass a particular sink. This is accomplished by comparing the strength of the sink against a user-defined threshold (S*). All sinks with strength greater than S* are treated as active; the particles stop at such sinks. The remaining sinks are treated as inactive, and particles entering cells containing such sinks simply bypass them. “Strong sinks” are defined as those that capture 100% of the cell inflow. Sinks with strength less than 100% are termed “weak sinks”. Thus, setting S* to 0 simulates the scenario of no bypass flow (both, weak and strong sinks are active), and setting S* to 1 simulates the scenario of maximum bypass flow (by activating only the strong sinks). The default value of S* was set to 0, and varied only in the simulation experiments conducted in chapter 4.

The raw travel times generated at each time step were then imported into a Microsoft Access database, and processed to generate a list of the cumulative travel time associated with each particle, along with information of its origin and final destination cell locations. The small fraction of particles with an unphysical travel time of zero years, obtained for the few particles that were released in cells containing an active sink, were removed. The travel

times associated with all the remaining particles were used to generate the mean travel time, that was interpreted as a representative of the travel time associated with two dimensional advective transport in the watershed. The shape of the travel time distribution was obtained by generating a normalized histogram (with a bin size of 6 years) such that the area under the travel time distribution equaled 1000 units (representing 1000 particles). The resulting travel time distributions and associated statistics are presented in the following chapters.

2.6. Model assumptions and limitations

As described at the end of the previous section, the distribution of cumulative travel times associated with advective transport are less sensitive to model errors, due to the fact that they are cumulative measures, and that the distribution has been obtained after normalizing the cumulative travel times of a large sample of particles. However, the construction and execution of any model involves some assumptions and limitations. For this particular model the key ones are listed below:

1. Steady state : One of the most important assumption is that the model is derived for steady-state, two dimensional flow. Therefore it is useful for applications that can be based on steady-state conditions. For instance, the model is useful for predictions of long-term trends of the order of a decade or more, such as the long-term response of groundwater flow in the watershed to land use or climate change measured in terms of the distribution of travel times and/or the volume of baseflow; and the effect that a deeper incision of the stream channel will have on the average water table levels. The model is not suitable for prediction and evaluation of short-term behavior, such as the response of the water table to a flood event.

2. Model dimension : The model is two-dimensional, and therefore incapable of simulating three dimensional aspects of groundwater flow, such as the variation of hydraulic head with depth, and the presence of vertical hydraulic gradients at the local scale. However, the model has variable elevation incorporated into it, by aligning the top of the layer with the land surface elevation. Therefore the model accounts for hydraulic differences established due to changes in elevation across cells (from one x-y location to another), but not within the cell (across a vertical profile for a fixed x-y location).

3. Transport by advection : The model has been constructed to simulate advective transport only. Other processes that influence contaminant transport, such as diffusion, adsorption, hydrodynamic and mechanical dispersion, solute dissolution, soil mineralization, chemical reaction, radioactive decay, biological degradation of organic contaminants, and similar reduction processes such as denitrification. Travel times associated with contaminant transport that is significantly influenced by any of these processes requires the use of more sophisticated models such as MT3DMS (Zheng and Wang, 1999).

4. Recharge : MODFLOW as a standalone model is limited by the fact that it can only simulate the groundwater component of the hydrology of a system. The influence of surface and vadose zone processes on subsurface flow has not been accounted for. Schwientek et al. (2009) through a series of field measurements observed the impact that variable thickness of the overlying unsaturated zone has on the vertical distribution of mean travel times in a heterogeneous, unconfined aquifer. Several authors have explored the interaction of the saturated and unsaturated zone processes (example, Wondzell et al., 2007; Kollet and Maxwell, 2008; Burns et al., 2005) and the interaction of the groundwater and surface water, such as flow exchanges and mixing near the stream boundary (example, Valett et al., 1997;

Harvey and Bencala, 1993; Wroblicky et al., 1998). These complex, nonlinear, hysteretic processes require one to account for various atmospheric and terrestrial variables such as plant growth, solar radiation, humidity, wind, land use, antecedent soil moisture conditions in the unsaturated zone, etc. By use of the net recharge to the aquifer as the aquifer recharge parameter, the model has been designed to account for average losses due to ET, lateral and overland flow. But these are averages across the entire watershed. In other words, spatial variation in recharge introduced due to the abovementioned processes has not been accounted for. The influence of these factors is very likely to modify the local distribution of hydraulic heads at any particular site within the watershed. Therefore, the model is not suitable in cases where an accurate prediction of the local hydraulic head distribution at a specific location within the watershed is desired.

5. Hydraulic conductivity : The presence of shale outcrops along the main channel and at places in the side slopes indicates that our design selection of uniform aquifer thickness is likely to not be true for certain locations in the watershed. Indeed, during model calibration we found that the introduction of a transition zone defined by a hydraulic conductivity in between the values of loess and till conductivities had a significant impact on the model results. This implies that the extent of low hydraulic conductivity zones might be underestimated in the model. Moreover, our baseline estimates using SSURGO hydraulic conductivity values might be high, since values obtained from the slug tests were nearly one order of magnitude lower. But, as discussed earlier, hydraulic conductivity estimates from slug tests are likely to underestimate conductivities representing larger scale flow. Therefore, there is uncertainty regarding the selection of the baseline estimates of hydraulic conductivity, with both sets of data possessing some advantages and disadvantages. In this

particular model, we found that considering both sets of data, by using the SSURGO values as baseline estimates that were then modified based on results from the slug tests, produced the best model calibration.

A bias in the model introduced by higher estimates of hydraulic conductivity would lower the water tables and lead to the creation of dry cells. Indeed, despite our best modeling efforts, the persistent presence of stray spots of dry cells indicates that hydraulic conductivity estimates might be higher than the actual range. The error might be stronger at some locations, for example, near the loess-till contact line and the streambed, where the outcropping of till indicates that equivalent horizontal hydraulic conductivity in that region starts decreasing rapidly over a certain unknown distance. We observed the model to be most sensitive to estimates of this region, since in the case of lateral flow across different conductivity units placed in series, the unit with the least conductivity is the limiting factor for flow. Thus, better estimation of the hydraulic conductivity in these regions is likely to improve the model, and eliminate the stray spots of dry cells.

Furthermore, the model calibration plot (Fig. 8) indicates a systematic underestimation of water table levels at the higher end of the observations. These calibration target locations would correspond to higher land surface elevations relative to the target locations in the floodplain, such as the side slope and upland areas. Therefore better estimation of the hydraulic conductivity of the till areas along the side slope is likely to improve model calibration.

6. Stream boundary condition : As discussed in the conceptual design section, delineation of the stream network used in the model involved the use of a variety of data sources, namely, the 2006 NAIP aerial photograph, the NWI remap stream lines derived from a 2002

CIR ortho-image of the region, and the analytic stream network derived from the reference DEM. This enabled us to arrive at the best estimate of the shape and extent of the stream. Estimates of the elevation of the stream stage and bottom, and other channel attributes such as channel width and streambed hydraulic conductivity, were based on a number of field studies conducted by researchers at the Iowa DNR.

However, there are some limitations in this design scheme. For example, there is no direct way to estimate the *steady-state* extent of the stream network. The presence of ephemeral tributaries and gullies through the spring and summer seasons at the watershed has been observed to be significant, especially in the form of several, short and steep gullies that develop along the length of the main channel. Therefore, the current extent of the network that was based on two images of the region depends on the specific time these images were taken. The images would have captured the stream profile based on the hydrologic conditions present at that time.

Moreover, spatially distributed estimates of the steady-state stream stage and width will be impacted by local variations in topography (land slope and channel incision), discharge from tile outlets, and the specific shape of the channel profile at each location. The model did not account for these factors. These parameters are used to determine water table elevations near the stream, and compute the flow rate between the aquifer and the stream, that in turn impact the water balance and final hydraulic head distribution within the aquifer. Estimates of streambed hydraulic conductivity would be influenced by the till and shale outcrops along the main channel, and possibly along some higher order tributaries. As discussed earlier, inclusion of these low conductivity zones would lower the flow from the aquifer to the

stream and therefore increase the local water table elevations. The model did not account for these fine scale heterogeneities.

7. Tile drain boundary condition : The impact of tile drainage in the headwaters located towards the north at the Walnut Creek watershed has not been quantified. Schilling et al. (2006a) observed streamflow behavior to vary by subwatershed. They observed the annual baseflow component to be larger from the tile-drained agricultural regions located at the headwaters of the watershed. This suggested that tile drainage has a significant impact on flow and the water table levels, and therefore streamwater quality, particularly in those parts of the watershed.

Thus, a complete mapping of all active tile drains, especially in the row cropped areas located in the headwater reaches, was an essential aspect of the model design. It is likely that the use of a 2006 NAIP aerial photograph of the region to locate the grassed waterways in this region and estimate the presence of the entire subsurface tile drainage network, could not account for many active tiles, in the headwaters and in fact, across the entire watershed. Therefore, a more accurate mapping of the tile drainage network using more data sources, especially in the headwater areas, is likely to be of great benefit to the model.

8. Calibration targets : Hydraulic head measurements at 84 wells across the watershed were used as calibration targets (Fig. 5). This data was obtained from field studies conducted by researchers at Iowa DNR and Iowa State University. The hydraulic head at each site was collected over a number of years at different times. We used the average of all hydraulic head values measured at each site however, the impact of the specific transient hydrologic conditions at the time of measurement is inescapable. Moreover, in ideal conditions, estimation of steady-state variables is not influenced by the time span over which the

measurements are made. In reality, under natural conditions that include annual and seasonal variability of precipitation, aquifer recharge is bound to vary with year and season. Thus, the season and year in which the measurements were made influenced the calibration data. Therefore, including measurements from a larger number of years into the averaging process is likely to improve estimates of the steady-state hydraulic head values at each site. The spatial distribution of the calibration targets also had an impact on our model results. The areas located in the headwaters for example were not represented in the calibration dataset. Therefore, expansion of the sample range to include locations that represent more diverse landscape positions is likely to improve the calibration dataset, and therefore improve our estimates of the model calibration error.

2.7. Kolmogorov-Smirnov statistical test

At different stages in the study, we perceived the need for comparing two distributions of travel times and quantifying the degree of closeness in their shapes. To achieve this purpose, we selected the Kolmogorov-Smirnov (KS) statistical test that quantifies the comparison of two sample distributions with each other (Daniel, 1978; Hollander and Wolfe, 1999). This technique was introduced in 1933 by a Russian mathematician, A. N. Kolmogorov for comparison of one sample distribution with a theoretical, continuous distribution. In 1939, another mathematician, named N.V. Smirnov, developed another variant of this test for comparison of two sample distributions with each other. Therefore, the first test became known as the KS one-sample test, while the latter came to be known as the KS two-sample test. The KS two-sample test was used for comparison of two empirical travel time distributions, while for comparison of an empirical distribution with an analytic distribution

the KS one-sample test was used. The concept behind both, the one and two sample tests is the same. Therefore, we first describe the one sample test and then generalize it to the two samples scenario.

To apply the KS one-sample test on a pair of distributions, we consider the cumulative distribution functions of both distributions. The cumulative distribution function of a random variable X, is denoted as F(x), and defines the probability that the value of the random variable X is less than or equal to x. Therefore, F(x) is characterized by a steadily increasing function that begins at 0 and continuously increases up to its upper bound 1 as the value of X is increased over the entire range of possible values the variable can take.

For the KS one-sample test, we compare two cumulative distributions, which describe the same random variable X, with each other. One cumulative distribution is defined by a theoretical, continuous form, $F_0(x)$, while the other, S(x), is an empirical distribution function that is derived from a random sample of the variable X. Assuming that we draw the random sample from a system that is represented by some unknown distribution function F(x), the KS one-sample test evaluates whether $F(x) = F_0(x)$, for all values of x. If the two distributions are equal, then the sample distribution S(x) and $F_0(x)$ are likely to closely agree with each other, especially for large sample sizes. To quantify this level of agreement, the KS one-sample test statistic is computed as described below.

Consider a random sample of size n, consisting of independent observations $X_1, X_2, \ldots, X_n$, derived from the population of a variable X that is represented by an unknown distribution function F(x). S(x) represents the sample's empirical distribution function, i.e. S(x) is the cumulative probability function evaluated from the sample data. In other words, S(x) is the proportion of sample observations that are less than or equal to x :

$$S(x) = \frac{(\text{number of observations } \le x)}{n} \tag{17}$$

Then the "distance" between S(x) and $F_0(x)$ is a measure of the degree of closeness between the distributions F(x) and $F_0(x)$. Therefore, we define the KS two-sided test statistic D as,

$$D = \max |S(x) - F_0(x)| \tag{18}$$

Graphically, this represents the maximum vertical distance between the two functions S(x) and $F_0(x)$. If the test statistic D, which is equal to the maximum difference between the two distributions at any value of x, is small then the differences at all other values of x will also be small, since they will be even smaller than D. Therefore D is a measure of the degree of closeness between the shapes of two cumulative distributions through the entire range of X. Thus, if the sample represented by S(x) has been drawn from the same system as the one that $F_0(x)$ represents then D will be close to 0. The maximum value that D can take is 1. Therefore, the closer D is to 0, the better the fit between the two distributions. The closer D is to 1, the greater is the mismatch between the two distributions.

The KS test statistic D defined above is easily generalized for the comparison of two samples as shown below.

Consider two independent random samples A and B, of sizes m and n, respectively. The observations in each sample are denoted as $A_1, A_2, \ldots, A_m$ and $B_1, B_2, \ldots, B_n$, respectively. Both observation sets are sampling a random variable X. The goal is to determine whether the two samples are representing the same system, in other words, whether the two samples have been drawn from the same population. If the samples A and B are represented by the

empirical distribution functions $S_A(x)$ and $S_B(x)$ (as defined in equation 17), then the KS two-sided test statistic D for the two sample case is given as,

$$D = \max | S_A(x) - S_B(x) | \tag{19}$$

Therefore, if both samples are representing the same system or population, then $S_A(x)$ and $S_B(x)$ should be close to each other for all values of x, and D should be close to 0.

Given the specific nature of the travel time distributions we sought to compare, this test statistic was found to be the most appropriate, given the fact that, (1) it allowed the comparison of distributions with different sample sizes, and (2) it accommodates a comparison of either a theoretical and empirical distribution, or a pair of empirical distributions. These conditions were necessary to enable us to use this test statistic in the comparison of travel time distributions where there were variations in the total number of particles with non-zero travel times, and in the comparison of a pair of travel time distributions that either comprised an empirical and a theoretical distribution, or two empirical distributions.

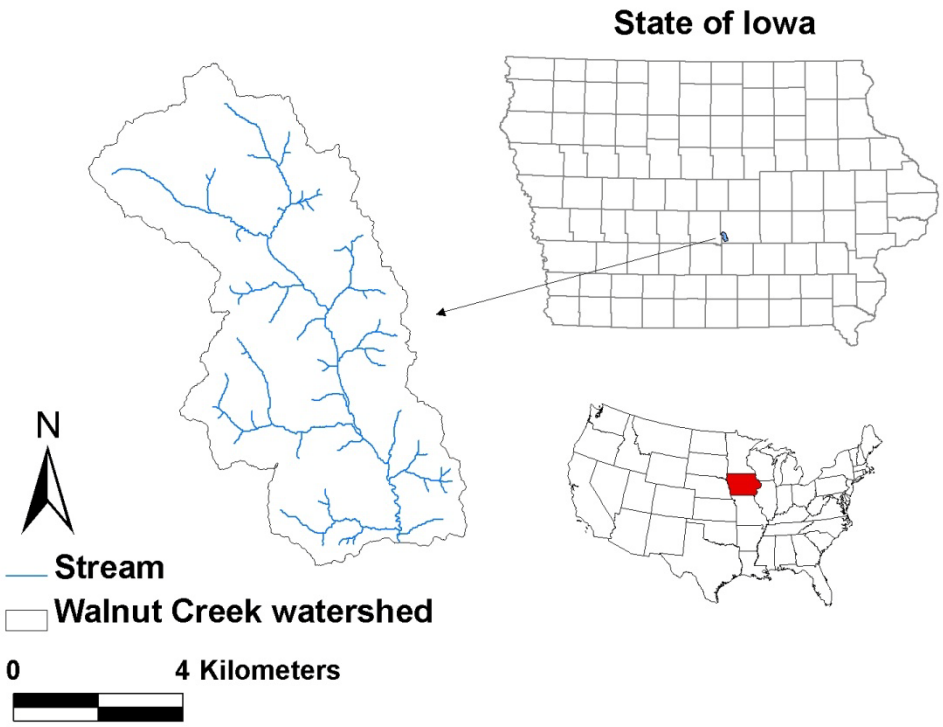

Fig. 1. Site location

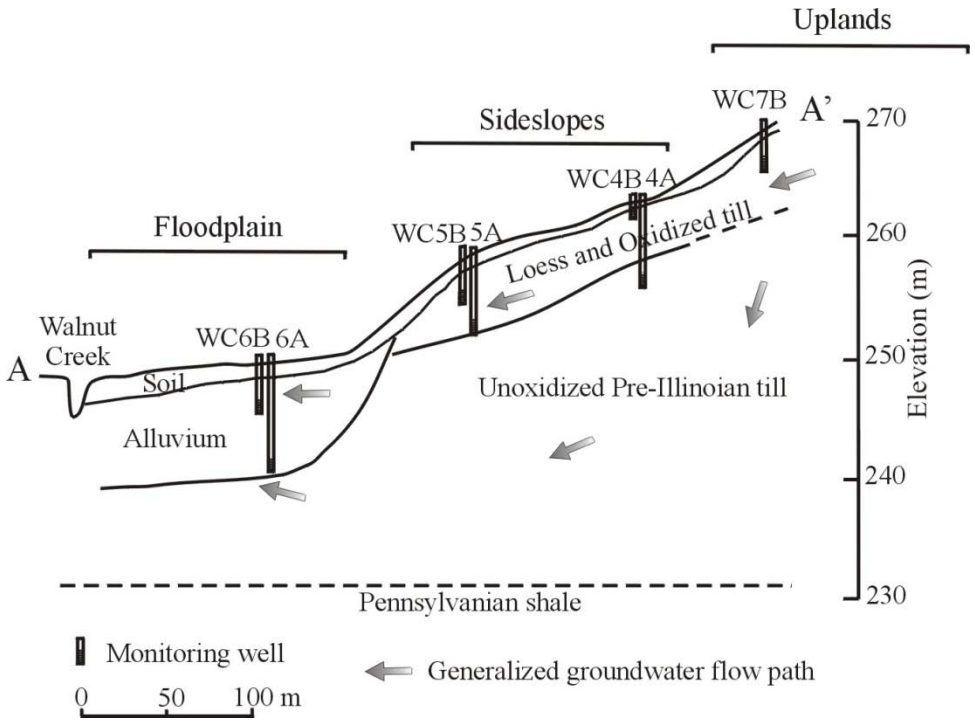

Fig. 2. Cross section along a representative well transect (From Schilling, 2009)

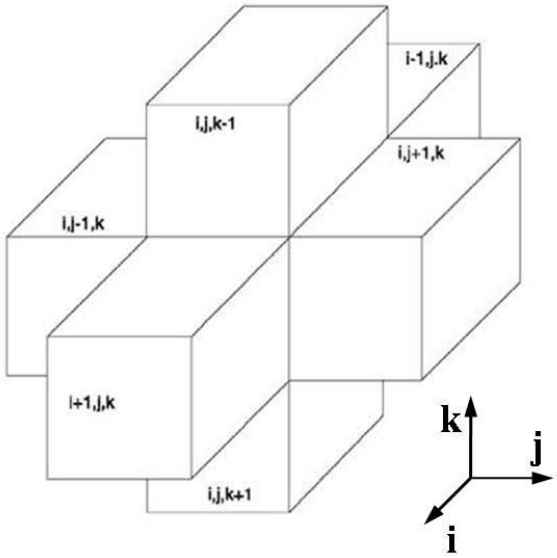

Fig. 3. MODFLOW cell and its six nearest neighbors along the three coordinate axes (Adapted from Harbaugh et al., 2000)

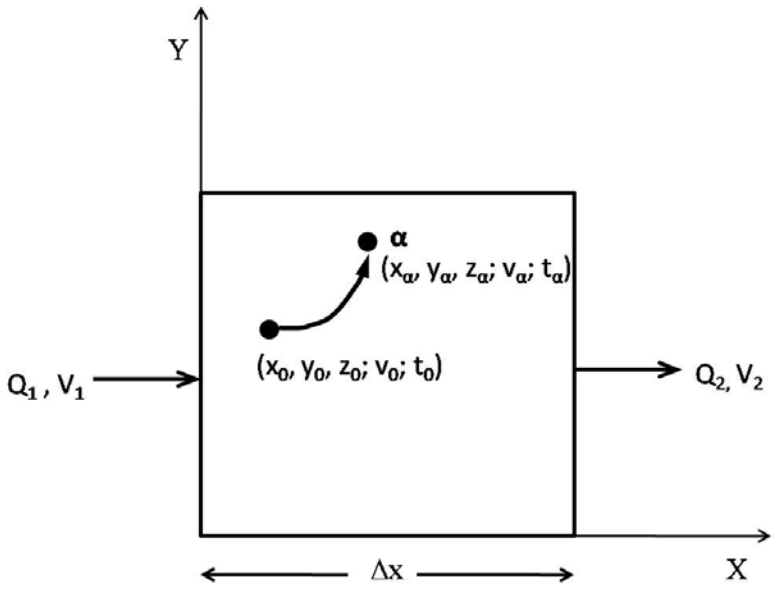

Fig. 4. Two dimensional profile of a cell inside the groundwater flow model. Q_1 and Q_2 are the flows across the cell faces in the X direction. v_1 and v_2 are the corresponding flow velocities. The particle tracking code MODPATH computes the position (x_α, y_α, z_α) and velocity v_α of a particle at a time t_α ; whose initial position and velocity is (x_0, y_0, z_0) and v_0 at time t_0 (Adapted from Pollock, 1994)

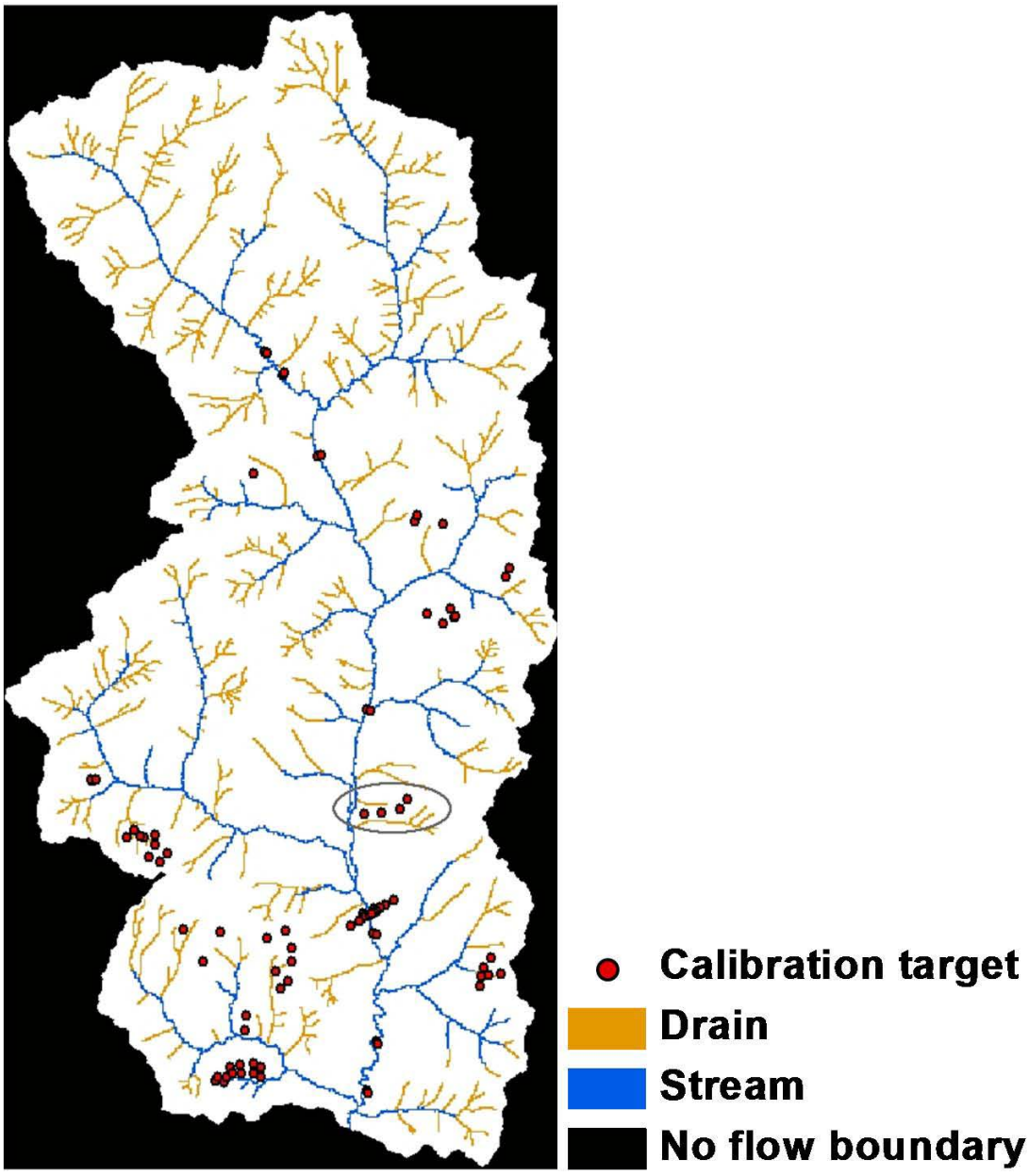

Fig. 5. MODFLOW boundary conditions and calibration target locations. The encircled area shows the location of the well transect whose stratigraphic cross section is shown in Fig. 2.

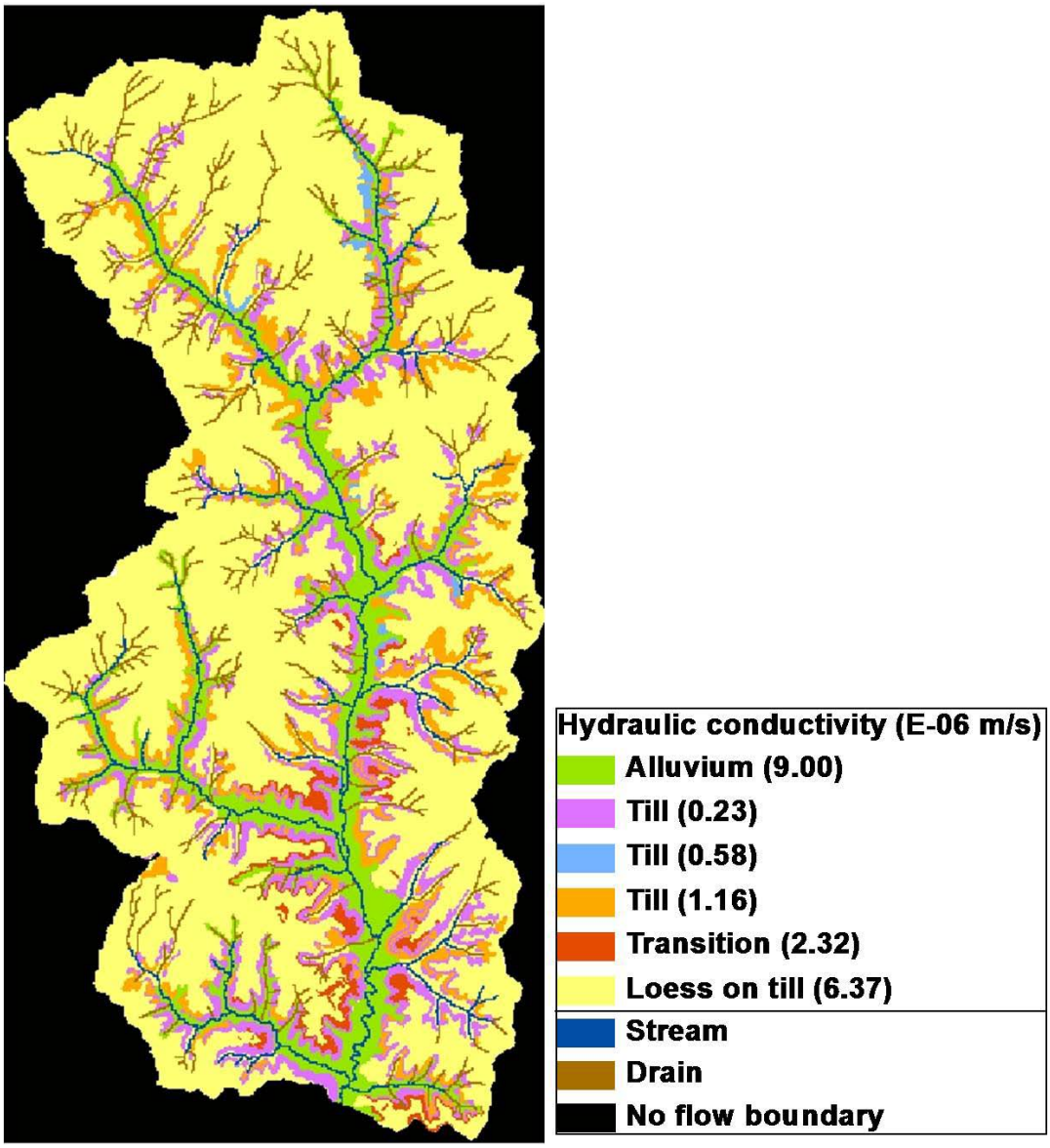

Fig. 6. Distribution and values of the calibrated hydraulic conductivity parameter

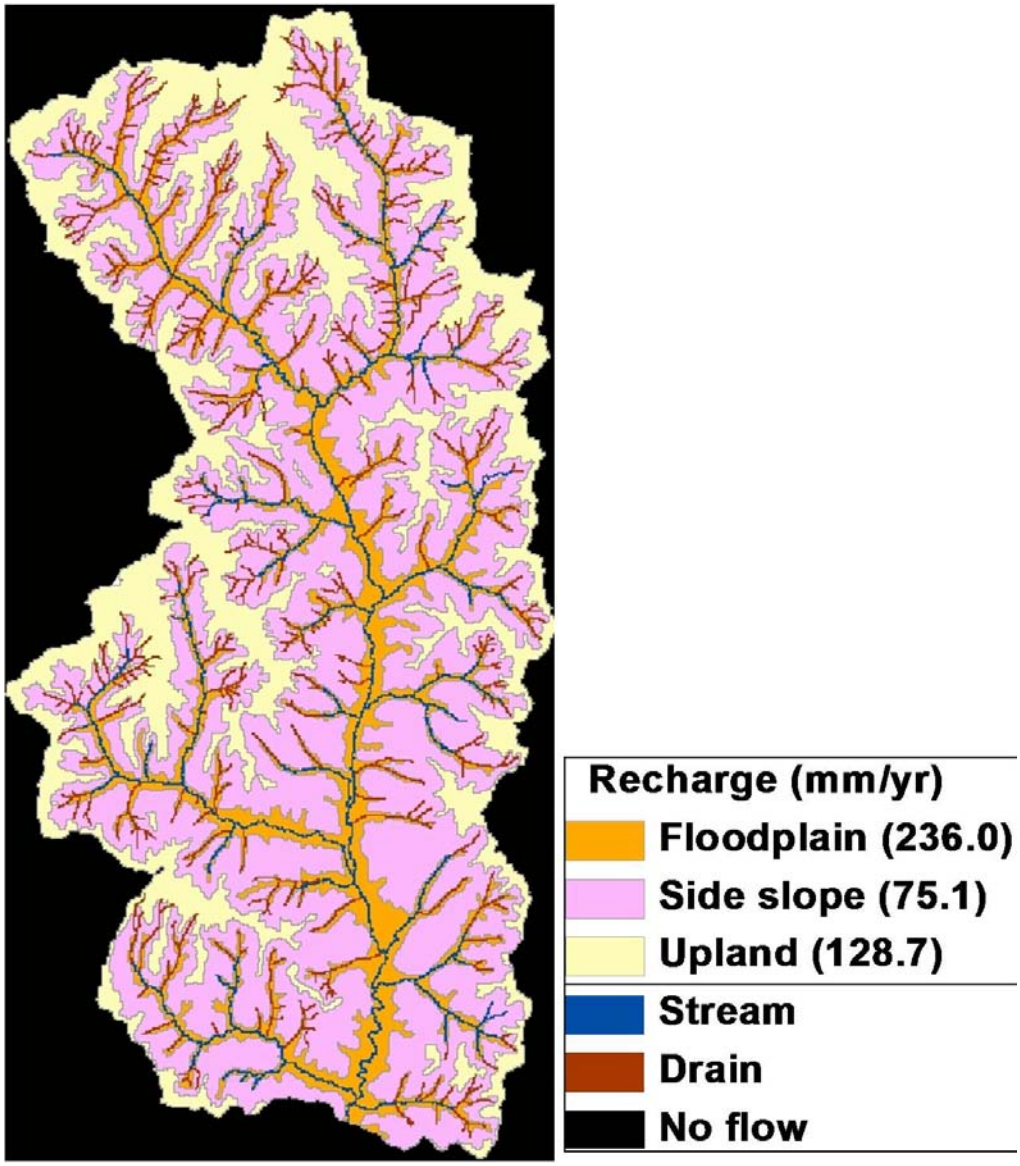

Fig. 7. Distribution and values of the calibrated net aquifer recharge parameter

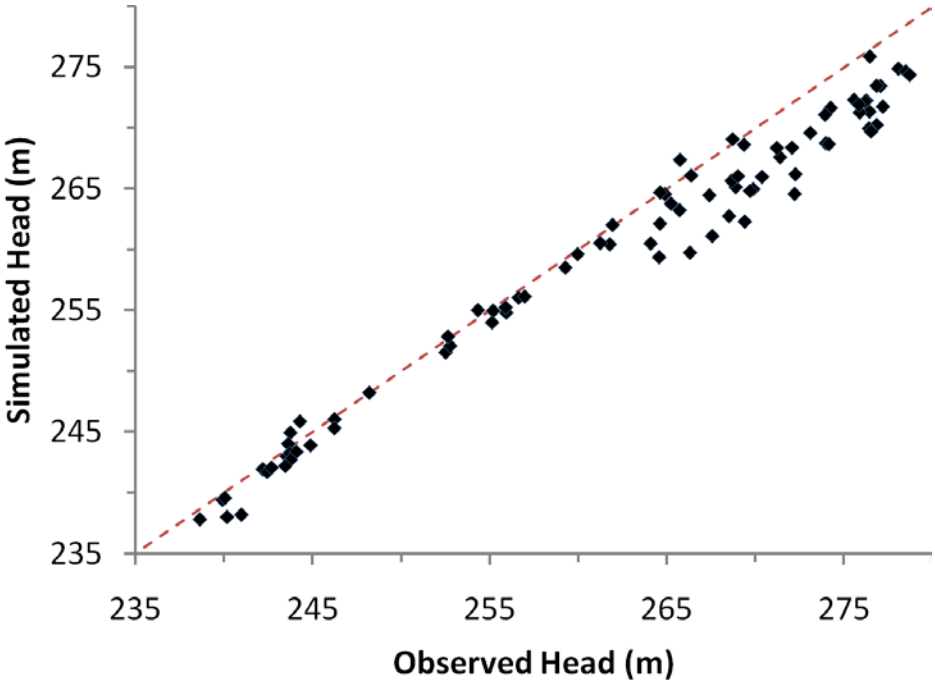

Fig. 8. Model calibration plot

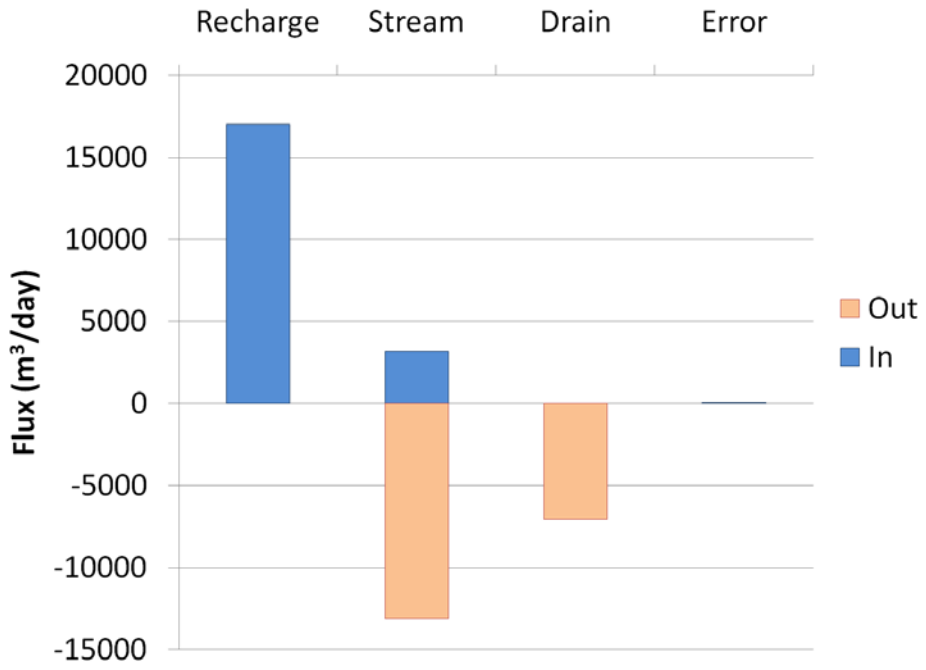

Fig. 9. Model mass balance

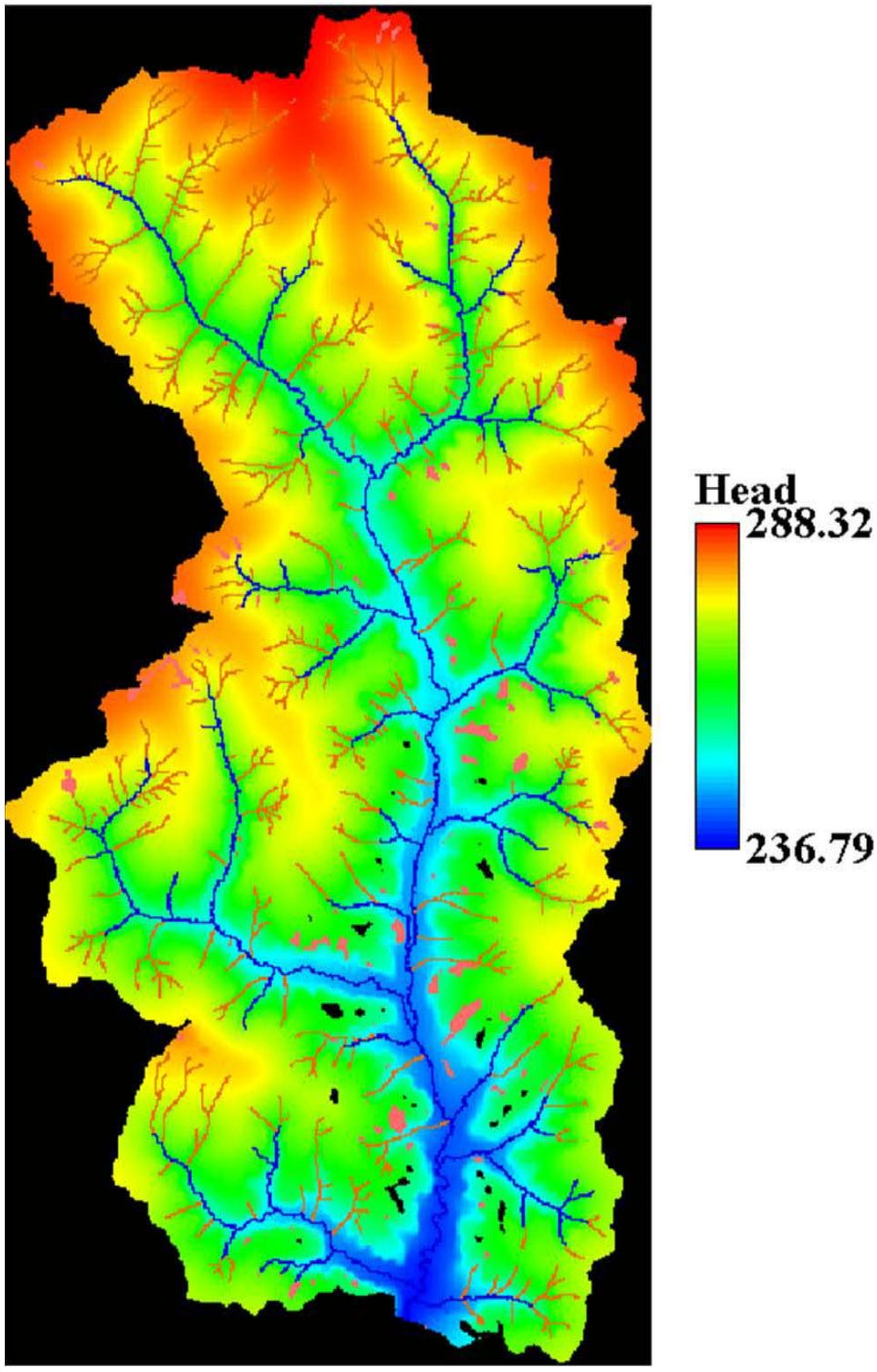

Fig. 10. Distribution of hydraulic head (in meters). The red and black spots represent stray flooded and dry cells, respectively. Stream and tile drains are represented by blue and brown lines, respectively.

III. A comparison of three models for estimation of the steady-state groundwater travel time distribution at the Walnut Creek watershed, Iowa

Adapted from a paper to be submitted to *Water Resources Research*

Priyanka Jindal, Keith E. Schilling, Nandita Basu, Calvin F. Wolter

Abstract

In light of the many conservation and remediation practices being implemented across many watersheds in the US to mitigate nonpoint source pollution, an estimate of the lag time necessary for such practices to demonstrate a positive impact on the streamwater quality is critical to the design, monitoring and evaluation of such projects. In particular, nitrate transport has been found to depend strongly on the characteristics of groundwater flow within the watershed. Thus, estimation of groundwater travel times is an essential component of any successful watershed improvement plan. We demonstrated the application of three models, spanning the range of model complexity, to the estimation of the two dimensional, steady state groundwater travel time distribution of a shallow, unconfined aquifer at a representative watershed. The analytic model, based on the theory proposed by Haitjema (1995), was the simplest and required estimates of the watershed-wide averages of porosity, saturated thickness, and areal recharge rate only. The GIS-based model (Schilling and Wolter, 2007) of intermediate complexity employed the land surface as a surrogate for the water table to compute flow path lengths and velocities at each spatial location within the watershed. A distributed hydrologic model constructed using MODFLOW represented the higher end of model complexity, and required detailed information of the spatial distribution of aquifer properties and boundary conditions. We obtained good agreement between all

three travel time distributions, with estimated mean travel times ranging from 16.2 to 20.5 years. The exponential distribution was found to best-fit all three distributions. An evaluation of the reasons behind the match between the MODFLOW and GIS-derived distributions revealed disagreements in the distributions of flow path lengths and velocities. But these differences did not penetrate to travel time distribution due to higher flow lengths and velocities in the GIS model leading to similar travel times as those generated by smaller flow lengths and velocities in the MODFLOW model. However, the flow length and velocity differences were visible in the comparison of the spatial distributions of the travel times. Comparison of travel time distributions representing each landscape position (upland, side slope, and floodplain) demonstrated that the travel time differences were dominant in the floodplain, where the land surface used by the GIS model fails to capture the convergence of the flow lines along the water table toward the stream. Based on these results, we inferred a set of guidelines to assist watershed managers in the process of model selection.

3.1. Introduction

The problem of nonpoint source pollution has been reported to afflict many watersheds across the United States (example, Shanks et al., 2006; Gentry et al, 2007; Tomer et al., 2008). Surface water quality has degraded, with stream water samples registering the presence of a variety of solute loadings in the form of sediment, nutrients, pathogens, pesticides, and metals (USEPA, 2008). This effect has propagated downstream and reached as far as the oceans, with zones of eutrophication and hypoxia of varying intensities being detected in many bays and estuaries bordering the eastern and western coasts of the country (Diaz and Rosenberg, 2008), such as the regions of the Gulf of Mexico, Chesapeake Bay,

Long Island Sound, and San Francisco Bay (Rabalais et al., 2002; Brush, 2009; Anderson and Taylor, 2001; Lehman et al., 2004).

In response to this threat a number of watershed nonpoint source projects have been implemented nation-wide (Hardy and Koontz, 2008), specifically targeted towards improving water quality through the adoption of various conservation and restoration schemes. The success of such programs depends strongly on many factors, including adequate landowner interest, accurate identification of the sources of pollution, proper selection and implementation of best management practices (BMPs), and effective monitoring of the water quality response (Meals et al., 2010). One such factor is the correct estimation of the characteristic lag time associated with the unique combination of the particular site, pollutant type, and the selected remediation procedure. In fact, the total time necessary for the effect of a distributed land use management practice to become visible at the stream includes the time required for the implemented practice to start producing an effect, the time needed for the effect to travel to the stream, and, once the effect reaches the stream, the time required for the stream to respond to that effect (Meals et al., 2010).

In the case of nitrate contamination, a major nonpoint source pollutant from agricultural watersheds (Carpenter et al., 1998; Burkart and James, 1999; Goolsby and Battaglin, 2000), whose primary mode of transport is shallow groundwater (Hallberg, 1987; Schilling, 2002; Schilling and Zhang, 2004), the total time elapsed before the effects of remediation practices are detectable in the stream water quality are typically very large (Bratton et al., 2004; Tomer and Burkhart, 2003). Even in very small watersheds (less than 2 ha) nitrate reductions have been observed to have lag times of the order of several years (Owens et al., 2008). Thus, we anticipate that in the case of nitrates, of all the three time scales listed above, the scale of

groundwater travel times from the location of remediation to the stream will be the most dominant, and determine the overall time delay necessary before the specific BMP implemented in the watershed yields significant results at the stream.

Advance knowledge of the distribution of groundwater travel times characterizing the watershed would facilitate prediction of the rate of nitrate removal from the stream waters that in turn would enable the project managers and stakeholders to set a realistic timeline for accomplishing project goals. This knowledge would also be very useful in the decision-making stages of selecting an appropriate set of BMPs and tailoring them to specifics of the particular watershed while keeping in mind the anticipated turnover time scales. Moreover, knowledge of the spatial distribution of groundwater travel times would be instrumental in optimal siting of the BMP to locations that are most likely to produce results within the allocated timeframe. An understanding of the characteristic travel time scales involved would also enable the project manager to better interpret monitoring results. Finally, this estimation would be critical to make a fair and scientifically-grounded evaluation of the efficacy of the implemented conservation and remediation strategies. Thus, we see that an understanding of the groundwater flow system, and the travel times associated with it, is important at every step of the watershed conservation plan and plays a central role in ensuring the success of such a program.

There exist many simulation schemes to estimate the distribution of travel times (see review by McGuire and McDonnell, 2006). In this study, we constructed the travel time distribution of steady-state groundwater flow in a watershed using three such methods derived from techniques based on theory, GIS analysis, and distributed hydrologic modeling. The three approaches represented different levels of generalization, and spanned the entire

range of model complexity from the simplest to the most detailed. The results obtained from each modeling approach were then compared with each other. This enabled us to gain a deeper understanding of the distribution of groundwater travel times in a watershed, and examine the relative importance of the two control factors that determine its form – flow path lengths and flow velocities.

Thereafter, we analyzed the spatial distribution of the travel times obtained from the GIS-based and distributed hydrologic models (since the analytic model does not incorporate spatial information in it). This enabled us to compare and contrast the travel times at the spatial level. As proposed in previous literature, the spatial mapping of travel times is important to identify the variables influencing groundwater flow at the watershed scale. Local flow effects introduced by spatial variability in topography, drainage, and hydraulic properties are known to have a significant impact on the spatial distribution of groundwater travel times (Modica et al., 1997; Broers, 2004; Darracq et al., 2010). Thus, incorporating spatial variability in the simulation is important when the project goals require a local assessment of the travel times from specific sub-domains within the watershed. Such situations arise in the case of contaminant transport from landfills, livestock confinement units, etc; and in the case of conservation and remediation strategies that are localized to specific areas within the watershed.

The comparison of the three models also helped us to gain a deeper understanding of the role of model structure on the final result. Thus, the culmination of the research effort produced a set of selection criterion that might prove to be beneficial to catchment managers and policy makers alike, who are faced with the challenge of estimating watershed lag times to a proposed scheme of watershed management practices.

A brief introduction to the three models herein is followed by the details of their implementation in the next section that in turn is followed by a presentation of the results and discussion. The analytic method, proposed by Haitjema (1995), was derived for steady state, two dimensional groundwater flow, that neglected flow variation in the vertical direction by assuming the Dupuit-Forchheimer conditions to be valid. A simple water balance for an area enclosed by a representative isochrone (contours of equal travel time) was shown to only depend on the areal recharge rate and the saturated thickness, which was assumed constant. This led to an exponential travel time distribution that was solely dependent on the ratio of porosity (n) times saturated thickness (H) divided by the rate of recharge (here denoted as R). The form of the distribution included no reference to the watershed area or shape, aquifer parameters such as hydraulic conductivity, or the shape and density of the stream network. The only pre-condition was the constancy of the ratio nH/R (as reinforced by Luther and Haitjema, 1998). Futhermore, the distribution was found to be a good approximation to unconfined aquifers characterized by variable saturated thickness, as long as the variation in heads was not too large compared to the overall aquifer depth.

The GIS-based model, outlined by Schilling and Wolter (2007), was also derived for steady state, two dimensional groundwater flow. The most striking feature of this model is its use of the land surface to replicate the water table surface. The fact that the water table is a subtle reflection of the land surface has been verified by many authors (Hubbert, 1940; Freeze and Cherry, 1979; Williams and Williamson, 1989). In the GIS-based model, the approximation is applied in reverse. In other words, estimates of flow path lengths and groundwater flow velocities at the water table are derived from the land surface topography that is easily accessible in the form of a digital elevation model (DEM).

We also constructed a steady state, two dimensional, spatially distributed hydrologic model of the unconfined aquifer in the watershed using MODFLOW, the USGS modular finite-difference groundwater flow model (Harbaugh et al., 2000). Travel times in the watershed were subsequently computed using the particle tracking post-processing model, MODPATH (Pollock, 1994). The design and construction phases of the MODFLOW model required detailed information of physical boundaries of the aquifer (horizontal and vertical extents) and drainage network (extent and stage); stream channel dimensions and properties; spatial distributions of the areal recharge, hydraulic conductivity; porosity; and field measurements of hydraulic head for model calibration. Thus, the distributed hydrologic model was constructed from a first principles approach that required the least assumptions (relative to the other two models). Note that the simulated travel times took into account only advective transport, and neglected the specific effects introduced by contaminant dispersion, adsorption and mixing. This was necessary to perform a valid comparison of the model with the other two abovementioned models that do not account for similar mechanisms of contaminant transport.

3.2. Site description

The study was conducted at the 51.94 km^2 Walnut Creek watershed in Jasper county, Iowa (Fig. 11). The watershed is located in the Southern Iowa Drift Plain landscape region, an area characterized by steeply rolling hills and well-developed drainage (Prior, 1991). The shallow, unconfined aquifer is a combination of Wisconsinan-age Peoria loess mantles overlying pre-Illinoian oxidized till in the uplands, and Holocene-age alluvial deposits (composed of around 60-80% silt; Schilling et al., 2004) in the floodplain. Intermittent

outcrops of Pre-Illinoian oxidized till and Late Sangamon paleosols are found along the side slopes. The 10-11 m deep aquifer is confined by a 6-30 m thick Pre-Illinoian unoxidized till layer whose hydraulic conductivity is estimated to be two orders of magnitude lower than the alluvial-loess aquifer. The impervious unoxidized till layer overlies bedrock comprising Pennsylvanian Cherokee group shale, limestone, sandstone, and coal.

Hydraulic conductivities of the abovementioned stratigraphic units were estimated using multiple sources comprising slug test results (Schilling and Wolter, 2001; Schilling et al., 2004; Weisbrod, 2005) and saturated hydraulic conductivity values of the soils in the Soil Survey Geographic (SSURGO) database of the region. The hydraulic conductivities of loess and alluvium, that have been estimated to be similar (Weisbrod, 2005; Schilling et al., 2004), were assigned a value of 9×10^{-6} m/s based on the values in the SSURGO database. The till and paleosol outcrops also have similar hydraulic conductivities, estimated to range from 2.3×10^{-7} m/s based on slug tests to 1.2×10^{-6} m/s based on the SSURGO database. Due to lack of field evidence to the contrary, we assumed the vertical and horizontal hydraulic conductivities of all units to be equal.

The watershed's predominantly gaining stream is characterized by a deeply incised channel, with incision depths starting at around 1 m at the tributary headwaters, and steadily increasing in the downstream direction to a depth of around 3 m along the main channel. High channel incision has significantly impacted the watershed hydrology (Schilling and Jacobson, 2008) and is associated with the stream's flashy discharge in response to storm events. An artificial subsurface drainage network at the site is used to drain the water table up to depths of around 1.2 m below the land surface. The drains are primarily branched along the first order drainageways, and underlie the grassed waterways in the watershed. The

watershed lies in a humid, continental region with annual precipitation averaging around 850 mm of which a total of around 129 mm reaches the water table (Schilling et al., 2006). Schilling (2009) estimated the recharge reaching the water table to vary with landscape position, with the floodplain receiving maximum recharge, and side slopes receiving the minimum amount, and uplands an intermediate amount. The ratio of recharge reaching the floodplain, side slope, and upland, was estimated to be 44:14:24, respectively.

3.3. Methods

3.3.1. Analytic model

The analytic model presented in Haitjema (1995), being the simplest, predict an exponential distribution for the travel times. It requires an input of only 3 numbers – estimates of the watershed-wide averages of porosity, saturated thickness, and areal recharge rate due to precipitation. Aquifer porosity was assigned a constant value of 0.3, based on data reported for pre-Illinoian till in eastern Iowa (Helmke et al., 2005). The watershed-wide average saturated thickness was estimated to be 7 meters. Annual recharge to the aquifer was estimated to be 129.5 mm based on the long-term average baseflow reported for the Walnut Creek watershed (Schilling et al., 2006).

3.3.2. GIS-based model

The GIS-based model, of intermediate complexity, was proposed by Schilling and Wolter (2007). The method constructs the groundwater travel time distribution (TTD) for the watershed using the formula:

$$T_i = \frac{L_i}{< v_i >}$$

where T_i is the travel time from the i-th cell to the stream, L_i is the cumulative flowpath length from the i-th cell to the stream, and $< v_i >$ is the average groundwater flow velocity along the flowpath from the i-th cell. $< v_i >$ is obtained by averaging over all the individual cell velocities along the flowpath between the i-th cell and the stream. Individual cell velocities are computed using Darcy's law, and are given as:

$$v_j = \frac{K_j * S_j}{n}$$

where v_j is the groundwater flow velocity at the j-th cell, K_j is the hydraulic conductivity at the j-th cell, S_j is the hydraulic gradient at the water table in the j-th cell, and n is the aquifer porosity. In the implementation of this method we employed the land surface slope obtained from a 20-meter resolution DEM as a surrogate for the hydraulic gradient at the water table. Saturated hydraulic conductivity values were obtained from the Soil Survey Geographic (SSURGO) soil database for Jasper County. The stream was delineated using the tools in Hydrology toolset of Spatial Analyst, ArcMap 9.2. A 20 meter resolution depressionless DEM and a stream initiation area of 100 acres (40.47 ha) were used for this purpose. The DEM was obtained by aggregating a 1 meter resolution LIDAR DEM, and was the same as the one used in the MODFLOW model.

3.3.3. MODFLOW model

A two dimensional, steady state groundwater flow model was constructed using MODFLOW-2000 (Harbaugh et al., 2000) and MODPATH (Pollock, 1994). The model is briefly described below. A detailed model description is given in Jindal (2010). The model grid was designed with a horizontal spacing of 20 m, and comprised 628 rows and 300

columns. The top elevation of the single layer model followed the land surface, while its bottom elevation was set to a uniform depth of 11 m. The boundaries of the shallow aquifer were estimated to align with the watershed boundaries. The stream and tile drain boundaries were defined using the RIV and DRN packages, respectively. Streambed sediment hydraulic conductivity and thickness were estimated using data in Schilling and Wolter (2000) and Schilling et al. (2004), and were estimated to be around 5×10^{-5} m/s and lie in the range 0.1-0.4 m, respectively. Drain conductance was selected as 8.7×10^{-4} m^2/s, close to typical literature values (Goswami and Kalita, 2009). The physical and hydrologic boundaries of the model are shown in Fig. 12. Effective porosity used for particle tracking was estimated to be around 0.3 (Helmke, 2005).

Hydraulic conductivity zones were delineated using the parent material index in the SSURGO database (loess, alluvium, till, or paleosol) and assigned values based on multiple data sources comprising slug test results (Schilling and Wolter, 2001; Schilling et al., 2004; Weisbrod, 2005) and the saturated hydraulic conductivity value obtained from the SSURGO database. It was observed that the hydraulic conductivity estimates based on the results from the slug tests consistently produced unrealistically high water table levels that exceeded the land surface elevation. This has been anticipated by a number of authors (Schulze-Makuch and Cherkauer, 1998; Rovey II, 1998) as reflective of the fact that groundwater flow is impacted by high-conductivity aquifer heterogeneities present at larger flow scales than the scale of flow created by localized slug tests. Indeed, estimates of saturated hydraulic conductivity obtained from the SSURGO database, that were approximately one order of magnitude higher than the slug test values, led to a significant improvement in water table

levels across the watershed. Thus, we selected the SSURGO values as baseline estimates, which were then used as calibration parameters during the stage of model calibration.

Recharge zones were delineated using the slope classification for each soil mapping unit in the SSURGO database, and assigned values such that the ratio of the recharges in the uplands to side slopes to floodplain was 24:14:44 (Schilling, 2009). The recharge values were constrained by the condition that the total or equivalent annual recharge over the entire watershed, computed as the area-weighted average of the recharges at each landscape position, be equal to the estimated long-term average value of annual baseflow. The aquifer parameters of groundwater recharge and hydraulic conductivity of the oxidized till zone were then adjusted during the stage of model calibration.

Model calibration was achieved by manual trial and error that produced the best results in comparison to other automated calibration procedures that were tested. The model was calibrated for 84 head targets situated at various locations in the watershed. Amongst the various calibration parameters included, the model was observed to be most responsive to hydraulic conductivity (both, value and spatial distribution) and total recharge. Specifically, the location of the loess-till contact and the hydraulic conductivity value of oxidized till had a significant impact on simulated heads. This hinted towards the presence of a transition zone along the loess-till contact line, with a hydraulic conductivity value that is intermediate between the corresponding loess and till values. The detailed spatial distribution and value of hydraulic conductivity for each zone is listed in Jindal (2010). The calibrated total or equivalent annual recharge was estimated to be 120 mm, which is slightly lower than the initial estimate of 129 mm (Schilling et al., 2006).

The final calibrated model produced reasonable agreement between the simulated and observed hydraulic head values at the calibration targets (Fig. 12). The absolute residual mean (ARM, the average of the absolute values of the residuals, or the difference between the simulated and observed heads) was 2.55 m, while the residual standard deviation was 2.29 m. The resultant distribution of water table elevations across the watershed is also shown in Fig. 12. For a model of covering an entire watershed of this size (51.94 km^2), an ARM of 2.55 m was considered reasonable. Moreover, for our specific project goals of evaluating the distribution of groundwater travel times, an error in hydraulic head generated at the scale of cell resolution is likely to not impact results significantly. This is because the travel time along the length of a flow path from its origin to the sink, is a cumulative measure that is liable to integrate out possible deviations in hydraulic gradient along its entire length. Furthermore, the travel time distribution was generated by aggregating the travel times of more than 120,000 particles, and then studying the distribution as a whole. Thus, possible errors introduced by some particle traces are likely to have negligible impact on the overall travel time distribution that is generated from a large sample size. These two reasons indicate that the few stray spots of dry and flooded cells (Fig. 12) that remained are expected to have a negligible impact on the distribution of cumulative travel times obtained from a large sample of tracer particles. Hints of the insensitivity of the distribution of cumulative travel times to localized model errors were evident in the earlier stages of model calibration when the distributions obtained for earlier model runs that had a higher number of dry and flooded cells (with the number of dry cells more than 100% of the number in the final model, and the number of flooded cells being similar) produced nearly the same results as the final calibrated model (with the mean travel time differing by 0.68% only).

Particle tracking in MODPATH was performed by releasing particles at the water table in every cell center of the active model domain and forward tracking them from source to sink. In particle tracking codes like MODPATH, the trace of a particle that enters a cell where the sink captures only a partial amount of the inflow relation cannot be resolved analytically. To overcome this problem, MODPATH defines the strength of a sink as the fraction of cell inflow that is captured by the sink, and uses the value of that parameter to determine whether the particle will stop or bypass a particular sink. This is accomplished by comparing the strength of the sink against a user-defined threshold (S*). All sinks with strength greater than S* are treated as active; the particles stop at such sinks. The remaining sinks are treated as inactive, and particles entering cells containing such sinks simply bypass them. “Strong sinks” are defined as those that capture 100% of the cell inflow. Sinks with strength less than 100% are termed “weak sinks”. Thus, setting S* to 0 simulates the scenario of no bypass flow (both, weak and strong sinks are active), and setting S* to 1 simulates the scenario of maximum bypass flow (by activating only the strong sinks).

Given the inability of the analytic and GIS models to simulate bypass flow, we chose S* to be 0. Thus, all sinks were treated as active, and there was no bypass flow. This enabled us to compare the travel times obtained using MODFLOW with those obtained from the other two models.

3.3.4. Kolmogorov-Smirnov statistical test for comparison of probability distributions

As part of the comparison between two distributions, we sought to quantify the degree of closeness in the shapes of both. We selected the Kolmogorov-Smirnov (KS) statistical test for this purpose (Daniel, 1978; Hollander and Wolfe, 1999). The comparison between the analytic distribution to an empirical distribution (derived from GIS or MODFLOW)

employed the KS one-sample test, while the comparison between the two empirical distributions (derived from GIS and MODFLOW) employed the KS two-sample test. Both tests utilize cumulative distributions. The cumulative distribution function of a random variable X, is denoted as F(x), and defines the probability that the value of the random variable X is less than or equal to x.

For the KS one-sample test, we compare two cumulative distributions of a random variable X, of which one is defined by a theoretical, continuous form, $F_0(x)$, while the other, S(x), is empirically derived based on a sample consisting of n observations of the variable and is given as,

$$S(x) = \frac{(\text{number of observations } \leq x)}{n}$$

Assuming that S(x) is based on a random sample from a system that is represented by some unknown distribution function F(x), the KS one-sample test evaluates whether F(x) = $F_0(x)$, for all values of x. If the two distributions are equal, then the sample distribution S(x) and $F_0(x)$ are likely to closely agree with each other, especially for large sample sizes. To quantify this degree of closeness, the KS one-sample test statistic D is computed as,

$$D = \max |S(x) - F_0(x)|$$

Similarly, the KS two-sample test compares two empirical distributions $S_1(x)$ and $S_2(x)$, using the test statistic,

$$D = \max |S_1(x) - S_2(x)|$$

Therefore, if both samples are representing the same system or population, then $S_1(x)$ and $S_2(x)$ should be close to each other for all values of x, and D should be close to 0. The maximum value D can take is 1.

3.3.5. Evaluation methods used for MODFLOW and GIS TTDs

Travel time distributions obtained from the three models were analyzed in greater detail. Travel time distributions are derived from two variables – flow path length, and groundwater flow velocity. Thus, to understand the parameters controlling the MODFLOW and GIS TTDs we examined the distribution of flow path lengths and groundwater flow velocities obtained from each model. The distributions of flow path length and groundwater flow velocity used in the GIS model were obtained using methods described in section 3.3.2. The values of groundwater flow velocity employed by the MODFLOW model were directly imported using the Groundwater Vistas graphical user interface. Values of flow path lengths used by the MODFLOW model were determined using the surface of water table elevations. The water table grid was treated similar to a DEM, and processed using the Hydrology toolset in Spatial Analyst toolbox of ArcMap (9.3) to obtain flow path lengths along the water table.

Analyzing the distributions of flow path lengths and groundwater flow velocities used by both models enabled us to understand the factors influencing the comparison of the derivative travel time distributions obtained from both the MODFLOW and GIS models.

3.3.6. Methods for spatial comparison of MODFLOW and GIS TTDs

The match between the MODFLOW and GIS TTDs was tested at the spatial level by comparing the spatial maps derived from both distributions. The spatial maps were generated by assigning the source cell of each particle a time stamp based on the amount of time it took for the particle from that cell to reach a sink. At each cell location, the travel time obtained by the GIS and MODFLOW models, were compared and plotted against each other. The degree of overlap between the scatter and the 45 degree line was used to demonstrate the extent of correlation between the two spatial distributions.

To gain further insight into the influence that physical location exercises on the travel times obtained from the MODFLOW and GIS models, we examined the impact that landscape position has on the watershed TTD obtained from both models. This was achieved by performing a TTD separation, akin to the separation that is performed on its transient, surface-water counterpart – the stream hydrograph. The separation was based on the landscape position where the particle was released – upland, side slope, or floodplain.

Delineation of each zone was performed using the Iowa Cooperative Soil Survey (ICSS) soil series database of Jasper County, IA. The soil mapping units located inside the Walnut Creek watershed were classified based on their slope class and type of parent material. Side slopes, comprising slopes belonging to the classes C (5-9%), D (9-14%) and E (14-18%), covered approximately 54% of the total watershed area. The remaining slope classes A (0-2%) and B (2-5%) were separated based on the parent material category in the soils database. Alluvium units fell in the floodplain region and covered around 19% of the watershed area, while loess units comprised the uplands and covered the remaining 27% of the watershed area.

MODFLOW and GIS travel times obtained at each landscape position were aggregated separately into component TTDs. The MODFLOW and GIS component TTD representing each region were then compared to each other, to demonstrate the level of agreement, and assess the relative strengths and weaknesses of both models in predicting travel time distributions for each individual landscape region.

3.4. Results and Discussion

3.4.1. Comparison of distribution shape and statistics

A comparison of the TTDs obtained by the 3 methods (analytic, GIS, and MODFLOW) and their corresponding statistics are shown in Fig. 13 and Table 1 respectively. Overall, there is very good visual agreement between the TTDs. The MODFLOW and GIS TTDs were found to be especially close to each other. The trend in all three distributions was observed to follow the form of a decaying exponential. For the analytic distribution this is true by definition. However, we also found the approximation to a decaying exponential to be valid even for the MODFLOW and GIS distributions. The resulting exponential best-fit scale parameters and corresponding standard errors are shown in Table 1. The values of the scale parameter were found to be nearly identical to the means of all three distributions.

Furthermore, a comparison of the distribution statistics (Table 1) showed that both the mean and median travel times representing all three distributions matched each other fairly well. The values of both parameters were the least for the analytic model, and maximum for the MODFLOW model. The mean and medians of the GIS and MODFLOW distributions were observed to be especially similar. Examining the mean first, we found the means of the MODFLOW and GIS distributions to differ by 4% only. The mean of the analytic distribution, that was the least of the three means, differed from the MODFLOW and GIS means to a greater extent, by around 21% and 17%, respectively.

To remove the influence of the distortion introduced by the positive skew of travel times in the analysis, an evaluation of the medians of the three distributions was considered essential. The medians of all the distributions were fairly close to each other. The MODFLOW and GIS medians agreed the best, and differed by 5% only. The differences between the median of the analytic distribution and those of the MODFLOW and GIS distributions were higher, varying by 28% and 24%, respectively.

The best-fit to an exponential form was further evident by examining the coefficient of variation for all three distributions. As discussed above, the mean of the MODFLOW and GIS distributions was higher than that of the analytic distribution. This trend was accompanied by a corresponding higher standard deviation for both distributions in comparison to the analytic distribution. Thus, the ratio of the standard deviation to the mean (namely, the coefficient of variation) was found to be more stable. The coefficients of variations of both the MODFLOW and GIS distribution stayed fairly steady (with values of 0.91 and 0.96, respectively) and close to the value of 1 for an ideal exponential distribution. The analytic distribution, by definition, had a coefficient of variation exactly equal to unity. Thus, the shape of the three distributions could be approximated fairly closely to that of a pure exponential distribution, notwithstanding the slight differences in the decay constants of the representative exponential distributions.

The level of agreement between each pair of distributions was quantified in terms of the Kolmogorov-Smirnov distance parameter, denoted by D (Table 2). As detailed in the methodology section, the measure D lies in the range of 0 to 1. The closer D is to 0, the higher is the degree of match between the two distributions. We observed the overlap to be maximum overlap between the MODFLOW and GIS distributions, with D (equal to 0.0268) being very close to 0. The maximum value of D (at 0.1175) was obtained for the comparison of the analytic and MODFLOW distributions, was still fairly close to 0. Overall, the values of D for all 3 pairs of distributions were close to 0, and underscored the close match between the three distributions.

This is especially surprising given the fact that the three distributions were derived from methods that (1) are based on radically different conceptual models, (2) vary widely in their

level of sophistication, and (3) utilize very different sets of input data. As detailed in the methodology section, the analytic distribution only required estimates of watershed wide averages of porosity, saturated thickness, and recharge rate. The GIS model utilized the value of aquifer porosity, watershed and stream network extent, and the spatial distributions of elevations and hydraulic conductivity. On the other hand, the MODFLOW model required spatially-detailed data inputs of watershed and aquifer extent, hydraulic conductivity, porosity, recharge, and specification of all boundary conditions including the stream and tile drainage network extents.

A closer inspection revealed some differences between the three distributions. The proportion of shorter transit times in the analytic model was higher than those observed in the GIS and MODFLOW models. Thus the MODFLOW and GIS models provide a larger estimate of the travel times that, in many cases of contaminant transport, is preferred. A comparison of the MODFLOW and GIS distributions reveals that though the overlap between the distributions is very strong, there was a small, but striking, difference in the shape of the two curves. The MODFLOW distribution displayed a smooth trend, versus the slightly jagged, meandering trend observed in the GIS distribution. This may be ascribed to the fact that computation of the travel times in the methods employed hydraulic head gradients from two different sources. It is a well known fact that the slope of the water table is a gentler reflection of the land surface that smoothens out abrupt changes in elevation. Thus, we may expect the gradients computed using water table elevations to vary more smoothly than those computed using land surface elevations. However, the extremely close match between the two distributions indicates that this difference might not pose a hurdle.

3.4.2. Evaluation of MODFLOW and GIS TTD overlap

At a fundamental level, length divided by velocity equals travel time. The cumulative travel time along a flow line is determined by dividing the total flow path length by the average velocity along its entire length. Therefore, a deeper analysis of the distribution of travel times necessitated an examination of the distributions of flow path lengths and velocities derived from both, the GIS and MODFLOW models.

The distribution of flow path lengths obtained from both models in shown in Fig. 14. Both distributions exhibit an initial stage of increase (over a very short range for the GIS model). As flow lengths continued to increase, the initial rise was followed by an overall declining trend. MODFLOW flow lengths were clustered around a peak near 225 m. Indeed, the mean of the flow length distribution was found to be 278.24 m. Flow lengths showed a steep decline beyond the 400-425 m range, with the distribution approaching zero rapidly beyond lengths of the order 725 m. Thus, the standard deviation of the MODFLOW distribution was relatively small with a value of 175.10 m. On the other hand, the GIS distribution of flow path lengths had a smoother, more gradual decline that was approximately monotonic. This trend led to the distribution being characterized by a larger mean and standard deviation of 382.47 and 252.77 meters, respectively.

Thus, the proportion of smaller flow lengths was significantly greater in the MODFLOW distribution. The appreciable difference between the two distributions can be understood in terms of the structure of the sink network used by both models, and the shape of the surface from which the flow path lengths were derived in each. In the MODFLOW model, the structure of the sink network was more detailed, and incorporated a large number of finer branches of shallow (tile) sinks. On the other hand, the GIS model employed a simpler sink network with coarser resolution, containing only the deeper (stream) sinks that are more

widely-spaced and distinct. Consequently, particle traces in the MODFLOW model were intersected by a sink more quickly than those evaluated by the GIS model. This resulted in shorter flow path lengths in the MODFLOW model. Moreover, the GIS model utilized the land surface as a surrogate for the water table surface to compute flow lengths. In general, land surface topography is a more dramatic reflection of the water table. The higher degree of curvature, and additional undulations distinguishing the land surface from the water table surface would lead to an increase the proportion of longer flow path lengths in the GIS model.

A comparison of the distribution of flow velocities is shown in Fig. 15. As flow velocity spanned the range from low to high, both distributions displayed an initial rise, followed by a continuous decrease. The period of initial rise was significantly shorter for the MODFLOW model. In fact, similar to the flow length distribution derived from the MODFLOW model, the velocity distribution displayed a sharp peak at a low flow velocity value of 0.03 m/day, and declined rapidly after that. The clustering of velocity values around 0.03 m/day was also obvious in the mean value of the entire distribution that was equal to 0.029 m/day. The velocity profile fell to near zero beyond 0.05 m/day. This was demonstrated by the relatively small standard deviation of 0.019 m/day. The trend in the GIS velocity distribution on the other hand was much more gradual, with a small peak observed at 0.08 m/s. The distribution of the velocities around the peak at 0.08 m/day was very diffuse, leading to larger values of the mean and standard deviation of 0.081 and 0.046 m/day, respectively.

To gain a deeper understanding of the physical reasons determining the distribution of flow velocities, we considered the variables that are used to determine flow velocity. Flow velocities in both models are determined using Darcy's law, and are given by the formula,

$$v = \frac{Ki}{n}$$

where v is the flow velocity, K is the hydraulic conductivity, i is the hydraulic gradient, and n is the porosity. The values of hydraulic conductivity in both models were primarily derived from the same source. Both models used saturated hydraulic conductivity values obtained from the SSURGO database. The calibration stage introduced some changes in the hydraulic conductivities of the MODFLOW model, though these changes were fairly localized and restricted to specific zones. The similarity in the GIS and MODFLOW values of hydraulic conductivity is reflected in their watershed-wide averages that were very close to each other (at 0.526 and 0.479 m/day, respectively). Both models used a porosity of 0.3. Thus, the differences in the distribution of velocities are primarily a reflection of differences in the hydraulic head gradients.

In the MODFLOW model, hydraulic head gradients were explicitly determined using the water table elevations. In contrast, the GIS model utilized land surface gradients as a surrogate for water table gradients. In general, the land surface slopes are steeper than slopes at the water table. Thus, hydraulic head gradients, and therefore flow velocities, were characterized by larger values for the GIS model.

The strong overlap between the GIS and MODFLOW TTDs can now be understood in terms of the specific structure of the flow path length and velocity distributions described above. The GIS model uses the land surface topography to derive flow path lengths and velocities. In comparison to the water table used in MODFLOW, this creates longer flow lengths for reasons discussed earlier. But the higher values of flow lengths do not translate to higher values of travel times, due to the fact that the same reasons also increase the values of

gradients (and therefore flow velocities). This “compensating effect” is the key factor that enabled travel times obtained using both models to transcend apparent differences and reach a good level of agreement.

3.4.3. Evaluation of overlap with analytic TTD

Haitjema (1995) and Luther and Haitjema (1998) predicted an exponential TTD for idealized groundwatersheds where the ratio of porosity (n) times saturated thickness (H) divided by recharge (here denoted as R) stays constant. They proposed this distribution regardless of the groundwatershed size, shape, and properties of the stream network. They also found this distribution to be a good approximation to the TTD of many types of aquifers, including unconfined aquifers, provided aquifer heterogeneities were not significant and distinct.

The agreeable match of the analytic TTD to those obtained from MODFLOW and GIS models suggests that these assumptions are indeed valid, and that for the purpose of estimating travel times, the essence of the entire dynamics of groundwater flow in a watershed can indeed be captured in the specifications of the watershed wide averages of porosity, saturated thickness, and rate of recharge. Other aquifer variables may indirectly influence travel times via these three factors. For example, the extent of the stream network and the distribution of hydraulic conductivities will influence the average saturated thickness. Hence, the dependence of travel time on the former two variables is likely to be expressed primarily through its dependence on average saturated thickness.

Moreover, the close agreement of the analytic TTD, that did not employ the watershed size, with the other two TTDs, that did employ the watershed size, suggests that watershed

travel times are scale invariant. In other words, as long as the ratio nH/R stays constant, the same travel time distribution may be applicable to watersheds of different orders.

The small degree of deviation observed between the analytic TTD and the other two distributions can be ascribed to the fact that the analytic formula is valid specifically for aquifers for the ratio nH/R is constant throughout. Thus, the formula is to be taken as an approximation for travel times in unconfined aquifers where the saturated thickness is variable. Also, the small degree of deviation is suggestive of the presence of small higher order corrections that might be used to refine the analytic formula. The correction terms might possibly depend more explicitly on other variables such as hydraulic conductivity, watershed size and shape, stream network details, etc.

3.4.4. Spatial comparison of MODFLOW and GIS TTDs

The agreement between the GIS and MODFLOW methods was tested at a greater level of detail by comparing their spatial maps (Fig. 16). We found the spatial maps to be similar to a certain extent. Both maps were consistent with the idea that particles released at the watershed boundaries and in the uplands exhibited longer travel times. Transit times shortened as the distance between the point of release and the sink network decreased. Therefore, heading in the downgradient direction, transit times were observed to decrease from the uplands to the side slopes to the floodplain. The one exception to this trend was observed in the GIS travel times computed for certain floodplain regions. A close inspection of the GIS spatial map revealed the presence of zones where long travel times extended from the upland divides all the way into the floodplain. This was due to the fact that as we approach the stream network, the flow lines at the water table converge to intersect the stream stage that is deeply incised into the watershed landscape. This local convergence is

not reflected at the land surface that stays relatively flat. Thus, the land surface gradients become incapable of capturing the rapid change in the water table. The flat gradients used by the GIS model are therefore reflected in an overestimation of travel times. The GIS model therefore breaks down in specific regions of the floodplain that are exceedingly flat.

Moreover, we found the maps to be very dissimilar in certain key aspects. Though there was an overall conceptual agreement in the spatial distribution of the travel times, we found the nature of the spread of travel times to be very different. There was a sharp contrast between the diffusive spread of travel times obtained from the GIS model, versus the fine scale structure apparent in the travel times derived from the MODFLOW model that showed areas of high and low travel times in close proximity. Indeed, regions with long transit times in the GIS map were primarily restricted to the bulk boundaries of the overall watershed, but were simulated by MODFLOW to penetrate deeper into the watershed following the subwatershed divides.

This lack of correlation at the fine spatial scale (i.e. at the level of cell resolution) was most obvious in the cell-by-cell correlation plot, as shown in Fig. 17. The GIS and MODFLOW travel times corresponding to each cell location were plotted against each other. The deviation from the 45 degree line demonstrated the lack of correlation between the two spatial distributions. The scatter of points was observed to be distributed on both sides of the 45% line in a dispersive manner. However, this disagreement at the level of cell resolution did not manifest in the TTD, due to overestimates of travel time in one area compensating for underestimates of travel time in another area (over/underestimates being defined relative to the MODFLOW model). In other words, we found the proportions of cells where MODFLOW travel time estimates were larger than GIS estimates to be similar to those

where the GIS estimates were larger than estimates based on MODFLOW. The summation over the entire watershed therefore led to a GIS probability distribution with very similar density profile as that obtained from the MODFLOW model.

3.4.5. Evaluation of landscape component TTDs

The hint of bias based on landscape position that was observed in the lack of correlation between the two spatial distributions, with floodplain travel times being a greater source of error, motivated us to decouple each TTD into individual component TTDs representing travel times for the upland, side slope and floodplain zones separately. The decoupling of the TTDs is shown in Fig. 18. In doing so, we sought to discover the degree to which the lack of spatial correlation was manifest in the TTDs representing each landscape position.

The landscape component TTDs obtained from both models were plotted separately and compared against each other (Fig. 19). We observed deviations in the component TTDs at each of the landscape position, but the deviation maximized at the floodplain, where the GIS travel times were much greater than those obtained from MODFLOW. In comparison, the deviation between the side slope and upland pairs of component TTDs were much smaller. For the latter regions, the GIS model was generally observed to moderately underestimate travel times relative to the MODFLOW model. This is because hydraulic head gradients based on the land surface will generally lead to higher estimates of flow velocities than those obtained from water table gradients. The deviations between the corresponding component TTDs were quantified using the Kolmogorov-Smirnov distance parameter, D, between each pair of distributions (Table 3). We found the distance measure, D, to be significantly higher at the floodplain (0.244), in comparison to the distance measures obtained for the upland and side slope regions (0.0805 and 0.1056, respectively).

Furthermore, a comparison of the distribution statistics for each pair of component TTDs was used to quantify the degree of agreement between travel times in each zone (Table 3). We found the mean travel times obtained from the MODFLOW and GIS models to overlap the most in the upland region, the two values being 31.61 and 33.42 years respectively. This amounts to a difference of only 6%. The variances in the distributions were also found to be nearly equal. The next best match was observed for the side slope region, with MODFLOW and GIS models predicting mean travel times of 19.82 and 15.28 years respectively (a difference of around 23%). On the other hand, the mean travel times representing the floodplain varied significantly, with MODFLOW predicting 3.64 years, and GIS predicting 9.68 years. Indeed, the standard deviation in the GIS model (at 18.46 years) was nearly double the value of its mean.

To gain further insight into the comparison between the component TTDs corresponding to each landscape position, we analyzed the box plots of all three sets of distributions (Fig. 20). Overall, the representative travel times were seen to decrease from the upland to the side slopes to the floodplain (left to right) in accordance with the decrease in flow path lengths from the uplands to the floodplain. All distributions had a strong positive skew, as visible in the long tail of outliers. The MODFLOW and GIS box plots characterizing the uplands and side slopes were very close to each other. Thus there is a good agreement in the statistical parameters (median, 25^{th} and 75^{th} percentiles) of both distributions in these two landscape regions. In fact, we observed the range of travel times in the uplands (including data outliers) that were simulated by the MODFLOW and GIS models to agree with each other.

On the other hand, there is a sharp contrast between the MODFLOW and GIS component TTDs at the floodplain. The box representing the GIS distribution is significantly wider than

the box representing the MODFLOW distribution. Also, the GIS distribution displays an extraordinarily high positive skew, with the long trail of data outliers extending up to 300 years. This is very different from the short tail of data outliers extending only up to 50 years in the MODFLOW distribution. Indeed, comparing the upland, side slope, and floodplain components of the GIS TTD with each other, we find that the floodplain component TTD possesses the largest skew of all the three distributions. Therefore, within the GIS model, the maximum value of travel time lies in the floodplain, which is physically unrealistic.

All these observations reinforce the idea that the GIS model fails in the presence of flat floodplain topography, where the water table ceases to imitate the land surface.

3.4.6. Comparison of the three models

Based on these results we derived several insights that address the problem of model selection that managers with limited data and computational resources often face. These are discussed below as follows:

The travel time distributions derived from the analytic, GIS, and MODFLOW were all found to agree well with each other, which was considered to be of great significance given the striking differences in their level of sophistication, model assumptions and setup, and input data requirements.

The close match between the analytic TTD with the other two distributions showed that for two dimensional, shallow, unconfined groundwater flow, a careful selection of the porosity, average saturated thickness, and recharge, can indeed produce an analytic TTD that is agrees reasonably well (in terms of the characteristic shape and statistics) with TTDs obtained using more detailed modeling approaches. Therefore, the analytic model presents an attractive alternative to more advanced models that typically require an intensive field data

collection, and investment of time and computational resources to construct the TTD at the watershed wide scale. The scale invariance of the analytic TTD is another unique feature of this approach. Indeed, if the project goals require a quick estimation of one single number that can be deemed a suitable measure of the travel times across a watershed, at any spatial scale, then the analytic model may be extremely beneficial.

However, if one seeks to incorporate more watershed-specific data, that embodies the variability of aquifer parameters and boundary conditions that are unique to the system into the prediction of the distribution of travel times, then more advanced models are necessary. Indeed, the inclusion of watershed-specific data that was unique to the study area in the GIS and MODFLOW models, such as data containing land surface elevations, stream network structure, and distribution of hydraulic conductivity, seemed to produce a stronger overlap between the simulated travel time distributions. This suggests that the travel times derived from these two models may be more accurate, and a closer representation of the real travel time distribution than the analytic distribution.

Out of the two spatially explicit models examined, the GIS model requires significantly less investment than the MODFLOW model, and still generates a TTD that matches the MODFLOW TTD surprisingly well. Indeed, the data required for the GIS model (topographic and digital soil data) is easily accessible via the numerous GIS servers maintained by most counties in the US. In contrast, the MODFLOW model demands extensive data inputs and more computational resources than the other two models. An evaluation of the reasons behind the close match between the GIS and MODFLOW distributions demonstrated that errors in both the flow path lengths and velocities profiles, introduced by the use of the land surface as a surrogate for the water table, did not transfer to

the profile of travel times. This was likely because, relative to the MODFLOW estimates, the higher estimates of flow lengths by the GIS model were compensated by higher estimates of flow velocities. This led to a good agreement between the travel times obtained from the GIS and MODFLOW models. Considering the relatively small cost incurred in its construction, the GIS model appears to be a valuable alternative to a MODFLOW model for predicting travel times that incorporate the specific parameters of a watershed to a greater detail than the analytic model. The transferability of this result needs to be further tested in the context of a wider variety of hydrologic landscapes.

Furthermore, if one seeks more spatially explicit information of travel times then the analytic model cannot be used, since it is not equipped to estimate spatial distributions of travel time. Spatial distributions of travel times are critical in a variety of scenarios, such as analysis of pesticide and nutrient transport from specific sub-regions within the watershed, and also to evaluate the performance of spatially focused restoration and conservation practices implemented within specific areas of a watershed. In such cases, it becomes necessary to select a more sophisticated technique, such as MODFLOW or GIS. We observed that in the case of spatial estimates of travel time, the choice between the MODFLOW and GIS models becomes more critical and is most likely to have a significant impact on the results. This was demonstrated by the great disparity in the spatial maps generated by the two models.

However, if high precision estimates (at the resolution of 10-20 meters) are not required, then the aggregation of travel times based on characteristic spatial scales (of the order of 100 meters), such as those based landscape position, was found to smoothen out these discrepancies. Moreover, the spatial bias in the cell-by-cell disparity suggested that the

magnitude of difference might be dependent on the specific landscape position of the area of interest for which the travel times are to be estimated. If the area of interest lies in the upland or side slope, then the GIS and MODFOW distributions of travel times may match reasonably well, particularly in the estimates of the representative statistics, such as the mean travel times. Thus, for such areas, the GIS model might suffice.

But in the floodplain region one must exercise greater caution in model selection. We found the GIS model to breakdown specifically in the flat regions of the floodplain, due to the inability of the land surface slope to simulate rapid variations in the water table gradients as the groundwater flow lines converged to the deeply incised stream channel. This indicates that the GIS and MODFLOW models are likely to disagree in areas where the land surface and the water table are observed to diverge from each other. This would occur either when the land surface fails to capture variability in the water table (when, for example, the water table approaches a stream boundary), or when the spatial variability in the land surface fails to capture a smoother water table (as might occur in the case of deeper water tables). We conclude that for estimating the lag times within such regions of the watershed, the travel times derived from methods utilizing the water table directly, such as a MODFLOW model are liable to be more accurate than those derived from the GIS model, or other similar models that employ the topography of the land surface as a surrogate for the water table surface.

3.5. Conclusions

In this study, we constructed the distribution of groundwater travel times for a representative agricultural watershed using three different modeling schemes (analytic, GIS-based, and MODFLOW) that were based on entirely different conceptual frameworks. A

favorable match was obtained between all three TTDs, in terms of its overall shape and representative statistics, with estimates of mean travel time representing groundwater flow in the watershed ranging from 16.22 years to 20.51 years (differing by 21% only). Thus, all three distributions might be useful to estimate the magnitude of lag times characterizing groundwater flow in the watershed. This showed that a careful selection of parameters for the analytic model produces travel time estimates that compare well with estimates generated by more complicated models. An examination of the contrast between the three distributions revealed the analytic travel times to be systematically lower than those obtained through the MODFLOW and GIS models. Therefore, for watershed conservation and restoration projects that require a conservative estimate of watershed lag times, the latter two models might be a better choice. The high degree of overlap between the TTDs obtained from the GIS and MODFLOW models was found to be sourced by a cancellation of differences introduced in the distribution of flow path lengths and velocities of both models. The GIS model, that employs land surface elevations as a surrogate for water table elevations, was found to generate longer flow path lengths and higher flow velocities due to the presence of greater spatial variability in the surface topography. Dividing the flow path lengths by the velocities mitigated the differences in the respective travel time distributions. Thus, both the variables – flow path lengths and velocities exercised significant influence in determining the final distribution of travel times in both models.

However, the differences between the GIS and MODFLOW models were most visible in an individual cell-by-cell comparison of the travel times. Differences in the flow path lengths and velocities at each spatial location caused a lack of correlation in the spatial distributions of the travel times obtained through both models. The differences were observed to grow at

certain landscape positions, where a divergence in the boundary conditions created a sharp inequality between the GIS and MODFLOW travel times. Specifically, the convergence of groundwater flowlines to the boundary of the deeply incised stream network in the floodplain indicated that the flat land surface topography no longer reflected the variability of the water table. This difference caused the GIS travel times to magnify in comparison to those obtained from the MODFLOW model. On the other hand, the GIS and MODFLOW distributions of travel times representing the upland and side slope regions were found to be reasonably agreeable. Thus, a GIS model may serve as a suitable substitute for a MODFLOW model only in regions where the land surface reflects the water table reasonably well.

The GIS and MODFLOW models fail to overlap in regions where the curvature of the water table is not reflected on the land surface, or vice versa, in regions when the land surface displays sharp undulations that are not visible at the water table (as might be the case for deeper water tables). We believe that to estimate travel times in such regions the construction of a full-fledged MODFLOW model might be a worthwhile exercise.

References

Anderson, T.H., Taylor, G.T., 2001. Nutrient pulses, plankton blooms, and seasonal hypoxia in western Long Island Sound. Estuaries, 24(2): 228-243.

Bratton, J.F., Bohlke, J.K., Manheim, F.T., Krantz, D.E., 2004. Ground water beneath coastal bays of the Delmarva Peninsula: Ages and nutrients. Ground Water, 42(7): 1021-1034.

Broers, H.P., 2004. The spatial distribution of groundwater age for different geohydrological situations in the Netherlands: implications for groundwater quality monitoring at the regional scale. Journal of Hydrology, 299(1-2): 84-106.

Brush, G.S., 2009. Historical land use, nitrogen, and coastal eutrophication: A paleoecological perspective. Estuaries and Coasts, 32(1): 18-28.

Burkart, M.R., James, D.E., 1999. Agricultural-nitrogen contributions to hypoxia in the Gulf of Mexico. Journal of Environmental Quality, 28(3): 850-859.

Carpenter, S.R. et al., 1998. Nonpoint pollution of surface waters with phosphorus and nitrogen. Ecological Applications, 8(3): 559-568.

Daniel, W.W., 1978. Applied nonparametric statistics. Houghton Mifflin Company, Boston, MA.

Darracq, A., Destouni, G., Persson, K., Prieto, C., Jarsjo, J., 2010. Quantification of advective solute travel times and mass transport through hydrological catchments. Environmental Fluid Mechanics, 10(1-2): 103-120.

Diaz, R.J., Rosenberg, R., 2008. Spreading dead zones and consequences for marine ecosystems. Science, 321(5891): 926-929.

Freeze, A.R., Cherry, J.A., 1979. Groundwater. Prentice Hall Inc., New Jersey, 604 pp.

Gentry, L.E., David, M.B., Royer, T.V., Mitchell, C.A., Starks, K.M., 2007. Phosphorus transport pathways to streams in tile-drained agricultural watersheds. Journal of Environmental Quality, 36(2): 408-415.

Goolsby, D.A., Battaglin, W.A., 2000. Nitrogen in the Mississippi basin-Estimating sources and predicting flux to the Gulf of Mexico: U.S. Geological Survey Fact Sheet 135-00, Reston, VA, pp. 6.

Goswami, D., Kalita, P.K., 2009. Simulation of base-flow and tile-flow for storm events in a subsurface drained watershed. Biosystems Engineering, 102(2): 227-235.

Haitjema, H.M., 1995. On the residence time distribution in idealized groundwatersheds. Journal of Hydrology, 172(1-4): 127-146.

Hallberg, G.R., 1987. Nitrates in ground water in Iowa. In: D'Itri, F.M., Wolfson, L.G. (Eds.), Rural ground water contamination. Lewis, Chelsea, MI, pp. 23-68.

Harbaugh, A.W., Banta, E.R., Hill, M.C., McDonald, M.G., 2000. MODFLOW-2000, the U.S. Geological Survey modular ground-water model -- User guide to modularization concepts and the Ground-water flow process: U.S. Geological Survey Open-File Report 00-92. Reston, VA, pp. 121.

Hardy, S.D., Koontz, T.M., 2008. Reducing nonpoint source pollution through collaboration: Policies and programs across the US States. Environmental Management, 41(3): 301-310.

Helmke, M.F., Simpkins, W.W., Horton, R., 2005. Fracture-controlled nitrate and atrazine transport in four Iowa till units. Journal of Environmental Quality, 34(1): 227-236.

Hollander, M., Wolfe, D.A., 1999. Nonparametric statistical methods. Wiley-Interscience.

Hubbert, M.K., 1940. The theory of ground-water motion. Journal of Geology, 48(8): 785-944.

Jindal, P., 2010. A study of the groundwater travel time distribution at a rural watershed in Iowa: A systems theory approach to groundwater flow analysis, Ph.D. thesis, Iowa State University, Ames, IA, 202 pp.

Lehman, P.W., Sevier, J., Giulianotti, J., Johnson, M., 2004. Sources of oxygen demand in the lower San Joaquin River, California. Estuaries, 27(3): 405-418.

Luther, K.H., Haitjema, H.M., 1998. Numerical experiments on the residence time distributions of heterogeneous groundwatersheds. Journal of Hydrology, 207(1-2): 1-17.

McGuire, K.J., McDonnell, J.J., 2006. A review and evaluation of catchment transit time modeling. Journal of Hydrology, 330(3-4): 543-563.

Meals, D.W., Dressing, S.A., Davenport, T.E., 2010. Lag time in water quality response to best management practices: A review. Journal of Environmental Quality, 39(1): 85-96.

Modica, E., Reilly, T.E., Pollock, D.W., 1997. Patterns and age distribution of ground-water flow to streams. Ground Water, 35(3): 523-537.

Owens, L.B., Shipitalo, M.J., Bonta, J.V., 2008. Water quality response times to pasture management changes in small and large watersheds. Journal of Soil and Water Conservation, 63(5): 292-299.

Pollock, D.W., 1994. User's guide for MODPATH/MODPATH-PLOT, version 3: A particle tracking post-processing package for MODFLOW, the U.S. Geological Survey finite-difference ground-water flow model: U.S. Geological Survey Open-File Report 94-464, Reston, VA, pp. 237.

Prior, J.C., 1991. Landforms of Iowa. University of Iowa Press, Iowa City, IA.

Rabalais, N.N., Turner, R.E., Scavia, D., 2002. Beyond science into policy: Gulf of Mexico hypoxia and the Mississippi river. Bioscience, 52(2): 129-142.

Rovey II, C.W., 1998. Digital simulation of the scale effect in hydraulic conductivity. Hydrogeology Journal, 6(2): 216-225.

Schilling, K., Zhang, Y.K., 2004. Baseflow contribution to nitrate-nitrogen export from a large, agricultural watershed, USA. Journal of Hydrology, 295(1-4): 305-316.

Schilling, K.E., 2002. Chemical transport from paired agricultural and restored prairie watersheds. Journal of Environmental Quality, 31(4): 1184-1193.

Schilling, K.E., 2009. Investigating local variation in groundwater recharge along a topographic gradient, Walnut Creek, Iowa, USA. Hydrogeology Journal, 17(2): 397-407.

Schilling, K.E., Hubbard, T., Luzier, J., Spooner, J., 2006. Walnut Creek watershed restoration and water quality monitoring project: final report. Iowa Department of Natural Resources, Geological Survey Bureau Technical Information Series 49, Iowa City, IA, pp. 124.

Schilling, K.E., Jacobson, P., 2008. Groundwater nutrient concentrations near an incised midwestern stream: effects of floodplain lithology and land management. Biogeochemistry, 87(2): 199-216.

Schilling, K.E., Wolter, C.F., 2000. Application of GPS and GIS to map channel features in Walnut Creek, Iowa. Journal of the American Water Resources Association, 36(6): 1423-1434.

Schilling, K.E., Wolter, C.F., 2001. Contribution of base flow to nonpoint source pollution loads in an agricultural watershed. Ground Water, 39(1): 49-58.

Schilling, K.E., Wolter, C.F., 2007. A GIS-based groundwater travel time model to evaluate stream nitrate concentration reductions from land use change. Environmental Geology, 53: 433-443.

Schilling, K.E., Zhang, Y.K., Drobney, P., 2004. Water table fluctuations near an incised stream, Walnut Creek, Iowa. Journal of Hydrology, 286(1-4): 236-248.

Schulze-Makuch, D., Cherkauer, D.S., 1998. Variations in hydraulic conductivity with scale of measurement during aquifer tests in heterogeneous, porous carbonate rocks. Hydrogeology Journal, 6(2): 204-215.

Shanks, O.C. et al., 2006. Basin-wide analysis of the dynamics of fecal contamination and fecal source identification in Tillamook Bay, Oregon. Applied and Environmental Microbiology, 72(8): 5537-5546.

Tomer, M.D., Burkart, M.R., 2003. Long-term effects of nitrogen fertilizer use on ground water nitrate in two small watersheds. Journal of Environmental Quality, 32(6): 2158-2171.

Tomer, M.D., Moorman, T.B., Rossi, C.G., 2008. Assessment of the Iowa River's South Fork watershed: Part 1. Water quality. Journal of Soil and Water Conservation, 63(6): 360-370.

USEPA, 2008. Handbook for developing watershed plans to restore and protect our waters. EPA 841-B-08-002, U.S. Environmental Protection Agency, Office of Water, Washington, DC, pp. 375.

Weisbrod, T.S., 2005. Modeling the influence of land use on shallow groundwater flow and nitrate transport, Neal Smith National Wildlife Refuge, Jasper county, Iowa, M.S. thesis, University of Iowa, Iowa City, IA, 136 pp.

Williams, T.A., Williamson, A.K., 1989. Estimating water-table altitudes for regional groundwater-flow modeling, U.S. Gulf coast. Ground Water, 27(3): 333-340.

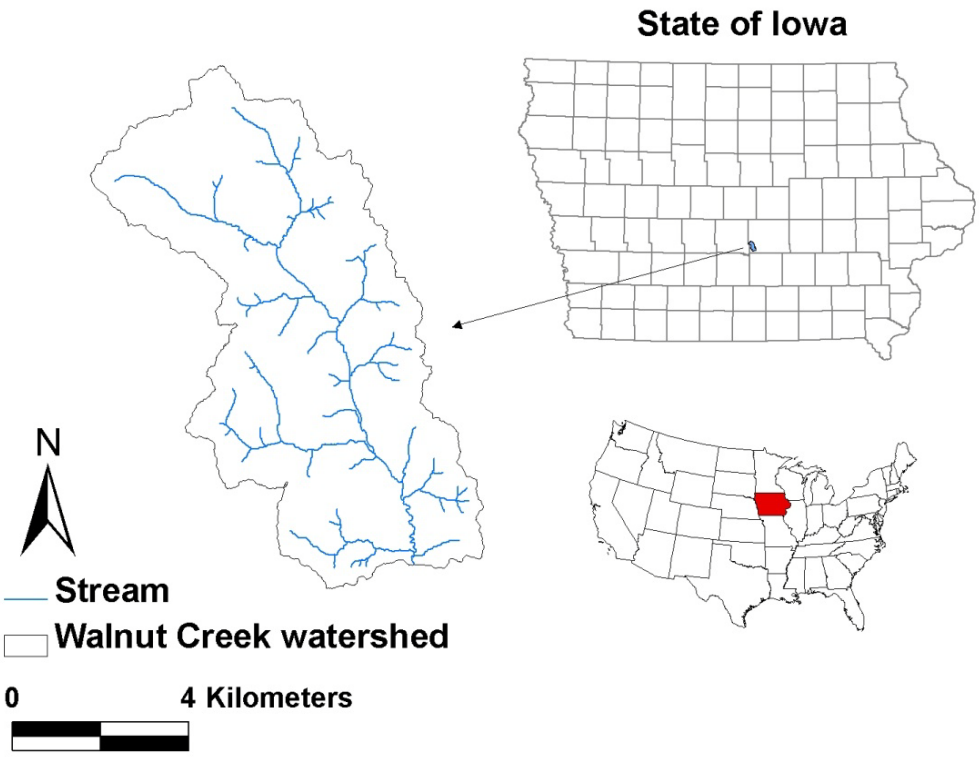

Fig. 11. Site location

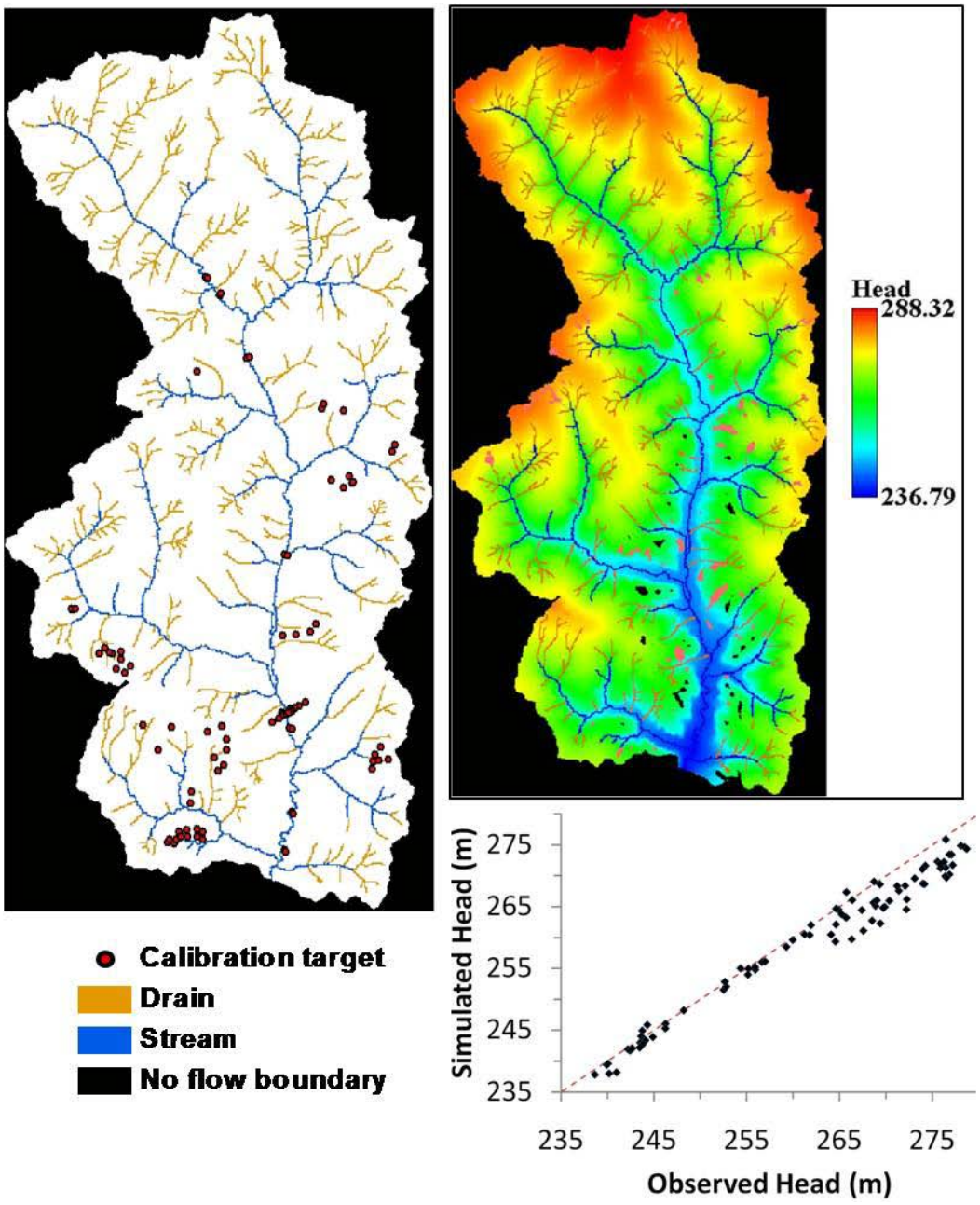

Fig. 12. MODFLOW model: boundary conditions and calibration target locations (left), distribution of hydraulic head (in meters, red and black spots represent stray flooded and dry cells, respectively) (top right); and final calibration plot (bottom right).

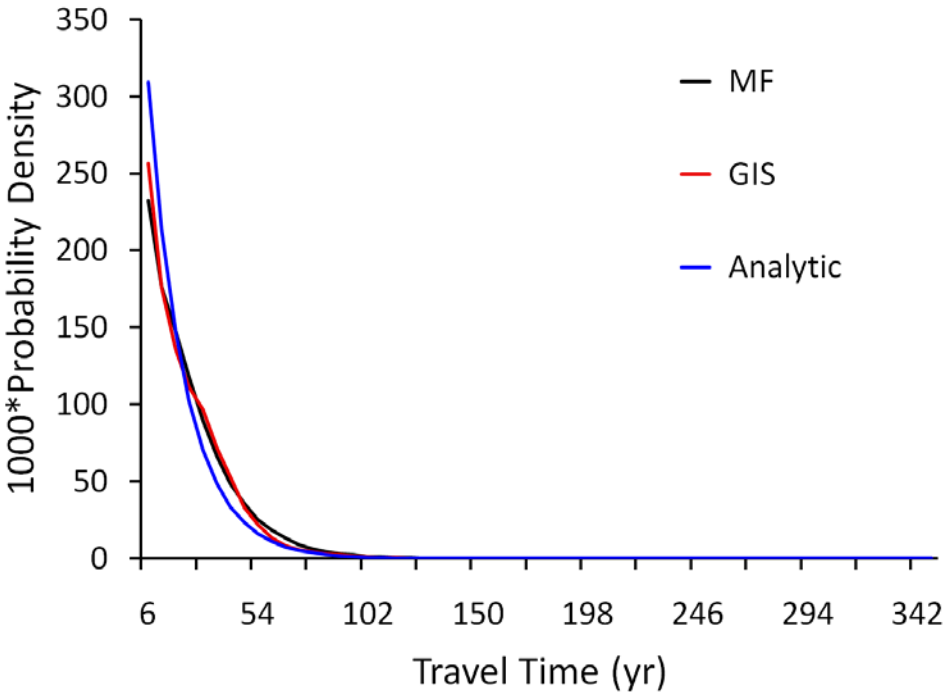

Fig. 13. The Walnut Creek watershed groundwater travel time distribution derived from three different models - analytic, GIS, and MODFLOW (MF). The distributions are normalized to 1000 particles.

Table 1. Summary of the characteristic travel times associated with distributions from three different models (analytic, GIS, and MODFLOW). Std dev and CV denote the standard deviation and coefficient of variation, respectively.

Model	Mean (yr)	Median (yr)	Maximum (yr)	Minimum (yr)	Std dev (yr)	CV	Best fit parameters	
							Scale parameter (yr)	Standard error (yr)
Analytic	16.22	11.24	N/A	N/A	16.22	1.00	16.22	N/A
GIS	19.61	14.80	328.45	0.06	18.84	0.96	19.606	0.055
MODFLOW	20.51	15.55	226.75	0.12	18.69	0.91	20.515	0.058

Table 2. Comparison of the Kolmogorov-Smirnov distance (D) between pairs of travel time distributions that were obtained from three different models (analytic, GIS, and MODFLOW).

Distribution pair	D
Analytic-GIS	0.1034
GIS-MODFLOW	0.0268
Analytic-MODFLOW	0.1175

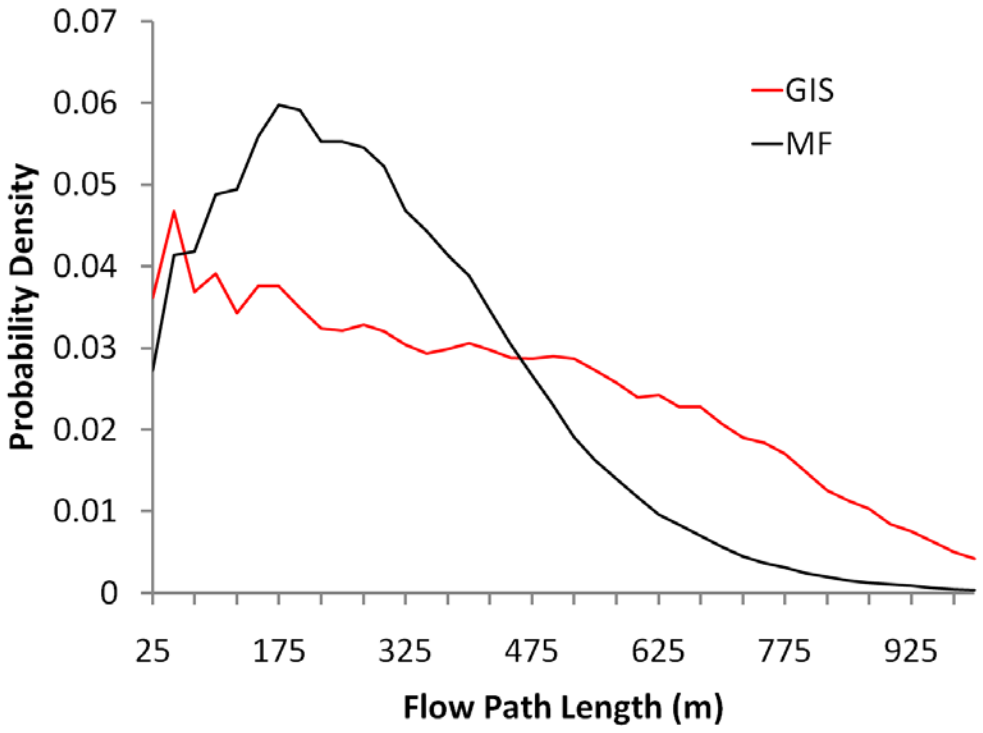

Fig. 14. The distribution of groundwater flow path lengths derived from two different models – the GIS model (in red) and the MODFLOW model (in blue). To facilitate comparison, the outliers in both distributions were cut off by focusing on flow path lengths less than 1000 m. Both distributions are normalized to 1000 particles.

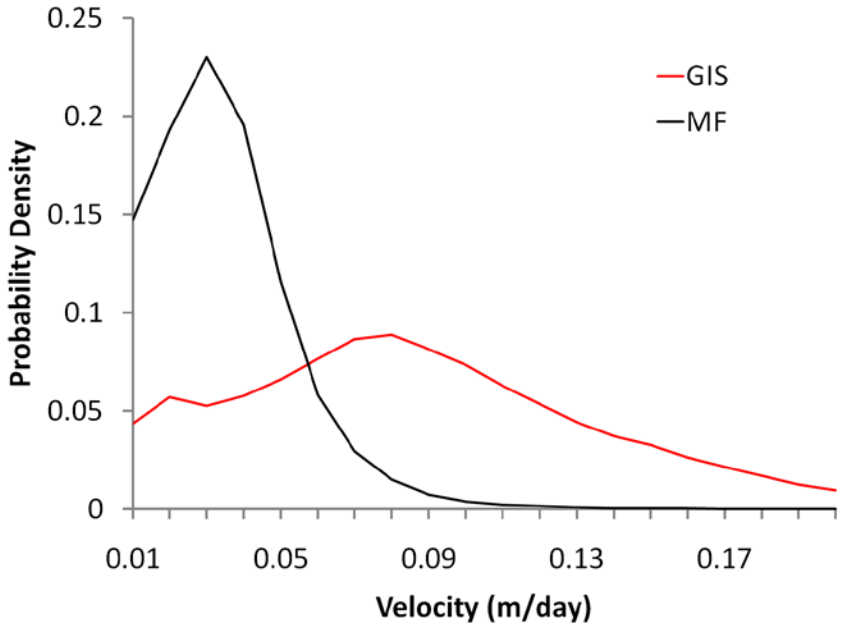

Fig. 15. The distribution of groundwater flow velocities derived from two different models – the GIS model (in red) and the MODFLOW model (in blue). To facilitate comparison, the outliers in both distributions were cut off by focusing on velocities less than 0.20 m/day. Both distributions are normalized to 1000 particles.

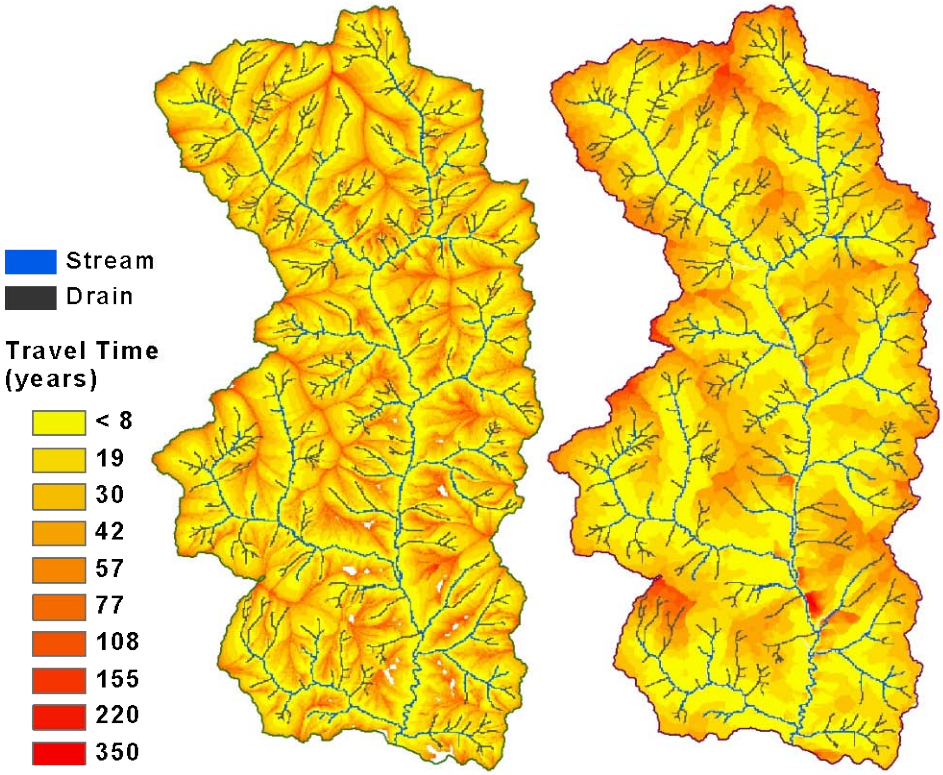

Fig. 16. Spatial distributions of travel times obtained from MODFLOW (left) and GIS (right)

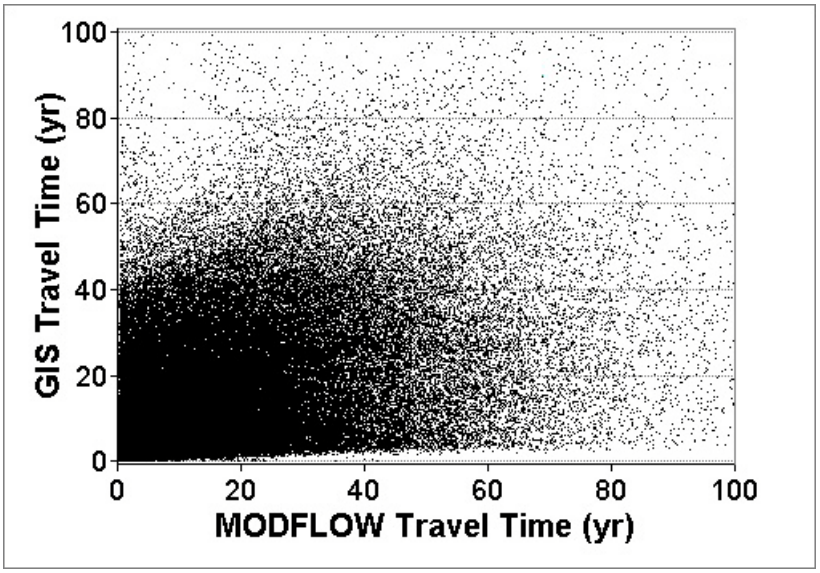

Fig. 17. Comparison of the travel time obtained at each cell location from the MODFLOW and GIS models (on the X and Y axes, respectively). The plot captures 99.24% of the entire data. Data outliers beyond 100 years were excluded.

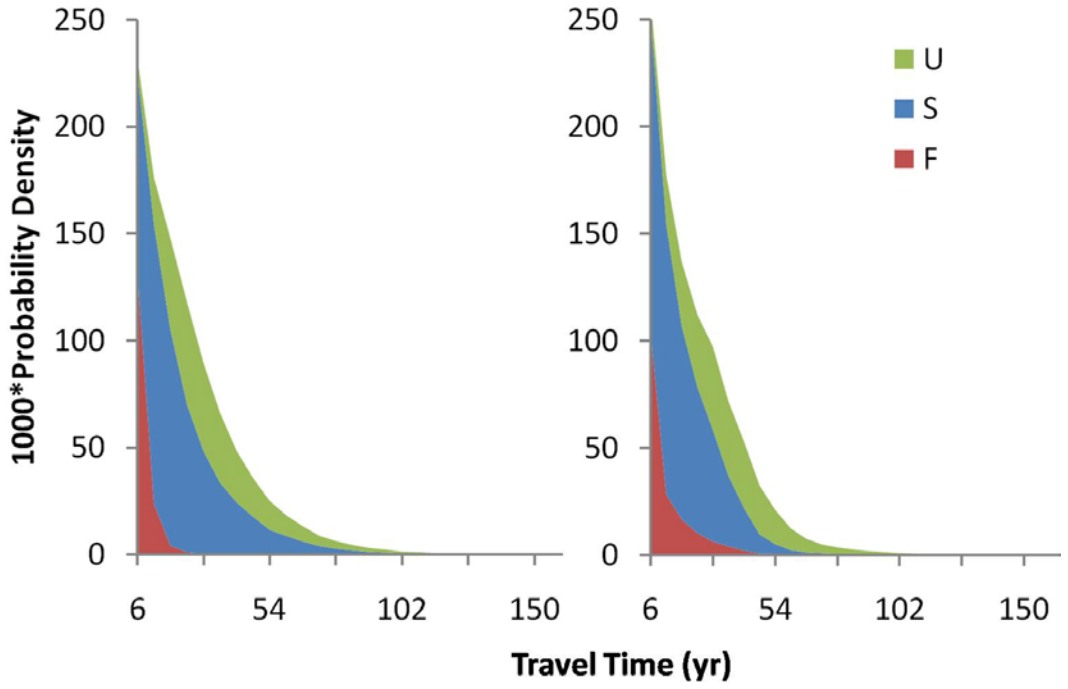

Fig. 18. Separation of the MODFLOW and GIS TTDs (left and right, respectively) based on the landscape position where the particle was released: upland (U), side slope (S), or floodplain (F). Both TTDs are normalized to 1000 particles.

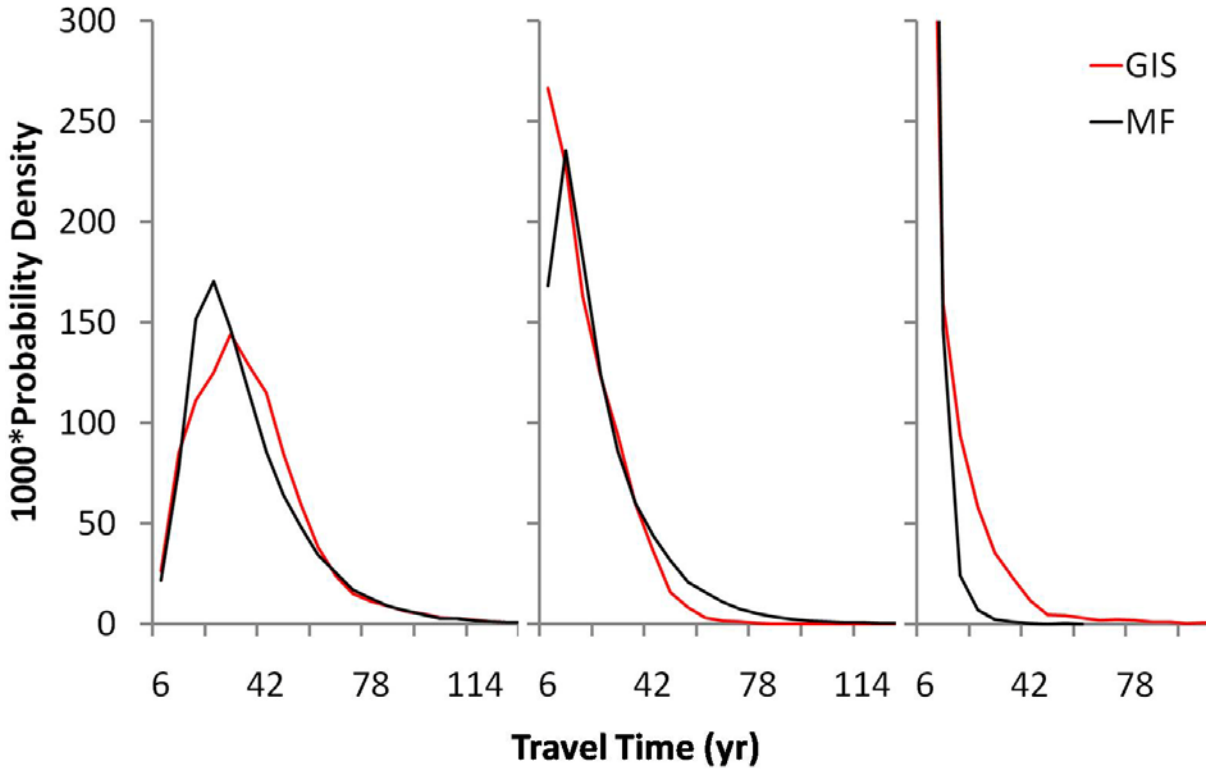

Fig. 19. A comparison of the component TTDs obtained from the MODFLOW (MF) and GIS models in the uplands (left), side slope (center), and floodplain (right). Each component TTD was normalized to 1000 particles.

Table 3.Summary of the mean and standard deviations of each component TTD (in the upland, side slope, and floodplain regions) obtained from the MODFLOW (MF) and GIS models. The Kolmogorov-Smirnov distance (D) between the component TTDs from both models at each location was also computed.

	Upland		Side slope		Floodplain	
	MF	**GIS**	**MF**	**GIS**	**MF**	**GIS**
Mean (yr)	31.61	33.42	19.82	15.28	3.64	9.68
Standard deviation (yr)	19.43	20.09	16.93	12.01	3.82	18.46
D (MF-GIS)	0.0805		0.1056		0.2440	

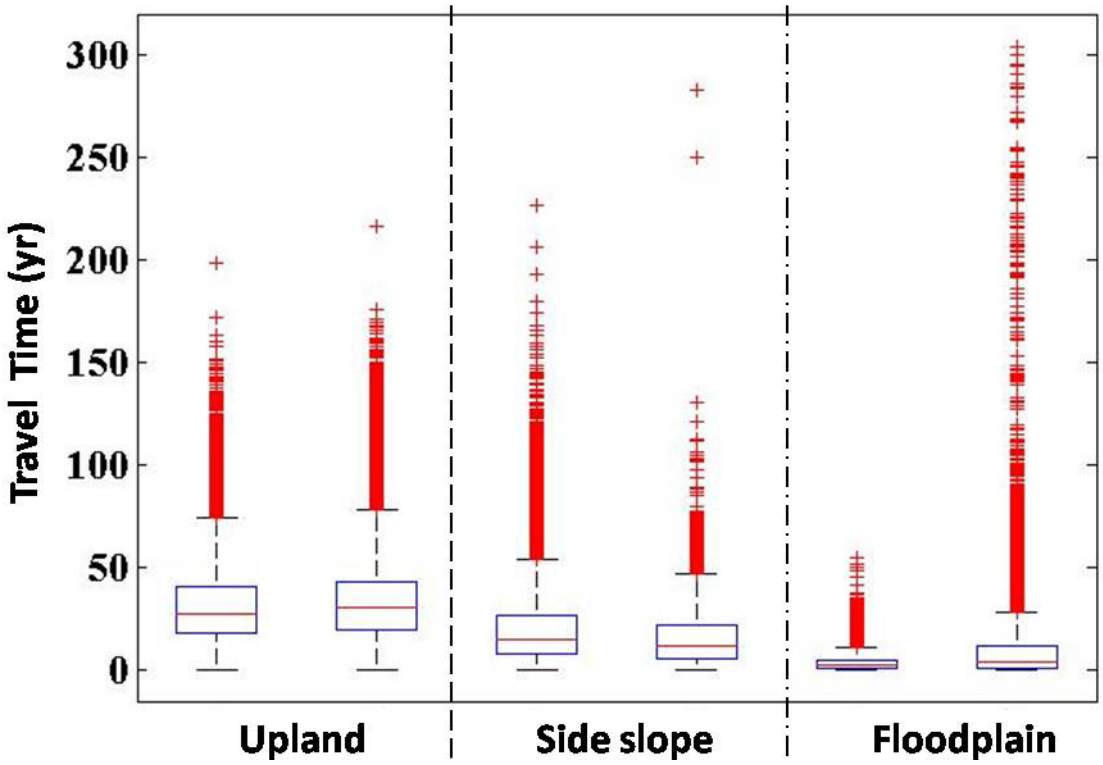

Fig. 20. Box plots of the three component TTDs obtained from the MODFLOW and GIS models (left and right, respectively), at each landscape position. Each box specifies the 25th, 50th, and 75th percentiles of each distribution. The whiskers represent the highest and lowest datum that is within a distance of 1.5 times the interquartile range (IQR) from the box edge. The red plus signs represent data outliers.

IV. Groundwater sink strength as a means to link watershed travel times and drainage network structure to depth of flow

Adapted from a paper to be submitted to *Ground Water*

Priyanka Jindal, Keith E. Schilling, Nandita Basu

Abstract

The relation between depth of groundwater flow and the distribution of travel times in a watershed is known to have a significant impact on the age composition and chemistry of stream water. Moreover, depth to groundwater and the structure of the stream network have been observed to be closely linked. We used a two-dimensional groundwater flow and advective transport model of a watershed, using a combination of MODFLOW and MODPATH, to examine the impact of flow depth on the distribution of travel times and the structure of the drainage network visible to flow. The dimension of depth was represented by a user-defined MODPATH variable, termed the sink strength threshold parameter (S*), as a control parameter. S*, was calibrated against depth of flow at the termination point of the path line of each tracer. We found average flow depth to increase with increase in S*. This relation enabled us to link the variation in travel times relative to S* with flow depth. Travel times were observed to increase with increasing flow depths. The distributions of travel times for shallow and deep groundwater flows were best represented by an exponential and gamma distribution, respectively. The transition between the two end-distributions was found to occur over a small range of depths (relative to the entire aquifer depth). Thus, the exponential distribution was determined to be a stable representation travel time distributions for shallow

flow. The structure of the sink network visible to deep flow was also examined. Sink density was found to decrease with increasing depth. The cluster of sinks at high depths displayed a spatial preference towards the higher order reaches within the sink network. The structure of the effective sink network visible at each depth was parameterized in terms of the bifurcation and length ratios, which are traditionally used to represent surface water stream networks. Bifurcation ratio of the effective sink network was observed to decrease with increasing flow depth in a nearly linear fashion. The relation of the bifurcation ratio to the mean travel time representing flow at each depth was found to be close to a power law, with the value of the scaling exponent (equal to -1.12) being close to -1. The length ratio increased with increasing depth over most of the simulated range of depths. A turnover point in the trend of length ratio at the higher end of depths is subject to further investigation.

4.1. Introduction

The travel times associated with groundwater flow are intimately linked with depth of flow in the aquifer. Travel time, or residence time, is a measure of the age of groundwater (Bethke and Johnson, 2008). The linkage between groundwater age and depth has been subject to much research since the late 1960s, when Vogel (1967) established a theory predicting the distribution of groundwater age relative to depth across a flow cross-section. Many studies have examined the nature of this relationship in the context of a variety of hydrologic scenarios (see for example; Solomon et al., 1995, Puckett and Hughes, 2005; Pabich et al., 2001; Delin et al., 2000). However, few studies have probed the distribution of groundwater age or residence times relative to depth at the watershed scale, particularly in the context of artificially drained agricultural landscapes. In the case of simulation studies,

such a mission would entail the construction of a three dimensional model covering the entire watershed. The sheer demand on computational resources, and extensive collection of field data required to capture the three dimensional variability of the groundwater flow system spanning the breadth and depth of the entire watershed render this to be a highly challenging task.

Regardless of the high costs involved, an estimation of groundwater travel times as a function of depth would be of great value to advance our understanding of hydrologic processes at the watershed scale. One area that highlights the importance of linking groundwater travel times to depth is the area of surface water-groundwater interaction. In one interesting study by Rozemeijer and Broers (2007), the authors found stream water quality at different rates of discharge to be a function of different mixing ratios of groundwater released from different depths in the aquifer. They found that during periods of low flow, when baseflow is the predominant contributor to total streamflow, surface water was primarily influenced by deeper groundwater. In contrast, during quick flow conditions, the contribution of shallower and upper groundwater became more important. Therefore, as confirmed in many other studies, the contribution of groundwater to streamflow measured at the outlet of a watershed typically involves the superposition of groundwater ages spanning many years (Pionke and Urban, 1985; Katz, 2004; Etcheverry and Perrochet, 2000). As the watershed order increases, the stream network intercepts greater depths, and the range of groundwater ages (and travel times) sampled by the stream increases.

This aspect of surface and ground waters interaction has significant implications for surface water quality. Rozemeijer and Broers (2007) observed an increase in the in-stream concentrations of many solutes with increasing contribution of quick flow. They found

nitrate concentrations during baseflow conditions to be very small, and reflective of the quality of deeper groundwater. On the other hand, highest nitrate concentrations were obtained during quick flow conditions when the more contaminated upper and shallow groundwaters began to contribute to total streamflow. However, the surface water nitrate concentrations were found to be less than those observed in the shallowest (upper) groundwater. This indicated that during periods of quick flow, stream water comprised a mixture of upper, shallow, and deep groundwaters. This work demonstrated the critical link between the quality of water in a stream and its groundwater sampling depths.

In other words, the water quality profile of a stream, as it travels from the headwaters to the watershed outlet, is primarily a reflection of the groundwater quality profile that represents the groundwater flow depths that are accessed by the stream. The decrease in concentrations of solutes, such as nitrates, with increasing depth in the aquifer has been analyzed by many authors (Scanlon et al., 2008; Bohlke, 2002; Tesoriero et al., 2005; Broers and van der Grift, 2004). Hence, stream water quality must reflect the improvement in groundwater quality in the downstream direction, as the stream water composition includes greater fractions of deeper and older groundwater (Bohlke and Denver, 1995).

Thus, a deeper understanding of the distribution of groundwater travel times across watershed depth is essential to determine the composition of groundwater ages comprising surface water at different values of stream stage, and to quantify the impact of groundwater solute concentrations on surface water quality. This work was an attempt to forge this critical link between groundwater travel times and depth of flow at the watershed scale.

An additional aspect of surface water-groundwater interaction is the relation between the structure of drainage networks and groundwater flow (Pederson, 2001; Nash, 1996;

Montgomery and Dietrich, 1989). A number of studies have been dedicated to relating surface water network parameters such as drainage density; and bifurcation, length, and area ratios, with various geologic, geomorphic, and hydrogeologic variables such as hydraulic conductivity, bedrock topography, drift thickness and groundwater depth (Luo et al., 2010; Cheng et al., 2001; De Vries, 1976, 1994, 1995; Troch et al., 1995).

In particular, the works of De Vries (1976, 1994 and 1995) focused on identifying the stream network as an outcrop of the groundwater flow system. He postulated stream order to represent a corresponding order in the groundwater drainage network, and related a decrease in depth to the water table with the resultant increase in surface water drainage densities and bifurcation ratio. In this study, we chose to examine the link between the two variables from a different angle. Different depths of a groundwater flow system have access to different reaches of the surface network. The deeper the contaminant particle lies in the aquifer, the more likely it is to travel longer distances and discharge into the higher order reaches of the stream network. We investigated the features of this "effective sink network" visible to groundwater at greater depths, by analyzing the dependence of the bifurcation and length ratios on depth of flow.

To realize the goals outlined above, we simulated the groundwater flow in the unconfined aquifer of a representative watershed in the two planar dimensions, and employed the variable termed "sink strength" as a surrogate for the third dimension of depth in the aquifer. The definition and background of this variable are introduced as follows:

The failure of traditional groundwater particle tracking codes (example, Pollock, 1988) to resolve the trace of a particle once it enters a cell containing a sink that captures only a part of the inflow into the cell has been a matter of great concern to groundwater model

developers and users alike (Zheng, 1994; Spitz et al., 2001; Shoemaker et al., 2004). This issue has been highlighted by numerous authors studying the capture areas of wells (Barlow, 1994; Buxton et al., 1991; Kelly, 2004; Clarke and West, 1998; Cherry and Clarke, 2007) and the distribution of travel times in such systems (Barlow and Dickerman, 2001; Kauffman et al., 2001; Renken et al., 2001).

To overcome this problem, a variable termed “sink strength” is used to distinguish sinks that capture only a partial amount of cell inflow from those that capture the entire amount. The strength of a sink is equal to the fraction of the total flow entering a model cell that is captured by the sink (Fig. 21). By definition, the value of sink strength ranges from 0 to 1. “Strong sinks” are defined as those with strength equal to 1, i.e. they capture 100% of the cell inflow. Therefore, the pathline of a particle that enters a cell containing a strong sink is fully determined. Sinks with strength less than 1 are termed “weak sinks”. The pathline of a particle that enters a cell containing a weak sink that does not capture all cell inflow is more ambiguous, since it is not clear whether the particle would exit through the sink, or continue past it and enter the next adjacent cell.

Currently, MODPATH, a USGS particle-tracking program, addresses this problem by allowing the user to set a model parameter (Pollock, 1994), termed as the “sink strength threshold” (S*) hereinafter. This parameter is used by the program to determine particle traces – all sinks with strength above this threshold value are set to capture particles. Sinks with strength below the threshold stay inactive; particles entering the cell containing an inactive sink simply “bypass” it. Here, “bypass” refers to the movement of particles (that are not intercepted) past the weak sink. This occurs until the particle enters a cell with a sink whose strength is greater than S*.

Methods to refine the particle tracking code that have been (and are currently being) developed (Visser et al., 2009; Abrams and Haitjema, personal communication) utilize the concept that a stream or drain will capture particles in proportion to its outflow, that in turn is sourced from the excess *hydraulic head* that develops in the cell above the sink's stage (Fig. 21). The remainder of the particles entering the cell will not be intercepted by the sink, and will instead bypass it. For an unconfined aquifer, where hydraulic heads are primarily determined by elevation (assuming Dupuit-Forchheimer conditions), this bypass flow is equivalent to the underflow that physically occurs below the sink.

We propose to use this aspect of the particle movement to link flow depth with sink strength. Conceptually, instead of setting a threshold to decide which sinks are capable of capturing a particle, we would like to invert the focus and ask which particles are in a position to be captured by a particular sink. What attributes of a particle might preclude it from being captured? In order to answer this question, we must ask, what permits a particle to bypass a sink? The answer: Depth. The deeper the particle, the less likely it is to be captured by a weak sink. Thus the two variables, strength of a sink and the depth of a particle, are inextricably linked. Fixing a higher sink strength threshold value amounts to accessing particles at greater depths (through the activation of stronger sinks). Indeed, setting a threshold for sink-activation could be taken as equivalent to setting a threshold for the depth of flow. Thus, it is likely that one may be able to directly translate S* in terms of depth of flow.

Note that from source to sink, the depth of flow of a tracer varies continuously, as the path of a subsurface contaminant intercepts variable depths. The final depth at which the flow path ends is simply the physical depth of the sink through which the particle exits the

aquifer, measured relative to an arbitrary datum. This implies that the cumulative travel time along the entire flow path length can only be associated with the depth of the discharge location, and not any other intermediate depth. Thus, the average sink depth is a suitable representative of the depth of flow measured at the termination point of each flow line. Indeed, as average depth of flow decreases, more particles exit from sinks that lie in the shallow, upgradient reaches of the watershed, and the average depth of all active sinks also decreases. Thus, we chose the average depth of all active sinks (at every given value of S*) as a measure to parameterize depth of flow. This allowed us to effectively "simulate" the dependence of groundwater travel times on depth, without explicitly including depth in the model.

Furthermore, since sink strength is derived from the proportion of flow captured by the sink, the spatial location of strong and weak sinks within the total sink network is not random. Stronger sinks are preferentially located along the downgradient reaches of the total drainage network. This correlation between the strength of a sink and its spatial location, along with the abovementioned relation between sink strength and flow depth, was used to uncover the relation between depth of flow and the structural properties of the "effective sink network" that is visible to particles at that depth.

4.2. Site description

The study was conducted at the 51.94 km^2 Walnut Creek watershed in Jasper county, Iowa (Fig. 22). The watershed is located in the Southern Iowa Drift Plain landscape region, an area characterized by steeply rolling hills and well-developed drainage (Prior, 1991). The shallow, unconfined aquifer is a combination of Wisconsinan-age Peoria loess mantles

overlying pre-Illinoian oxidized till in the uplands, and Holocene-age alluvial deposits (composed of around 60-80% silt; Schilling et al., 2004) in the floodplain. Intermittent outcrops of Pre-Illinoian oxidized till and Late Sangamon paleosols are found along the side slopes. The 10-11 m deep aquifer is confined by a 6-30 m thick Pre-Illinoian unoxidized till layer whose hydraulic conductivity is estimated to be two orders of magnitude lower than the alluvial-loess aquifer. The impervious unoxidized till layer overlies bedrock comprising Pennsylvanian Cherokee group shale, limestone, sandstone, and coal.

Hydraulic conductivities of the abovementioned stratigraphic units were estimated using multiple sources comprising slug test results (Schilling and Wolter, 2001; Schilling et al., 2004; Weisbrod, 2005) and saturated hydraulic conductivity values of the soils in the Soil Survey Geographic (SSURGO) database of the region. The hydraulic conductivities of loess and alluvium, that have been estimated to be similar (Weisbrod, 2005; Schilling et al., 2004), were assigned a value of 9×10^{-6} m/s based on the values in the SSURGO database. The till and paleosol outcrops also have similar hydraulic conductivities, estimated to range from 2.3×10^{-7} m/s based on slug tests to 1.2×10^{-6} m/s based on the SSURGO database. Due to lack of field evidence to the contrary, we assumed the vertical and horizontal hydraulic conductivities of all units to be equal.

The watershed's predominantly gaining stream is characterized by a deeply incised channel, with incision depths starting at around 1 m at the tributary headwaters, and steadily increasing in the downstream direction to a depth of around 3 m along the main channel. High channel incision has significantly impacted the watershed hydrology (Schilling and Jacobson, 2008) and is associated with the stream's flashy discharge in response to storm events. An artificial subsurface drainage network at the site is used to drain the water table up

to depths of around 1.2 m below the land surface. The drains are primarily branched along the first order drainageways, and underlie the grassed waterways in the watershed. The watershed lies in a humid, continental region with annual precipitation averaging around 850 mm of which a total of around 129 mm reaches the water table (Schilling et al., 2006). Schilling (2009) estimated the recharge reaching the water table to vary with landscape position, with the floodplain receiving maximum recharge, and side slopes receiving the minimum amount, and uplands an intermediate amount. The ratio of recharge reaching the floodplain, side slope, and upland, was estimated to be 44:14:24, respectively.

4.3. Methods

4.3.1. Groundwater flow model

A two dimensional, steady state groundwater flow model was constructed using MODFLOW-2000 (Harbaugh et al., 2000) and MODPATH (Pollock, 1994). The model is briefly described below. A detailed model description is given in Jindal (2010). The model grid was designed with a horizontal spacing of 20 m, and comprised 628 rows and 300 columns. The top elevation of the single layer model followed the land surface, while its bottom elevation was set to a uniform depth of 11 m. The boundaries of the shallow aquifer were estimated to align with the watershed boundaries. The stream and tile drain boundaries were defined using the RIV and DRN packages, respectively. Streambed sediment hydraulic conductivity and thickness were estimated using data in Schilling and Wolter (2000) and Schilling et al. (2004), and were estimated to be around 5×10^{-5} m/s and lie in the range 0.1-0.4 m, respectively. Drain conductance was selected as 8.7×10^{-4} m^2/s, close to typical literature values (Goswami and Kalita, 2009). The physical and hydrologic boundaries of the

model are shown in Fig. 23. Effective porosity used for particle tracking was estimated to be around 0.3 (Helmke, 2005).

Hydraulic conductivity zones were delineated using the parent material index in the SSURGO database (loess, alluvium, till, or paleosol) and assigned values based on multiple data sources comprising slug test results (Schilling and Wolter, 2001; Schilling et al., 2004; Weisbrod, 2005) and the saturated hydraulic conductivity value obtained from the SSURGO database. It was observed that the hydraulic conductivity estimates based on the results from the slug tests consistently produced unrealistically high water table levels that exceeded the land surface elevation. This has been anticipated by a number of authors (Schulze-Makuch and Cherkauer, 1998; Rovey II, 1998) as reflective of the fact that groundwater flow is impacted by high-conductivity aquifer heterogeneities present at larger flow scales than the scale of flow created by localized slug tests. Indeed, estimates of saturated hydraulic conductivity obtained from the Soil Survey Geographic (SSURGO) database, that were approximately one order of magnitude higher than the slug test values, led to a significant improvement in water table levels across the watershed. Thus, we selected the SSURGO values as baseline estimates, which were then used as calibration parameters during the stage of model calibration.

Recharge zones were delineated using the slope classification for each soil mapping unit in the SSURGO database, and assigned values such that the ratio of the recharges in the uplands to side slopes to floodplain was 24:14:44 (Schilling, 2009). The recharge values were constrained by the condition that the total or equivalent annual recharge over the entire watershed, computed as the area-weighted average of the recharges at each landscape position, be equal to the estimated long-term average value of annual baseflow. The aquifer

parameters of groundwater recharge and hydraulic conductivity of the oxidized till zone were then adjusted during the stage of model calibration.

Model calibration was achieved by manual trial and error that produced the best results in comparison to other automated calibration procedures that were tested. The model was calibrated for 84 head targets situated at various locations in the watershed. Amongst the various calibration parameters included, the model was observed to be most responsive to hydraulic conductivity (both, value and spatial distribution) and total recharge. Specifically, the location of the loess-till contact and the hydraulic conductivity value of oxidized till had a significant impact on simulated heads. This hinted towards the presence of a transition zone along the loess-till contact line, with a hydraulic conductivity value that is intermediate between the corresponding loess and till values. The detailed spatial distribution and value of hydraulic conductivity for each zone is listed in Jindal (2010). The calibrated total or equivalent annual recharge was estimated to be 120 mm, which is slightly lower than the initial estimate of 129 mm (Schilling et al., 2006).

The final calibrated model produced reasonable agreement between the simulated and observed hydraulic head values at the calibration targets (Fig. 23). The absolute residual mean (ARM, the average of the absolute values of the residuals, or the difference between the simulated and observed heads) was 2.55 m, while the residual standard deviation was 2.29 m. The resultant distribution of water table elevations across the watershed is also shown in Fig. 23. For a model of covering an entire watershed of this size (51.94 km^2), an ARM of 2.55 m was considered reasonable. Moreover, for our specific project goals of evaluating the distribution of groundwater travel times, an error in hydraulic head generated at the scale of cell resolution is likely to not impact results significantly. This is because the

travel time along the length of a flow path from its origin to the sink, is a cumulative measure that is liable to integrate out possible deviations in hydraulic gradient along its entire length. Furthermore, the travel time distribution was generated by aggregating the travel times of more than 120,000 particles, and then studying the distribution as a whole. Thus, possible errors introduced by some particle traces are likely to have negligible impact on the overall travel time distribution that is generated from a large sample size. These two reasons indicate that the few stray spots of dry and flooded cells (Fig. 23) that remained are expected to have a negligible impact on the distribution of cumulative travel times obtained from a large sample of tracer particles. Hints of the insensitivity of the distribution of cumulative travel times to localized model errors were evident in the earlier stages of model calibration when the distributions obtained for earlier model runs that had a higher number of dry and flooded cells (with the number of dry cells more than 100% of the number in the final model, and the number of flooded cells being similar) produced nearly the same results as the final calibrated model (with the mean travel time differing by 0.68% only).

Particle tracking in MODPATH was performed by releasing particles at the water table in every cell center of the active model domain and forward tracking them from source to sink. To establish the relation between the sink strength threshold parameter and simulated travel times, separate simulations were run for values of S* spanning the entire range from 0 to 1. The distributions at the low and high extremities (S*=0 and 1) were best-fit to standard probability distributions. The best-fit analysis was performed using the Distribution Fitting tool that is part of the MATLAB Statistics toolbox.

4.3.2. Kolmogorov-Smirnov statistical test

As part of the comparison between two distributions, we sought to quantify the degree of closeness in the shapes of both. We selected the Kolmogorov-Smirnov (KS) two-sample statistical test for this purpose (Daniel, 1978; Hollander and Wolfe, 1999). The test utilizes two cumulative distributions that are empirically derived from two independent, random samples of a random variable X. The cumulative distribution function of a random variable X, is denoted as F(x), and defines the probability that the value of the random variable X is less than or equal to x. Similarly, the sample cumulative distribution, S(x), that is empirically derived from a discrete sample comprising n observations of the random variable X is defined as,

$$S(x) = \frac{(\text{number of observations } \leq x)}{n}$$

Let $S_1(x)$ and $S_2(x)$ be the empirical distributions of the random variable X based on two samples of size n and m observations, respectively. To quantify their degree of closeness, the KS two-sample test statistic D is computed as,

$$D = \max | S_1(x) - S_2(x) |$$

If both samples are representing the same system or population, then $S_1(x)$ and $S_2(x)$ should be close to each other for all values of x, and D should be close to 0. The maximum value D can take is 1.

4.3.3. Methods to relate travel time with depth and network properties

To establish the relation between travel time and depth of flow we first performed particle tracking for multiple scenarios where S* was varied systematically between the two end points of 0 and 1. This gave us the travel time distribution at each value of S*. We then performed a calibration that related S* to the depth of flow in the watershed, as represented

by the average depth of flow at the outlet. This was done by first summarizing all particles by the location of their final destination sinks for every simulation. We then computed the average depth of all the sinks active at each value S*, relative to the average land surface elevation along the total sink network. This represents the average depth of flow at the discharge location at each given value of S*. Note that the choice of the datum has no bearing on these results. It was chosen to represent a depth of flow relative to the elevation of the local land area running along the sink network, versus the surface elevation of the entire watershed. This enables us to better capture the intuitive notion of "depth of flow", that, for instance, would be the depth of the stream relative to the stream bank. Having established the relation between S* and travel time and the corresponding one between S* and depth of flow, we were able to successfully relate travel times with depth of flow.

We also observed a clear visual trend in the spatial pattern of the active destination sinks with variation in S*. To capture this trend more effectively we examined the structural form, namely the geomorphic properties, of the active sink network, and its variation with S*. We parameterized the structure of the "effective sink network" at each S* by employing an order and associated parameters traditionally used to delineate surface water stream networks, that were defined and developed by Horton (1945) and Strahler (1952, 1957). In contrast to traditional stream networks, the sink network here (1) corresponds to that visible to groundwater flow, and (2) unifies stream and tile drainage networks into a single "sink network". The parameters chosen to classify the structure of the effective sink network were (1) the bifurcation ratio, R_b, and (2) the length ratio, R_L.

We first created the combined sink network. Each "reach" (individual segment of the sink network that was not intersected by another line) was then assigned an order based on the

Horton-Strahler ordering system. Upland reaches with no parent reach were assigned an order 1, and a join of 2 reaches of equal order increased the order of the downgradient reach by 1. Thus, the reach order gradually increased downgradient from 1 to 5, that turned out to be the order of the stream main channel.

The bifurcation ratio, R_b, and length ratio, R_L, are defined as

$$R_b = \frac{N(k)}{N(k+1)} \quad \text{and} \quad R_L = \frac{\bar{L}(k+1)}{\bar{L}(k)}$$

where $N(k)$ is the number of reaches with order k, and $\bar{L}(k)$ is the average length of all reaches with order k. The watershed bifurcation and length ratios representing the entire network were computed by taking the average of their respective values obtained for every consecutive pair of orders. It has been observed that typically, for most naturally developed surface water stream networks, the value of R_b is within the range between 3 and 5, and for R_L between 1.5 and 3.5 (Rodriguez-Iturbe and Rinaldo, 1997).

To compute R_b and R_L for the active sink network, we assigned each sink a unique reach ID based on specific reach it belonged to. The sinks were then aggregated by the reach ID, to evaluate the active length of each reach. The active reaches (and their corresponding active length) were then matched to their assigned order, and used to compute R_b and R_L between every pair of consecutive orders. The value of each ratio for all such pairs was then averaged over, to obtain the representative R_b and R_L of the effective sink network at every value of sink strength threshold S*. These ratios were then analyzed, and via the sink strength, related to the other physical variables of flow depth and watershed travel time.

4.4. Results and Discussion

4.4.1. Impact of the sink strength threshold parameter on watershed travel times

As has been acknowledged by the abovementioned authors, a user-defined setting of a sink strength threshold parameter (S*) in the particle-tracking code, MODPATH, introduces considerable arbitrariness in the particle pathlines, and hence in the watershed travel times derived from it. The extent of this problem was gauged by quantifying the impact that S* has on the TTD shape and statistics as S* was varied systematically from 0 (stop at all sinks), to 1 (stop at strong sinks only). We conducted a best-fit analysis and found the probability distribution that best-fit the simulated distribution to change from an exponential distribution at S*=0 (best-fit scale parameter: 20.51, with standard error: 0.06), to a gamma distribution for S*=1 (with best-fit scale and shape parameters: 1.43 and 28.10; and standard errors: 0.005 and 0.12, respectively). The distribution corresponding to S*=0 was found to match the idealized exponential TTD as proposed by Haitjema (1995).

Interestingly, the transformation in the shape of the travel time distribution from a gamma to an exponential distribution (as shown in Fig. 24) did not occur at a uniform pace. Fig. 25 shows the switch from the gamma distribution as S* was decreased, to be initially rapid and slow down as the value of S* was decreased further. To quantify (1) the non-uniform rate of transition in the TTD shape and, (2) the degree of deviation from the idealized exponential distribution, we computed the level of agreement in terms of the Kolmogorov-Smirnov distance parameter (D) between the pair of distributions defined by the “baseline” exponential TTD obtained at S* = 0, and every individual TTD with a non-zero value of S*. In the case of a perfect match with the exponential, D equals 0. Thus, the degree of deviation observed in D from 0 at each S* was a measure of the deviation of each TTD from the baseline exponential form.

As expected, maximum deviation was observed for the TTD at S*=1 (that was best-fit to a gamma distribution). The deviations of all TTDs were computed as a percent of this maximum value. These normalized percent deviations are shown in Fig. 26. The near-zero deviation of the TTD shape for most S* values confirmed the observation that deviation from the exponential distribution became dominant only at the higher end of S* values (≥ 0.6). Note that this approximate conformity in the shape of the TTD to an exponential over a large range of S* values was not due to the number of active sinks possibly staying constant regardless of what value S* was set at (as would happen, if for example, all sinks in a flow system were strong). This was evidenced by a near linear decrease ($R^2 = 0.98$) in the total number of sink destinations at which the particles stopped as the value of S* was increased (Fig. 27). This result made it certain that there was a definite increase in bypass flow as S* increases, yet, for small to moderate values of S*, the TTD stays close to an exponential-like decay.

The relatively high value of S* below which all the distributions resembled an exponential suggests that the exponential distribution, as proposed by Haitjema (1995) is fairly robust and stable, and can even tolerate a small degree of “perturbation” (in the form of bypass flow in the watershed). In other words, our results suggest that the exponential distribution might be considered to be a good approximation to MODFLOW TTDs that might contain some bypass flow in it.

Also, an examination of the statistics of the distributions (Table 4) revealed that for most S* values, the span of the travel times stays fairly constant (in terms of both the maximum and minimum values). But within that range, there is a dramatic change in the proportion of high and low transit times as S* is varied. Raising the sink strength threshold increased the

proportion of higher transit times, but the transition did not occur at a uniform pace, as was evidenced by its impact on the mean travel time. The variation in mean travel time became prominent only at higher threshold values (S* > 0.5) as shown in Fig. 28. We also observed the pace at which the median and the mean of the distributions vary to be comparable. Overall, as S* was varied over the entire range from 0 to 1, the mean and median travel times approximately doubled (from 20.51 to 40.2 years, and from 15.55 to 32.47 years, respectively).

Thus, a change in the particle stop criteria, for the *same* set of boundary conditions and aquifer parameters, altered the MODFLOW TTD significantly, though most of the variation was restricted to the higher end values of the sink strength threshold parameter. The apparent arbitrariness of the travel time results was used to our advantage, by physically interpreting the concept of sink strength in terms of average flow depth across the watershed, as demonstrated below.

4.4.2. Relation between travel times and depth of flow

The intuitive correlation between depth of flow and strength of a sink suggested in the introduction was examined by estimating the depth of flow (as represented by the average depth of active sinks in the model) as a function of the sink strength threshold, S*. Note that S* forms the lower bound of the sink strengths of all active sinks in the watershed, and is thus a valid representative instead of the average value of these sink strengths. We found that the depth of flow did indeed increase systematically as the sink strength minima (S*) was increased (Table 4 and Fig. 29). Variation of S* over its entire range from 0 to 1 was found to represent a depth variation of nearly 8 meters in the 11 meter deep aquifer. Thus, S* can

simulate the effect of depth of flow, and can therefore be used as a surrogate measure for the vertical dimension.

The quantitative relation between S* and flow depth shall vary based on the watershed and sink network characteristics, aquifer properties, and boundary conditions. But for a typical system, there should be a one-to-one correspondence between the active sink strength in the model (be it measured in terms of its average, or its lower bound S*) and the depth at which the particles are discharged.

The relationships between mean travel time and S*, and between the depth of flow and S*, presented above provided an opportunity to indirectly simulate the variation of groundwater travel times with flow depth in a watershed. Linking the depth of flow back to the TTD via S* provided some valuable insights into the behavior of the distribution of travel times with respect to depth. The TTD at shallow depths was found to be an exponential. As depth increased, the form of the TTD transitioned to a gamma distribution.

Also, we found the mean travel time to increase with increasing depth of flow (Fig. 30). The best-fit curve to the simulated trend was a quadratic polynomial. The functional dependence of the 3 best-fit coefficients on the various physical variables characterizing the watershed is not yet known to us and requires further research. It is also possible that this trend is a subset to a broader trend that might have a different functional form. Future work needs to examine this issue more deeply.

As noted in the introduction, the variation of groundwater travel time with depth has been subject to much research since the theory proposed by Vogel (1967) predicted a logarithmic dependence on saturated thickness. His theory was established for depth variations within a cross-sectional profile. Thus the 1-D relation predicted therein does not apply to our model,

and to the best of our knowledge, there has been no theory to predict the variation of mean travel time with respect to depth for groundwater flow in a watershed.

A number of points of discussion can be garnered from these results. Firstly, for a watershed where the scale of its vertical dimensions is 100 times smaller than that the scale of its horizontal dimension, one may anticipate the distribution of travel times to be sensitive to variations in the vertical dimension. This was been established herein. Secondly, the representative turnover depth at which the shape of the TTD switches from an exponential to a gamma distribution would constitute a characteristic depth scale for the watershed, that would represent the transition from deep flow (with a gamma-like TTD) to shallow flow (with an exponential-like TTD). What is its value, and how does it depend on the physical properties of the watershed and aquifer, is a question that requires further research. Thirdly, does the mean TT vary quadratically with respect to depth when we expand the range of simulated depths, and if so, why? Does the result apply for watersheds too?

Fourth, this research illustrated the critical role that depth plays in determining the distribution of groundwater travel times and ages that is sampled by the stream of a particular order. This distribution would govern the in-stream mixing ratio of groundwater of different ages, and the resultant stream water quality. Furthermore, this work brings forth the need to consider the role that depth plays in determining conservative solute travel times, and the associated turnover time necessary to detect the impact of distributed environmental conservation and restoration practices that are implemented for the removal of the particular contaminant from the surface water bodies in the watershed. Indeed, our results show that the higher the watershed order, the higher is the proportion of deep groundwater that is associated with longer travel times. Therefore, we anticipate higher order watersheds to

require longer periods of times before the effects of remediation and conservation practices implemented on the land surface can be visible at the stream outlet.

Finally, it should be noted that though this is a two dimensional model, the effect of depth could be simulated via the sink strength variable, that is governed by a ratio of fluxes. Both, cell-to-cell and cell-to-sink fluxes are dependent on the hydraulic head differences between them. Head differences, in turn, are dependent on the cell head and the stage of the sink. For an unconfined aquifer where vertical dimensions (of both aquifer and sinks) are negligible compared to the horizontal dimension, the cell head (water table) and stage of the sink shall follow the absolute land surface elevation. Thus, it was possible to indirectly account for the effect of flow depth via control over the strength of the active sinks, the value of which can be traced back to depend on the variability in the land surface elevation. Thus, a comparison of fluxes can be used to gain insight into aspects of the model that are not directly simulated.

4.4.3. Relation between depth of flow and network structure

We examined the spatial patterns of the sink network, and its dependence on the sink strength parameter. The spatial maps of the sink distributions at three different values of S* were juxtaposed (Fig. 31). These three maps correspond to the active sink distributions at the low, intermediate, and high end of S* (S* = 0, 0.5 and 1, respectively), and show the range in the sink network that is possible in this model. As the comparison of maps clearly shows, strong sinks are preferentially located along the main channel of the stream, and other higher order tributary reaches of the sink network. This bias manifested in the unnatural appearance of the strong sinks network, that we sought to quantify explicitly using two parameters that are traditionally used to designate surface water stream networks, namely, the bifurcation ratio, R_b, and the length ratio, R_L.

Trends of both R_b and R_L are shown in Fig. 32. As the sink strength threshold decreases, and more sinks become active, the network starts resembling the full surficial network. Thus, the values of R_b and R_L tend toward the natural range (3-5 for R_b and 1.5-3.5 for R_L). But both chart their approach toward their respective natural range from opposite directions. In other words, at higher values of sink strength threshold, the bifurcation ratio is suppressed, due to the fact that sinks with higher strengths will preferentially lie along higher order reaches located further downgradient in the sink network. Thus, the number of active lower order reaches relative to the number of active higher order reaches will be biased negatively, and be less than would be the case for the full network. This leads to the average ratio of the number of lower to higher order reaches, defined as R_b, to be smaller than the ratio obtained when the entire sink network is activated at the lower extremity of S*.

On the other hand, the same factor, namely, the preferential activation of higher order, implies that the average length of active sinks of higher order relative to those of lower order will be biased positively, and be greater than what would be computed for the entire network. Thus, the ratio of the average length of higher to lower order reaches, defined as R_L, will be greater than the ratio obtained when the entire sink network becomes active at S*=0. This implies that as the active sink network approaches the full network, the bifurcation ratio will increase, and the length ratio will decrease. Both these predictions are manifest in the trends, except in the behavior of the length ratio at the higher extremity of S*, where R_L initially increases with a decrease in S*. The circumstances governing the turnover point at S*=0.8 are yet unknown to us, and subject to further investigation. We chose to focus instead on the bifurcation ratio, and on building a deeper understanding of its significance and relation to the other physical variables characterizing groundwater flow in the watershed.

The relations established between the bifurcation ratio and sink strength, and the one between sink strength and flow depth explored earlier, were used to gain further insight into the characteristics of deep contaminant flow. The variation of average depth of flow (measured in terms of average sink depth) with respect to S*, and the variation of R_b with respect to S*, were correlated, to probe how the bifurcation ratio of the effective sink network varied with respect to flow depth (Fig. 33). The relation between R_b and flow depth was gauged to be close to linear for the modeled range of S* and associated flow depths. We would like to note that this obviously documents only a small window of a larger trend, since physically, R_b cannot become nonpositive if depth of flow was to increase further. Regardless of this fact, the relation provides some valuable insights as discussed below.

The rapid decrease in the bifurcation ratio as depth increases, suggests that the effective sink network "visible" to deeper contaminants can be remarkably different from the sink network visible to shallow/surface contaminants. As depth increases, contaminants bypass an increasing number of upgradient sinks, and thus perceive an entirely different sink network that contains a much lower density of sinks than that observed at the surface. Moreover, the location of such sinks is strongly biased towards the higher order reaches of the sink network.

The relation between the depth of flow and the structure of the effective sink network has possible implications for water quality impacts, and remediation practices targeted towards improving water quality at specific reaches of drainage network. Not only must we take into account the capture area that contributes to a particular reach, but also consider the "capture depth", that is contributing to outflow at the specific stream reach that requires improvements in water quality. In other words, the spatial focus of conservation and remediation efforts implemented on the land surface to improve the water quality of specific segments of the

stream network must be directed not only over specific areal extents, but also be targeted at the specific range of depths where the particular stream segment is visible.

Further works needs to be conducted to quantify the broader trend of the bifurcation ratio of the effective sink network with depth, in the context of different landscapes and a wider variety of sink networks. The factors governing the turnover point in the length ratio of the effective sink network at the higher end extremity of sink strength (hence, at the higher end of flow depth) also need to be examined.

4.4.4. Relation between travel times and network structure

As noted above, the observed trend of R_b with respect to flow depth is certainly limited due to the limited range of flow depths the model could capture for the particular watershed, and needs to be expanded over a larger range of flow depths. In contrast, we observed the relation between travel time and bifurcation ratio to seem more universal. The connections between travel time and sink strength, and between the bifurcation ratio and sink strength established above were used to relate travel time with network properties visible to deeper flow. As expected, an increase in the mean travel time (denoted as T* in the following discussion) of contaminant flow at a specific depth is accompanied by a decrease in R_b of the effective sink network observed by the flow.

Interestingly, the results suggested a power law relation between the two variables (Fig. 34). The value of the scaling exponent (equal to -1.12), was very close to -1. Though we cannot test or prove whether there is indeed a simple inverse relation between the two variables, the form of this relation was explored deeper. The asymptotic limits of this near inverse relation, albeit theoretical, were useful gedanken experiments that helped gain a deeper appreciation of its possible widespread applicability, as follows:

(a) Does the limit $T^* \to \infty$ imply $R_b \to 0$?

As depth increases , one starts to access to regional groundwater flows that can potentially have mean travel times of the order of tens of thousands of years. Such flow discharges into the most downgradient, highest order reaches of the sink network, that are indeed very few in number. Thus, our results suggest that in the limit of deep flow, the R_b of the effective sink network visible to such deep flow does indeed tend to zero.

(b) Does the limit $R_b \to \infty$ imply $T^* \to 0$?

A large bifurcation ratio corresponds to a large number of lower order reaches per unit higher order reach. This would typically correspond to increasingly high drainage densities of the sink network. For such networks, a particle released in the watershed would immediately be taken up by a sink, and that would indeed result in a mean travel time tending towards zero.

The analysis of the limiting cases, in conjunction with the observed relation between the two variables, and the closeness of the exponent in that relation to -1 suggests the presence of a close link between the groundwater travel times and the structure of the sink network visible to contaminants as the depth of flow in a watershed increases. The validity of this relation in the context of different watershed landscapes needs to be further investigated.

4.5. Conclusions

We examined the impact that depth has on two aspects of the groundwater flow system of a watershed – the distribution of groundwater travel times and the structure of the drainage network visible to flow at a specific depth. This goal was accomplished by the

implementation of a coupled, two-dimensional groundwater flow and advective transport model at the Walnut Creek watershed, a representative watershed located in Jasper County, Iowa. The user-defined setting of a sink strength threshold parameter (S*) designed to determine the location of active sinks in the advective transport model was used as a surrogate for the vertical dimension in the watershed. We found higher values of S* to represent deeper flow.

The variation of the travel time distribution from an exponential to a gamma distribution as S* increased could then be translated in terms of a variation with respect to depth. Thus, shallow flow was found to be best represented by the exponential distribution, while deeper flow was well represented by the gamma distribution. Travel times were observed to increase as S*, and therefore depth, were increased.

The relation between the drainage pattern and S* was then used to describe the properties of the drainage network at variable depths within the watershed. The distribution of sinks was observed to be spatially biased towards the higher order reaches, as depth of flow increased. Parameterizing the effective sink network visible to deeper flow by the bifurcation and length ratios, we found that both ratios to vary continuously and head towards their natural range as S* was decreased. Length ratio was observed to mostly decrease, while the bifurcation ratio was observed to increase, as S* was decreased. The latter relation established a near linear relation between the bifurcation ratio of the effective sink network and depth of flow. Also, the mean travel time and bifurcation ratio seemed to be inversely related to each other via a power law whose exponent was close to -1.

The results demonstrate how the appropriate selection of a model parameter, S*, can reveal facets of the groundwater flow system that would be hidden otherwise, namely, the

dependence of groundwater travel times and drainage patterns on flow depth within the watershed.

References

Barlow, P.M., 1994. Two- and three-dimensional pathline analysis of contributing areas to public-supply wells of Cape Cod, Massachusetts. Ground Water, 32(3): 399-410.

Barlow, P.M., Dickerman, D.C., 2001. Numerical-simulation and conjunctive-management models of the Hunt–Annaquatucket–Pettaquamscutt stream-aquifer system, Rhode Island: U.S. Geological Survey Professional Paper 1636, Reston, VA, pp. 88.

Bethke, C.M., Johnson, T.M., 2008. Groundwater age and groundwater age dating. Annual Review of Earth and Planetary Sciences, 36: 121-152.

Bohlke, J.K., 2002. Groundwater recharge and agricultural contamination. Hydrogeology Journal, 10(1): 153-179.

Bohlke, J.K., Denver, J.M., 1995. Combined use of groundwater dating, chemical, and isotopic analyses to resolve the history and fate of nitrate contamination in two agricultural watersheds, Atlantic coastal plain, Maryland. Water Resources Research, 31(9): 2319-2339.

Broers, H.P., van der Grift, B., 2004. Regional monitoring of temporal changes in groundwater quality. Journal of Hydrology, 296(1-4): 192-220.

Buxton, H.T., Reilly, T.E., Pollock, D.W., Smolensky, D.A., 1991. Particle tracking analysis of recharge areas on Long Island, New York. Ground Water, 29(1): 63-71.

Cheng, Q.M., Russell, H., Sharpe, D., Kenny, F., Qin, P., 2001. GIS-based statistical and fractal/multifractal analysis of surface stream patterns in the Oak Ridges Moraine. Computers & Geosciences, 27(5): 513-526.

Cherry, G.S., Clarke, J.S., 2007. Simulation and particle-tracking analysis of selected ground-water pumping scenarios at Vogtle Electric Generation Plant, Burke County, Georgia: U.S. Geological Survey Open-File Report 2007-1363, Reston, VA, pp. 51.

Clarke, J.S., West, 1998. Simulation of ground-water flow and stream-aquifer relations in the vicinity of the Savannah River Site, Georgia and South Carolina, predevelopment through 1992: U.S. Geological Survey Water-Resources Investigations Report 98-4062, Reston, VA, pp. 135.

Daniel, W.W., 1978. Applied nonparametric statistics. Houghton Mifflin Company, Boston, MA.

Delin, G.N., Healy, R.W., Landon, M.K., Bohlke, J.K., 2000. Effects of topography and soil properties on recharge at two sites in an agricultural field. Journal of the American Water Resources Association, 36(6): 1401-1416.

Devries, J.J., 1976. The groundwater outcrop-erosion model; evolution of stream network in the Netherlands. Journal of Hydrology, 29(1-2): 43-50.

Devries, J.J., 1994. Dynamics of the interface between streams and groundwater systems in lowland areas, with reference to stream net evolution. Journal of Hydrology, 155(1-2): 39-56.

Devries, J.J., 1995. Seasonal expansion and contraction of stream networks in shallow groundwater systems. Journal of Hydrology, 170(1-4): 15-26.

Etcheverry, D., Perrochet, P., 2000. Direct simulation of groundwater transit-time distributions using the reservoir theory. Hydrogeology Journal, 8(2): 200-208.

Goswami, D., Kalita, P.K., 2009. Simulation of base-flow and tile-flow for storm events in a subsurface drained watershed. Biosystems Engineering, 102(2): 227-235.

Haitjema, H.M., 1995. On the residence time distribution in idealized groundwatersheds. Journal of Hydrology, 172(1-4): 127-146.

Harbaugh, A.W., Banta, E.R., Hill, M.C., McDonald, M.G., 2000. MODFLOW-2000, the U.S. Geological Survey modular ground-water model -- User guide to modularization concepts and the Ground-water flow process: U.S. Geological Survey Open-File Report 00-92. Reston, VA, pp. 121.

Helmke, M.F., Simpkins, W.W., Horton, R., 2005. Fracture-controlled nitrate and atrazine transport in four Iowa till units. Journal of Environmental Quality, 34(1): 227-236.

Hollander, M., Wolfe, D.A., 1999. Nonparametric statistical methods. Wiley-Interscience.

Horton, R.E., 1945. Erosional development of streams and their drainage basins; hydrophysical approach to quantitative morphology. Geological Society of America Bulletin, 56(3): 275-370.

Jindal, P., 2010. A study of the groundwater travel time distribution at a rural watershed in Iowa: A systems theory approach to groundwater flow analysis, Ph.D. thesis, Iowa State University, Ames, IA, 202 pp.

Katz, B.G., 2004. Sources of nitrate contamination and age of water in large karstic springs of Florida. Environmental Geology, 46(6-7): 689-706.

Kauffman, L.J., Baehr, A.L., Ayers, M.A., Stackelberg, P.E., 2001. Effects of land use and travel time on the distribution of nitrate in the Kirkwood-Cohansey Aquifer System in southern New Jersey: U.S. Geological Survey Water-Resources Investigations Report 01-4117, Reston, VA, pp. 49.

Kelly, B.P., 2004. Simulation of ground-water flow, contributing recharge areas, and ground-water travel time in the Missouri River Alluvial Aquifer near Ft. Leavenworth, Kansas: U.S. Geological Survey Scientific Investigations Report 2004– 5215, Reston, VA, pp. 70.

Luo, W., Grudzinski, B.P., Pederson, D., 2010. Estimating hydraulic conductivity from drainage patterns-A case study in the Oregon Cascades. Geology, 38(4): 335-338.

Montgomery, D.R., Dietrich, W.E., 1989. Source areas, drainage density, and channel initiation. Water Resources Research, 25(8): 1907-1918.

Nash, D.J., 1996. Groundwater sapping and valley development in the Hackness hills, north Yorkshire, England. Earth Surface Processes and Landforms, 21(9): 781-795.

Pabich, W.J., Valiela, I., Hemond, H.F., 2001. Relation between DOC concentration and vadose zone thickness and depth below water table in groundwater of Cape Cod, U.S.A. Biogeochemistry, 55(3): 247-268.

Pederson, D.T., 2001. Stream piracy revisited: A groundwater-sapping solution. GSA Today, 11(9): 4-10.

Pionke, H.B., Urban, J.B., 1985. Effect of agricultural land use on ground-water quality in a small Pennsylvania watershed. Ground Water, 23(1): 68-80.

Pollock, D.W., 1988. Semianalytical computation of path lines for finite-difference models. Ground Water, 26(6): 743-750.

Pollock, D.W., 1994. User's guide for MODPATH/MODPATH-PLOT, version 3: A particle tracking post-processing package for MODFLOW, the U.S. Geological Survey finite-difference ground-water flow model: U.S. Geological Survey Open-File Report 94-464, Reston, VA, pp. 237.

Prior, J.C., 1991. Landforms of Iowa. University of Iowa Press, Iowa City, IA.

Puckett, L.J., Hughes, W.B., 2005. Transport and fate of nitrate and pesticides: Hydrogeology and riparian zone processes. Journal of Environmental Quality, 34(6): 2278-2292.

Renken, R.A., Patterson, R.D., Orzol, L.L., Dixon, J., 2001. Approach for delineation of contributing areas and zones of transport to selected public-supply wells using a regional ground-water flow model, Palm Beach County, Florida: U.S. Geological Survey Water-Resources Investigations Report 01-4158, Reston, VA, pp. 216.

Rodriguez-Iturbe, I., Rinaldo, A., 1997. Fractal river basins: chance and self-organization. Cambridge University Press, Cambridge, U.K.

Rovey II, C.W., 1998. Digital simulation of the scale effect in hydraulic conductivity. Hydrogeology Journal, 6(2): 216-225.

Rozemeijer, J.C., Broers, H.P., 2007. The groundwater contribution to surface water contamination in a region with intensive agricultural land use (Noord-Brabant, the Netherlands). Environmental Pollution, 148(3): 695-706.

Scanlon, B.R., Reedy, R.C., Bronson, K.F., 2008. Impacts of land use change on nitrogen cycling archived in semiarid unsaturated zone nitrate profiles, Southern High Plains, Texas. Environmental Science & Technology, 42(20): 7566-7572.

Schilling, K.E., 2009. Investigating local variation in groundwater recharge along a topographic gradient, Walnut Creek, Iowa, USA. Hydrogeology Journal, 17(2): 397-407.

Schilling, K.E., Hubbard, T., Luzier, J., Spooner, J., 2006. Walnut Creek watershed restoration and water quality monitoring project: final report. Iowa Department of Natural Resources, Geological Survey Bureau Technical Information Series 49, Iowa City, IA, pp. 124.

Schilling, K.E., Jacobson, P., 2008. Groundwater nutrient concentrations near an incised midwestern stream: effects of floodplain lithology and land management. Biogeochemistry, 87(2): 199-216.

Schilling, K.E., Wolter, C.F., 2000. Application of GPS and GIS to map channel features in Walnut Creek, Iowa. Journal of the American Water Resources Association, 36(6): 1423-1434.

Schilling, K.E., Wolter, C.F., 2001. Contribution of base flow to nonpoint source pollution loads in an agricultural watershed. Ground Water, 39(1): 49-58.

Schilling, K.E., Zhang, Y.K., Drobney, P., 2004. Water table fluctuations near an incised stream, Walnut Creek, Iowa. Journal of Hydrology, 286(1-4): 236-248.

Schulze-Makuch, D., Cherkauer, D.S., 1998. Variations in hydraulic conductivity with scale of measurement during aquifer tests in heterogeneous, porous carbonate rocks. Hydrogeology Journal, 6(2): 204-215.

Shoemaker, W.B. et al., 2004. Comparison of estimated areas contributing recharge to selected springs in North-Central Florida by using multiple ground-water flow models: U.S. Geological Survey Open-File Report 03-448, Reston, VA, pp. 32.

Solomon, D.K., Poreda, R.J., Cook, P.G., Hunt, A., 1995. Site characterization using $^{3}H/^{3}He$ ground-water ages, Cape Cod, MA. Ground Water, 33(6): 988-996.

Spitz, F.J., Nicholson, R.S., Pope, D.A., 2001. A nested rediscretization method to improve pathline resolution by eliminating weak sinks representing wells. Ground Water, 39(5): 778-785.

Strahler, A.N., 1952. Dynamic basis of geomorphology. Geological Society of America Bulletin, 63(9): 923-938.

Strahler, A.N., 1957. Quantitative analysis of watershed geomorphology. Transactions of the American Geophysical Union, 38(6): 913-920.

Tesoriero, A.J., Spruill, T.B., Mew, H.E., Farrell, K.M., Harden, S.L., 2005. Nitrogen transport and transformations in a coastal plain watershed: Influence of geomorphology on flow paths and residence times. Water Resources Research, 41(2).

Troch, P.A., Detroch, F.P., Mancini, M., Wood, E.F., 1995. Stream network morphology and storm response in humid catchments. Hydrological Processes, 9(5-6): 575-587.

Visser, A., Heerdink, R., Broers, H.P., Bierkens, M.F.P., 2009. Travel time distributions derived from particle tracking in models containing weak sinks. Ground Water, 47(2): 237-245.

Vogel, J.C., 1967. Investigation of groundwater flow with radiocarbon. In: Isotopes in Hydrology. IAEA-SM-83/24, Vienna: 355–369.

Weisbrod, T.S., 2005. Modeling the influence of land use on shallow groundwater flow and nitrate transport, Neal Smith National Wildlife Refuge, Jasper county, Iowa, M.S. thesis, University of Iowa, Iowa City, IA, 136 pp.

Zheng, C., 1994. Analysis of particle tracking errors associated with spatial discretization. Ground Water, 32(5): 821-828.

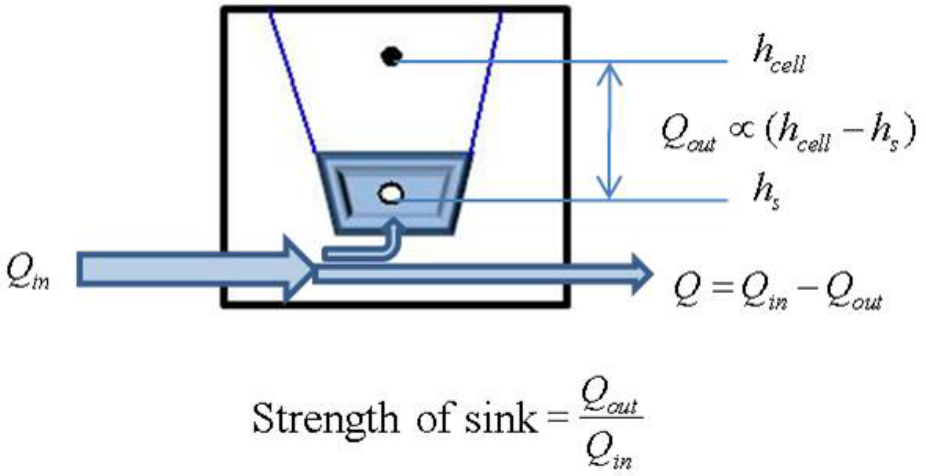

Fig. 21. Representative model cell containing a sink to demonstrate the concept of sink strength

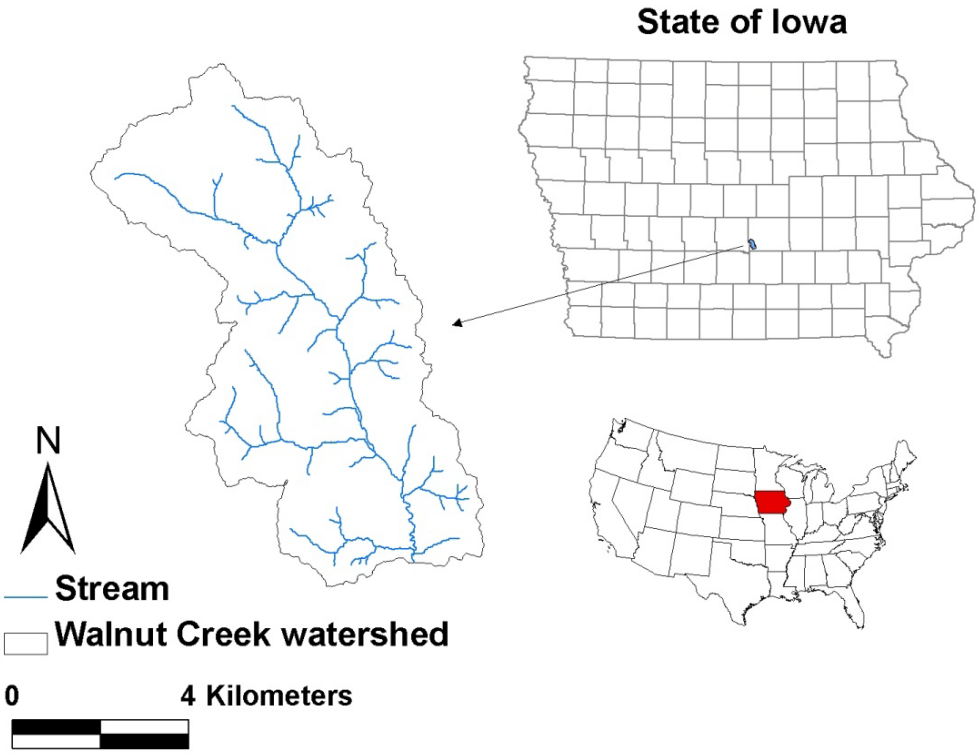

Fig. 22. Site location

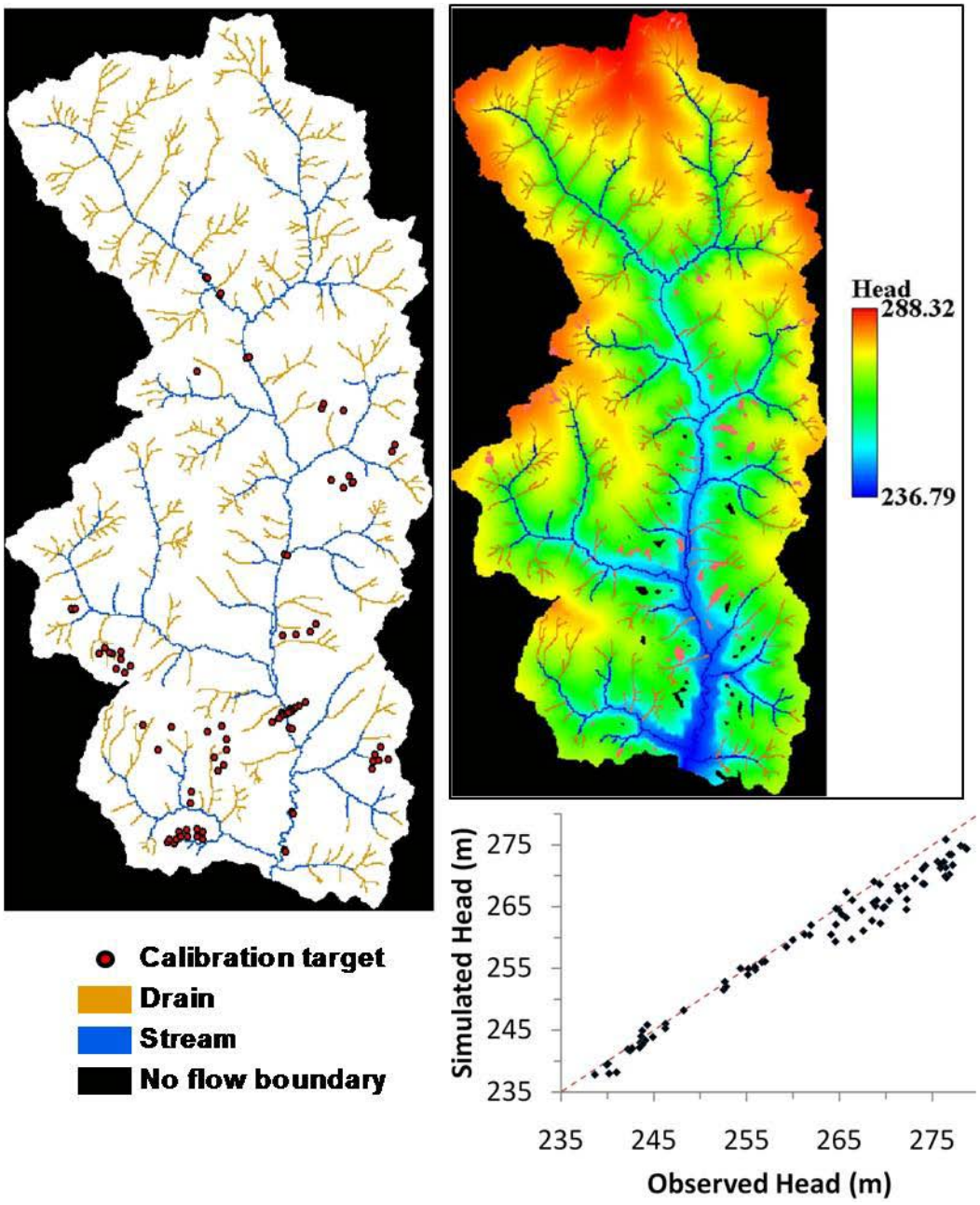

Fig. 23. MODFLOW model: boundary conditions and calibration target locations (left), distribution of hydraulic head (in meters, red and black spots represent stray flooded and dry cells, respectively) (top right); and final calibration plot (bottom right).

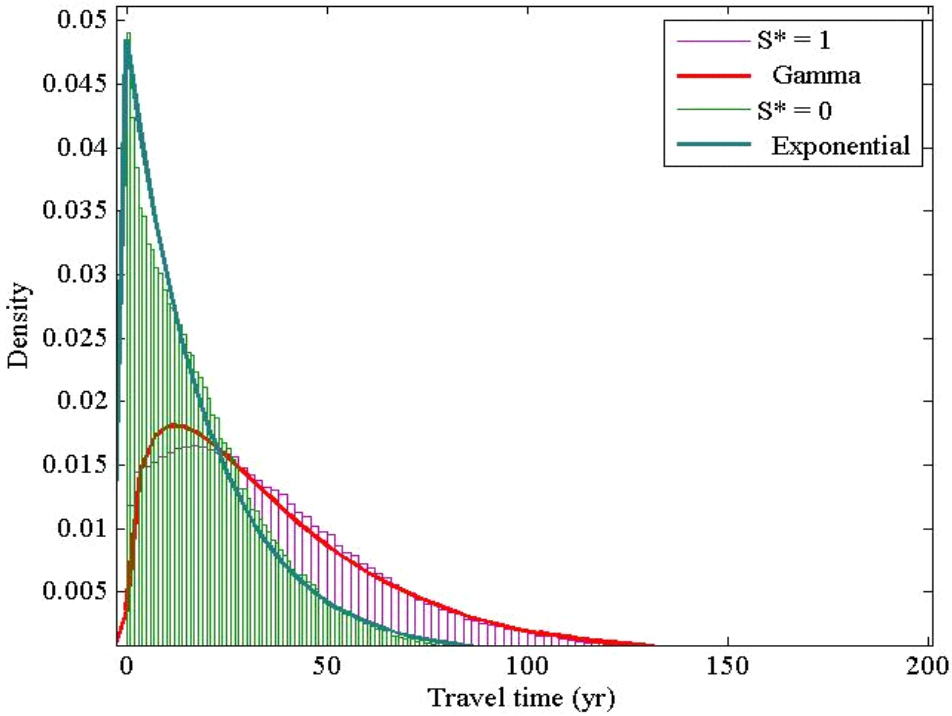

Fig. 24. MODFLOW travel time distributions for the sink strength threshold (S*) values 0 and 1, along with their best-fit probability density functions, an exponential and a gamma distribution, respectively.

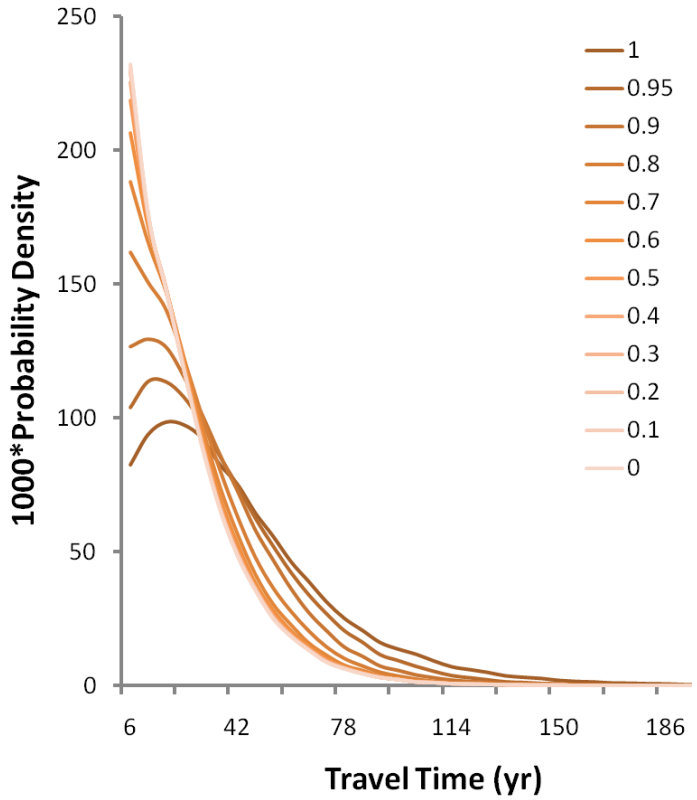

Fig. 25. Impact of the sink strength threshold parameter (S*) on the MODFLOW TTD. The model was run for different values of S* (listed in the legend). The distributions are normalized to 1000 particles.

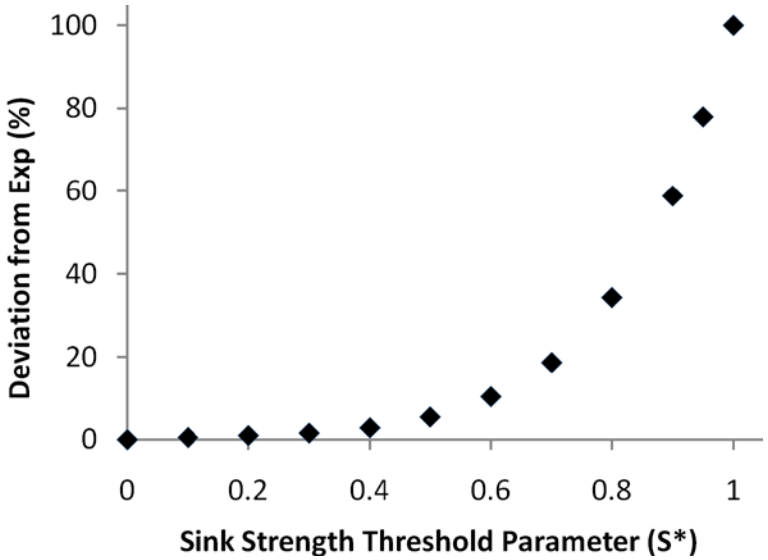

Fig. 26. Deviation in the TTD shape from the exponential shape of the baseline TTD (S*=0) as a function of the sink strength threshold parameter (S*)

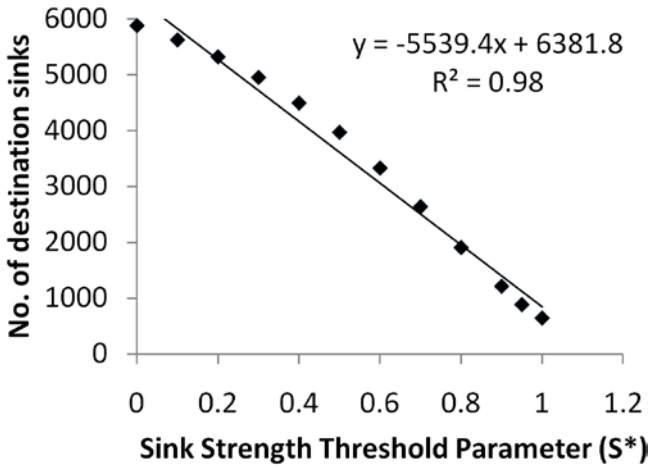

Fig. 27. A decrease in the number of destination sinks with increase in the sink strength threshold (S*) indicates the increase in bypass flow

Table 4. Summary of the characteristic time scales, average sink depth, and effective bifurcation ratio (R_b) values associated with TTDs obtained from model runs using different values of the sink strength threshold parameter (S*)

S*	Mean (yr)	Median (yr)	Maximum (yr)	Minimum (yr)	Standard deviation (yr)	Average sink depth (m)	Effective R_b
1.0	40.20	32.47	342.69	0.12	33.1	10.81	1.503
0.95	33.68	27.65	342.69	0.12	27.225	9.83	1.807
0.9	29.34	24.14	228.24	0.12	23.29	8.74	2.099
0.8	25.17	20.2	226.75	0.12	20.76	7.32	2.481
0.7	22.85	17.96	226.75	0.12	19.6	6.11	2.703
0.6	21.78	16.84	226.75	0.12	19.2	5.32	2.887
0.5	21.18	16.23	226.75	0.12	18.99	4.71	3.022
0.4	20.86	15.9	226.75	0.12	18.87	4.31	3.100
0.3	20.71	15.73	226.75	0.12	18.78	4.00	3.135
0.2	20.63	15.67	226.75	0.12	18.74	3.8	3.173
0.1	20.57	15.6	226.75	0.12	18.71	3.66	3.202
0	20.51	15.55	226.75	0.12	18.69	3.55	3.214

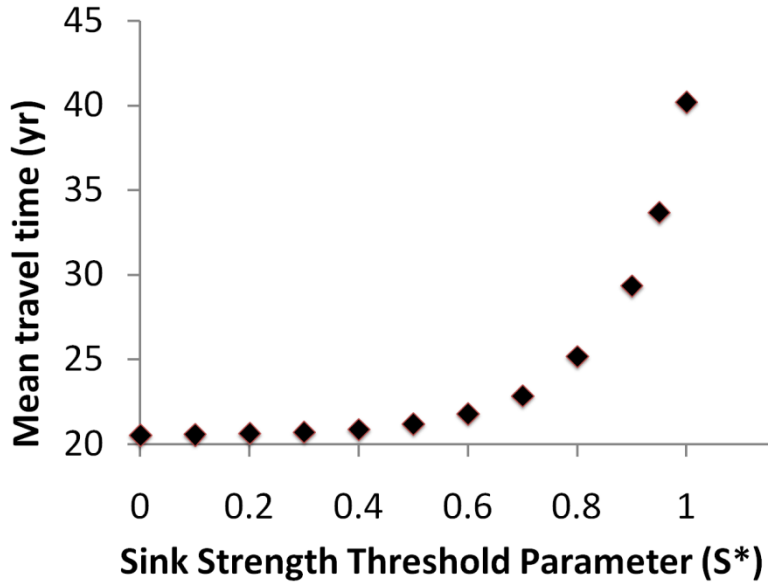

Fig. 28. Impact of the sink strength threshold parameter (S*) on the mean of the travel time distribution

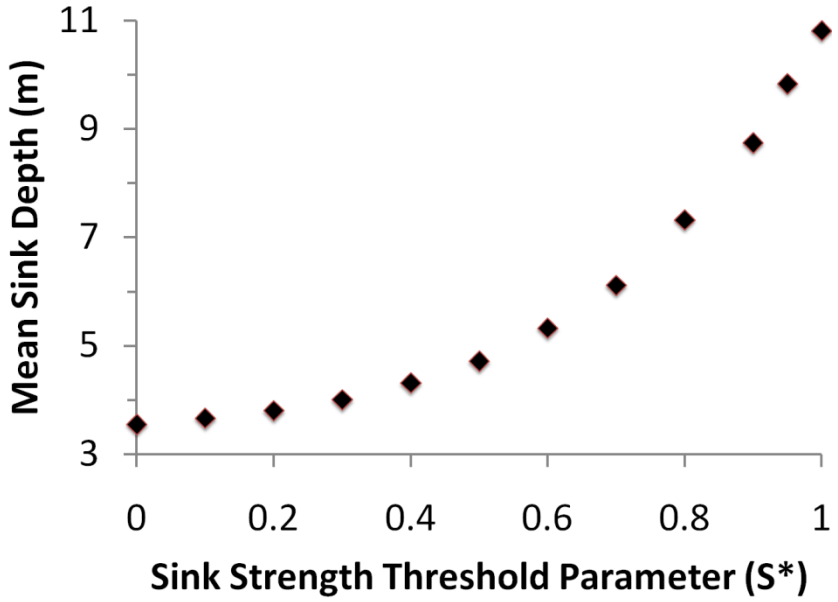

Fig. 29. Relation between the depth of flow (represented by the mean depth of sinks at all discharge locations) and the strength of all active sinks (represented by their lower bound, the sink strength threshold S*)

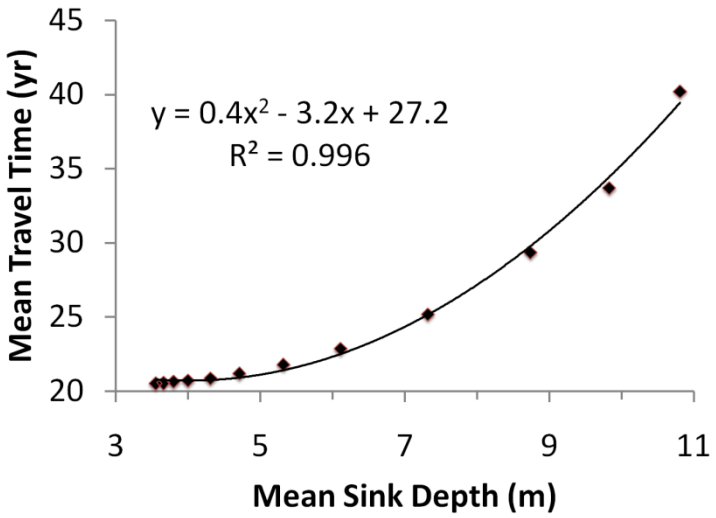

Fig. 30. Variation of the mean travel times with depth of flow (as measured by the average depth of active sinks)

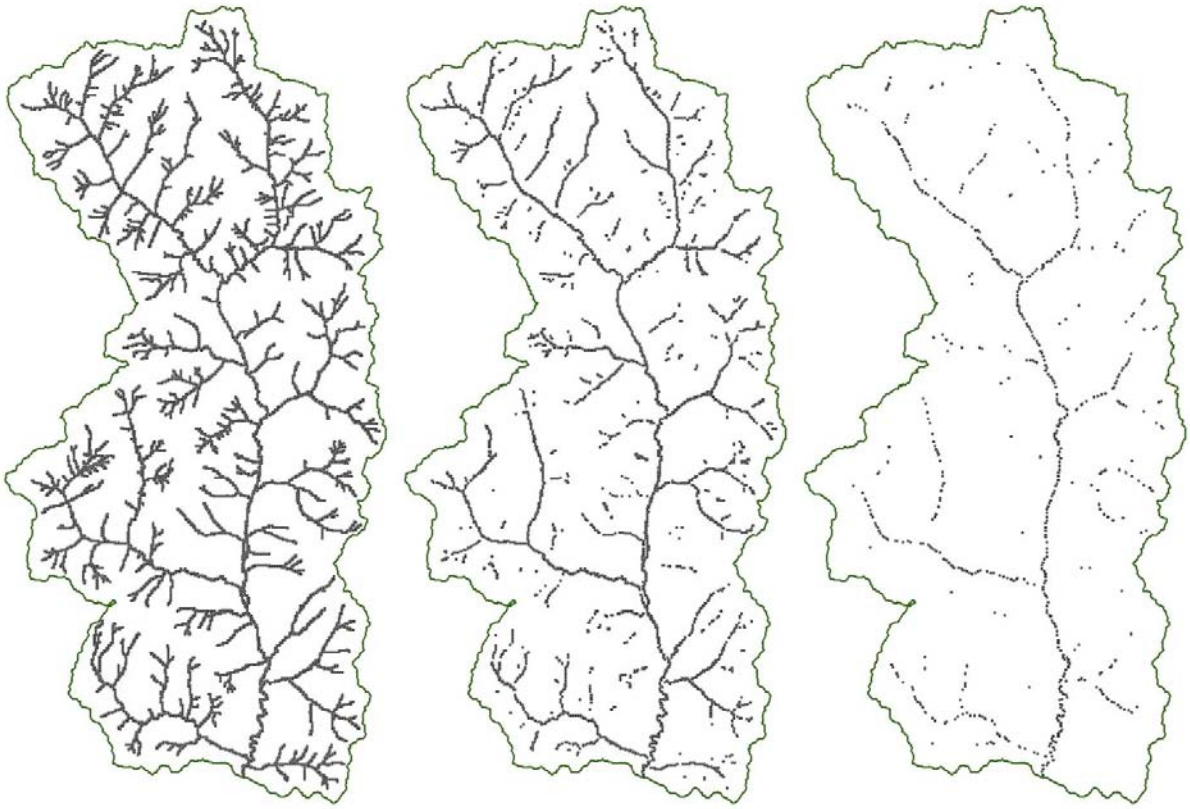

Fig. 31. Spatial distribution of the active sinks in the model at the low end (S*=0, left), intermediate (S*=0.5, center), and high end (S*=1, right) extremities of the sink strength threshold (S*). The sinks are buffered by 5 m to assist visibility.

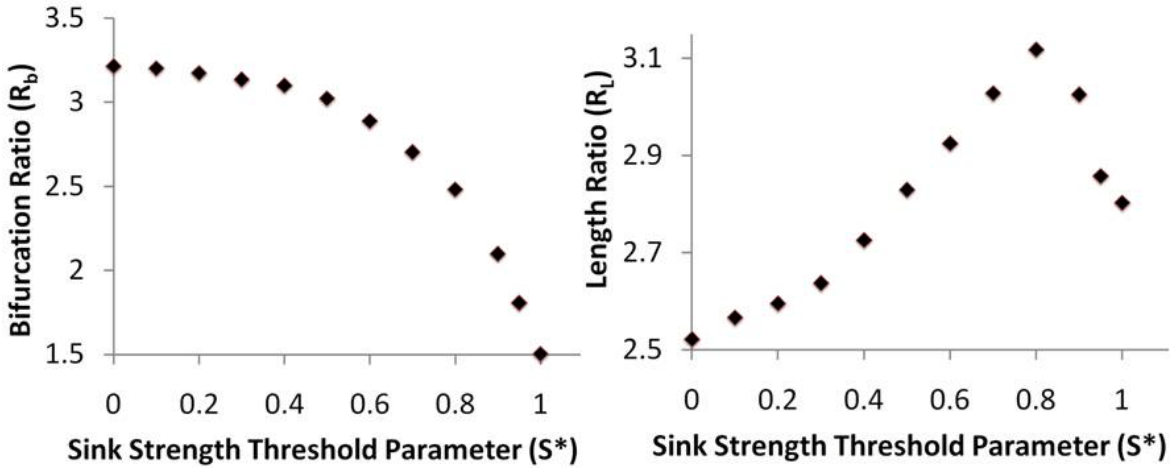

Fig. 32. Dependence of the structural parameters of the effective sink network on the sink strength threshold (S*)

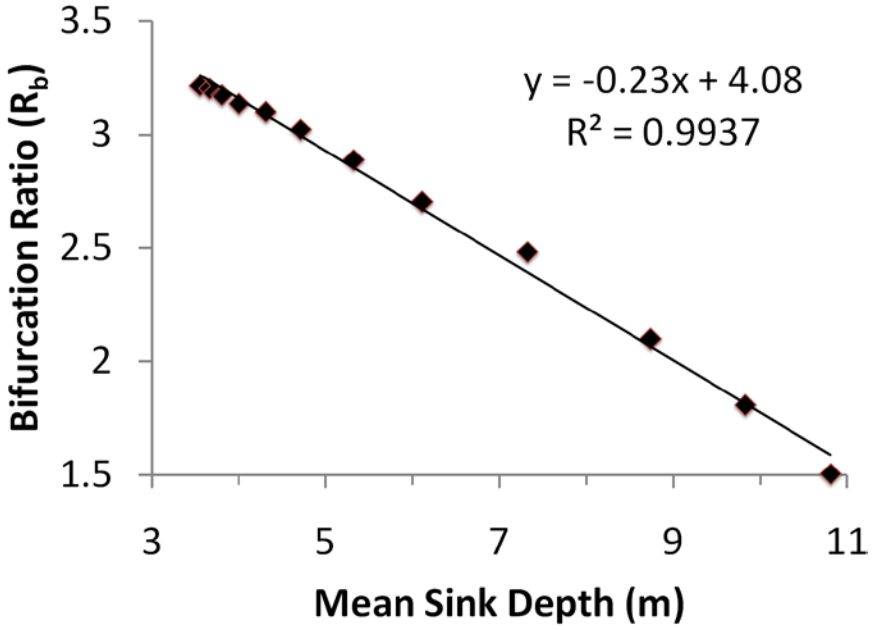

Fig. 33. Variation in the bifurcation ratio, R_b, of the effective sink network that is apparent to flow as a function of the average depth of the flow in the watershed (quantified in terms of the average depth of active sinks). Note that the best-fit linear trendline captures the variation of R_b for this particular range of flow depths only, since R_b cannot become nonpositive with increasing depth.

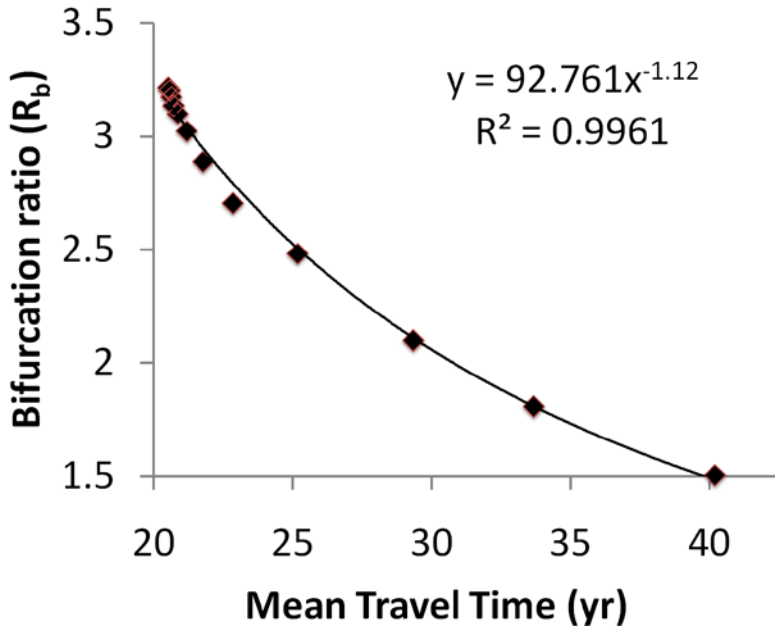

Fig. 34. Relation between the mean travel time of flow and the structure of the sink network visible to the flow (quantified in terms of the bifurcation ratio R_b). The best-fit curve was a power law with the value of the exponent very close to -1.

V. Impact of artificial subsurface drainage network density and incision depth on groundwater travel times and baseflow at the watershed scale

Adapted from a paper to be submitted to *Journal of Hydrology*

Priyanka Jindal, Keith E. Schilling, Nandita Basu, Matthew J. Helmers

Abstract

We analyzed the impact of artificial subsurface drainage networks on the groundwater hydrology at a representative watershed. This was done by simulating the impact of hypothetical tile drainage networks with variable tile drainage density and incision depths on groundwater travel times and proportion of baseflow captured by the tile drains using a two dimensional, steady state groundwater flow model at a representative watershed. In all simulated scenarios, the distribution of groundwater transit times was best represented by an exponential distribution with variable values of the decay constant. Variation in the tile drainage density from 0 to 0.0038 m^{-1}, while maintaining a constant tile incision depth at 1.2 m, caused the mean travel time to decrease exponentially from 40.29 years and tend towards a lower bound of 19.20 years asymptotically. The scale parameter of this trend represented a characteristic drainage density equal to 0.00104 m^{-1}. Increasing tile drainage density increased the tile contribution to baseflow from 0% to an upper bound of 37.27% that the system approached asymptotically. The characteristic scale parameter of the best fit to the trend was 0.00119 m^{-1}. The similar form of the trend (exponential) observed in both dependent variables as a function of tile drainage density suggested an inverse correlation between them that was found to be approximately linear (with a slope of -0.52 years). Variation in the tile incision depth from 0.3 to 2.7 m, while maintaining a constant tile

drainage density of 0.0038 m^{-1}, caused mean travel time to decrease linearly from 21.54 to 18.05 years. The best-fit slope and y-intercept were -1.45 yr/m and 21.96 years, respectively. A conceptual analysis of this relation produced a slope and y-intercept of -1.54 yr/m and 15.45 years, respectively, that were found to be in close agreement with the simulated results. Increasing tile incision depth increased the tile contribution to baseflow from 29.94% to 54.44% in a near-linear manner. The best-fit slope and y-intercept were 10.45m^{-1} and 24.88% respectively. The similar form of the trend (linear) observed in both variables as a function of tile incision depth was again suggestive of an inverse correlation that was found to be close to linear. The best-fit slope of -0.14 years was significantly smaller in magnitude than the best-fit slope of the inverse correlation observed between the two variables in the case of variable tile drainage density. The results qualitatively suggested that tile incision depths have a stronger impact on the volume of baseflow captured by tiles than groundwater travel times. On the other hand, tile drainage density, impacted groundwater travel times more strongly than the tile outflow volume. Thus, the impact of the tile network on the hydrology of the watershed is likely to vary depending on the specific network parameter and dependent hydrologic variable being considered, though the overall impact of the network parameters might be similar, in this case it being the fact that increases in both drainage density and incision depths cause an overall decrease in groundwater travel times and increase in the tile contribution to baseflow.

5.1. Introduction

Amongst the myriad variables affecting the groundwater hydrology of a watershed, such as precipitation, soil properties, land surface topography, watershed size and shape, stream

channel morphology, artificial drainage network structure and properties, intrinsic aquifer properties, etc; subsurface artificial drainage is known to have a great impact on the hydrology of a system (Blann et al., 2009). Yet, a quantification of its environmental impact at the watershed scale is not well documented (Eidem et al., 1999).

Flow from subsurface artificial drainage channels is a major component of baseflow (Schilling and Helmers, 2008). A study of the baseflow trends of the rivers in the state of Iowa revealed significant increases in their contribution to total streamflow in the second half of the 20th century that was concluded to be partly sourced from increasing contributions from the artificial drainage network (Schilling and Libra, 2003). Therefore, in the context of nonpoint source pollution, flow from subsurface tile drainage is likely to have a great impact on the overall water quality of a stream. Focusing specifically on stream water quality degradation due to nitrate losses from agricultural landscapes, it has been observed that groundwater discharge in the form of direct baseflow and that derived from tile drains is the primary medium of nitrate transport to surface waters (Hallberg, 1987; Schilling, 2002; Schilling and Zhang, 2004). High nitrate loads have degraded water quality to the extent of impacting its use by industry, agriculture, municipal water supplies, amongst many other users. It has created the problem of nutrient enrichment of the stream and ocean waters that has led to a degradation of the aquatic ecosystem in terms of eutrophication, fish kills, loss of biodiversity, hypoxia, and other associated problems (Carpenter et al., 1998; Rabalais, 1998; Bricker et al., 1999). Therefore, a scientific evaluation of the impact of tile drainage on various hydrologic aspects of the watershed, especially in the context of agricultural landscapes, is essential for the design and development of best management practices that can protect and restore the surface water quality in the region (Tomer et al., 2003).

Among the various factors influencing the magnitude of nitrate losses to streams through the medium of subsurface drainage in agricultural watersheds, such as precipitation; soil mineralization; the rate of timing of nitrogen fertilizer application; choice of cropping and tillage systems; conservation practices like cover crops and vegetative filter strips; etc, the design of the subsurface drainage network is one factor that can be controlled and optimized so as to minimize nitrate losses to the stream (Randall and Goss, 2008). The tile drain spacing and incision depth are two important design parameters that determine the structure of the tile drainage network. Therefore, a research to assess the hydrologic impact of tile drain spacing and incision depth in a tile-drained agricultural watershed is necessary to help decision makers choose the best drainage design and management practices that will strike an optimum balance between the economic and environmental interests of the stakeholders and community at large.

One key aspect of the hydrologic impact of artificial subsurface drainage on watershed hydrology is its effect on the travel times associated with groundwater contaminant transport within the watershed (Molénat et al., 2000). The distribution of groundwater travel times in a watershed is a critical factor that determines the success of the various conservation and remediation practices targeted to decrease nitrate losses to surface water (Meals et al., 2010). The distributed impact of such practices implemented at the land surface can only be realized at the stream when the groundwater flow system has transmitted the change from the land surface to the discharge location, be it a tile inlet or a stream reach. Thus, a study of the impact of tile drainage on this hydrologic parameter is considered essential to the estimation of the time scales involved in a watershed improvement plan, and to the evaluation of the efficacy of such practices.

Studies by a number of authors have also documented the hydrologic impact that changes in tile drain spacing and depth have on tile outflow volumes (Kladivko et al., 2004; Skaggs and Chescheir, 2003; Burchell et al., 2003; Davis et al., 2000; Nangia et al., 2010). These studies demonstrated the positive correlation between tile outflow volumes and nitrate losses; an increase in the outflow through tiles is observed to increase nitrate losses to the stream. Thus, the impact of tile drainage network properties on tile outflow volumes at the watershed scale would be highly valuable in the estimation of nitrate losses to stream in a given watershed. Moreover, some of these studies (Skaggs and Chescheir, 2003; Burchell et al., 2003; Nangia et al., 2010) considered the combined impact of varying tile drain spacing and depth on the outflow volumes and nitrate losses. Their results suggest that an optimal analysis of tile network design should account for both degrees of freedom – tile drain spacing and depth.

Our study was designed to meet these requirements and build on the abovementioned research studies by conducting an analysis of the impact of tile network parameters at the watershed scale. We also sought to meet the scientific goals outlined earlier that expressed the need to quantify the hydrologic impact of subsurface drainage, especially on groundwater travel times, at the watershed scale. This was done by quantifying the systematic trend in both the groundwater travel times and the volume of baseflow, as a function of both tile drainage density and incision depth for a representative watershed, the Walnut Creek watershed, located in South Central Iowa.

This was done using a calibrated groundwater flow model of the two dimensional, steady state groundwater flow at the watershed. The two parameters characterizing the tile network, namely, the tile drainage density and incision depth, were treated as independent variables,

whose impact was assessed on two dependent variables that characterize the hydrology of the watershed, namely, the distribution of groundwater travel times and the fraction of outflow captured by the tile drains. The resultant four relations were qualitatively analyzed in detail to gain insight into the physical factors influencing the hydrologic response. These insights might be of value in the design and selection of best drainage management practices, and in the evaluation of current practices vis-à-vis their impact on the hydrology of the watershed.

Note that we chose to quantify the horizontal extent of the tile network in terms of a tile drainage density instead of tile drain spacing. This was necessary given the specific structure of the tile network present at the Walnut Creek watershed. As opposed to the system of patterned tiling, the current tile network at the Walnut Creek watershed is primarily branched along the first order drainageways, and underlies the grassed waterways in the watershed. This is a recommended design practice for grassed waterways to prevent the buildup of excessive wetness, so as to maintain the vegetative cover, prevent formation of further gullies, and facilitate accessibility to farm equipment (Stone and McKague, 2009; Green and Haney, 2005; NRCS, 2004).

Thus, to analyze the impact of tile drainage density on the hydrology of the watershed we constructed alternative subsurface tile networks branching out along the first order drainageways that underlie the grassed waterways in the watershed. Moreover, given the pattern of the branched tile network, we quantified variations in the extent of the tile drainage network in terms of a branching density, or tile drainage density. The tile drainage density parameter was structured along the same lines as the drainage density parameter that characterizes stream networks in surface water hydrology, was considered to be a more appropriate measure than drain spacing to describe the extent of the branched tile network for

each scenario. Thus, the branching density of the artificial subsurface drainage network, hereafter termed as the tile drainage density for the sake of brevity, was defined as the total tile length per unit watershed area, and was used to symbolize each scenario.

5.2. Site description

The study was conducted at the 51.94 km^2 Walnut Creek watershed in Jasper county, Iowa (Fig. 35). The watershed is located in the Southern Iowa Drift Plain landscape region, an area characterized by steeply rolling hills and well-developed drainage (Prior, 1991). The shallow, unconfined aquifer is a combination of Wisconsinan-age Peoria loess mantles overlying pre-Illinoian oxidized till in the uplands, and Holocene-age alluvial deposits (composed of around 60-80% silt; Schilling et al., 2004) in the floodplain. Intermittent outcrops of Pre-Illinoian oxidized till and Late Sangamon paleosols are found along the side slopes. The 10-11 m deep aquifer is confined by a 6-30 m thick Pre-Illinoian unoxidized till layer whose hydraulic conductivity is estimated to be two orders of magnitude lower than the alluvial-loess aquifer. The impervious unoxidized till layer overlies bedrock comprising Pennsylvanian Cherokee group shale, limestone, sandstone, and coal.

Hydraulic conductivities of the abovementioned stratigraphic units were estimated using multiple sources comprising slug test results (Schilling and Wolter, 2001; Schilling et al., 2004; Weisbrod, 2005) and saturated hydraulic conductivity values of the soils in the Soil Survey Geographic (SSURGO) database of the region. The hydraulic conductivities of loess and alluvium, that have been estimated to be similar (Weisbrod, 2005; Schilling et al., 2004), were assigned a value of 9×10^{-6} m/s based on the values in the SSURGO database. The till and paleosol outcrops also have similar hydraulic conductivities, estimated to range from 2.3

x 10^{-7} m/s based on slug tests to 1.2 x 10^{-6} m/s based on the SSURGO database. Due to lack of field evidence to the contrary, we assumed the vertical and horizontal hydraulic conductivities of all units to be equal.

The watershed's predominantly gaining stream is characterized by a deeply incised channel, with incision depths starting at around 1 m at the tributary headwaters, and steadily increasing in the downstream direction to a depth of around 3 m along the main channel. High channel incision has significantly impacted the watershed hydrology (Schilling and Jacobson, 2008) and is associated with the stream's flashy discharge in response to storm events. An artificial subsurface drainage network at the site is used to drain the water table up to depths of around 1.2 m below the land surface. The drains are primarily branched along the first order drainageways, and underlie the grassed waterways in the watershed. The watershed lies in a humid, continental region with annual precipitation averaging around 850 mm of which a total of around 129 mm reaches the water table (Schilling et al., 2006). Schilling (2009) estimated the recharge reaching the water table to vary with landscape position, with the floodplain receiving maximum recharge, and side slopes receiving the minimum amount, and uplands an intermediate amount. The ratio of recharge reaching the floodplain, side slope, and upland, was estimated to be 44:14:24, respectively.

5.3. Methods

To achieve the abovementioned objectives we chose to quantify the impact of the two independent parameters characterizing tile drainage networks, namely, tile drainage density and incision depth, on two dependent hydrologic variables, namely, groundwater travel times and baseflow. This was done using the methods outlined below.

5.3.1. Groundwater flow model

A two dimensional, steady state groundwater flow model was constructed using MODFLOW-2000 (Harbaugh et al., 2000) and MODPATH (Pollock, 1994). The model is briefly described below. A detailed model description is given in Jindal (2010). The model grid was designed with a horizontal spacing of 20 m, and comprised 628 rows and 300 columns. The top elevation of the single layer model followed the land surface, while its bottom elevation was set to a uniform depth of 11 m. The boundaries of the shallow aquifer were estimated to align with the watershed boundaries. The stream and tile drain boundaries were defined using the RIV and DRN packages, respectively. Streambed sediment hydraulic conductivity and thickness were estimated using data in Schilling and Wolter (2000) and Schilling et al. (2004), and were estimated to be around 5×10^{-5} m/s and lie in the range 0.1-0.4 m, respectively. Drain conductance was selected as 8.7×10^{-4} m^2/s, close to typical literature values (Goswami and Kalita, 2009). The physical and hydrologic boundaries of the model are shown in Fig. 36. Effective porosity used for particle tracking was estimated to be around 0.3 (Helmke, 2005).

Hydraulic conductivity zones were delineated using the parent material index in the SSURGO database (loess, alluvium, till, or paleosol) and assigned values based on multiple data sources comprising slug test results (Schilling and Wolter, 2001; Schilling et al., 2004; Weisbrod, 2005) and the saturated hydraulic conductivity value obtained from the SSURGO database. It was observed that the hydraulic conductivity estimates based on the results from the slug tests consistently produced unrealistically high water table levels that exceeded the land surface elevation. This has been anticipated by a number of authors (Schulze-Makuch and Cherkauer, 1998; Rovey II, 1998) as reflective of the fact that groundwater flow is

impacted by high-conductivity aquifer heterogeneities present at larger flow scales than the scale of flow created by localized slug tests. Indeed, estimates of saturated hydraulic conductivity obtained from the Soil Survey Geographic (SSURGO) database, that were approximately one order of magnitude higher than the slug test values, led to a significant improvement in water table levels across the watershed. Thus, we selected the SSURGO values as baseline estimates, which were then used as calibration parameters during the stage of model calibration.

Recharge zones were delineated using the slope classification for each soil mapping unit in the SSURGO database, and assigned values such that the ratio of the recharges in the uplands to side slopes to floodplain was 24:14:44 (Schilling, 2009). The recharge values were constrained by the condition that the total or equivalent annual recharge over the entire watershed, computed as the area-weighted average of the recharges at each landscape position, be equal to the estimated long-term average value of annual baseflow. The aquifer parameters of groundwater recharge and hydraulic conductivity of the oxidized till zone were then adjusted during the stage of model calibration.

Model calibration was achieved by manual trial and error that produced the best results in comparison to other automated calibration procedures that were tested. The model was calibrated for 84 head targets situated at various locations in the watershed. Amongst the various calibration parameters included, the model was observed to be most responsive to hydraulic conductivity (both, value and spatial distribution) and total recharge. Specifically, the location of the loess-till contact and the hydraulic conductivity value of oxidized till had a significant impact on simulated heads. This hinted towards the presence of a transition zone along the loess-till contact line, with a hydraulic conductivity value that is intermediate

between the corresponding loess and till values. The detailed spatial distribution and value of hydraulic conductivity for each zone is listed in Jindal (2010). The calibrated total or equivalent annual recharge was estimated to be 120 mm, which is slightly lower than the initial estimate of 129 mm (Schilling et al., 2006).

The final calibrated model produced reasonable agreement between the simulated and observed hydraulic head values at the calibration targets (Fig. 36). The absolute residual mean (ARM, the average of the absolute values of the residuals, or the difference between the simulated and observed heads) was 2.55 m, while the residual standard deviation was 2.29 m. The resultant distribution of water table elevations across the watershed is also shown in Fig. 36. For a model of covering an entire watershed of this size (51.94 km^2), an ARM of 2.55 m was considered reasonable. Moreover, for our specific project goals of evaluating the distribution of groundwater travel times, an error in hydraulic head generated at the scale of cell resolution is likely to not impact results significantly. This is because the travel time along the length of a flow path from its origin to the sink, is a cumulative measure that is liable to integrate out possible deviations in hydraulic gradient along its entire length. Furthermore, the travel time distribution was generated by aggregating the travel times of more than 120,000 particles, and then studying the distribution as a whole. Thus, possible errors introduced by some particle traces are likely to have negligible impact on the overall travel time distribution that is generated from a large sample size. These two reasons indicate that the few stray spots of dry and flooded cells (Fig. 36) that remained are expected to have a negligible impact on the distribution of cumulative travel times obtained from a large sample of tracer particles. Hints of the insensitivity of the distribution of cumulative travel times to localized model errors were evident in the earlier stages of model calibration when

the distributions obtained for earlier model runs that had a higher number of dry and flooded cells (with the number of dry cells more than 100% of the number in the final model, and the number of flooded cells being similar) produced nearly the same results as the final calibrated model (with the mean travel time differing by 0.68% only).

Particle tracking in MODPATH was performed by releasing particles at the water table in every cell center of the active model domain and forward tracking them from source to sink. The particle traces were determined with the default value of the sink strength threshold parameter (S*) set to 0. In particle tracking codes like MODPATH, the trace of a particle that enters a cell where the sink captures only a partial amount of the inflow relation cannot be resolved analytically. To overcome this problem, MODPATH defines the strength of a sink as the fraction of cell inflow that is captured by the sink. It then compares this sink strength to a user-defined threshold parameter (S*). All sinks with strength greater than S* are treated as active; the particles stop at such sinks. The remaining sinks are treated as inactive, and particles entering cells containing such sinks simply bypass them. “Strong sinks” are defined as those that capture 100% of the cell inflow. Sinks with strength less than 100% are termed “weak sinks”. Thus, setting S* to 0 simulates the scenario of no bypass flow (both, weak and strong sinks are active), and setting S* to 1 simulates the scenario of maximum bypass flow (by activating only the strong sinks). The tile simulations were generated for the case of no bypass flow (S*=0) so as to incorporate the impact of all sinks, including tile drains that are classified as weak sinks, on the groundwater travel time distribution.

5.3.2. Construction of alternative scenarios of tile drainage density and incision depth

We first constructed alternative scenarios of tile drainage density. Given the fact that the current placement of tile drains in the watershed runs along the first order drainageways

underlying grassed waterways, this was done by mapping all grassed waterways in the watershed using the 2006 National Agriculture Imagery Program (NAIP) aerial photograph of the region. Thirteen such hypothetical scenarios were constructed such that the tile drainage density gradually increased from a minimum of 0 m^{-1} to a maximum of 0.0038 m^{-1}, while maintaining a constant tile incision depth of 1.2 meters. The current extent of the tile network, calibrated against the hydraulic heads across the watershed, corresponds to a tile drainage density of 0.0027 m^{-1}. This was selected as the baseline drainage density scenario. Fig. 37 shows three such simulated tile density scenarios - the drainage pattern extent for the baseline, low and high end drainage density simulations. The values of the simulated drainage densities are listed in Table 5.

The dependence of travel times and tile contribution to baseflow on tile incision depth of the tile network was then explored by fixing the tile drainage density to an arbitrary constant value (equal to 0.0038 m^{-1}), and systematically varying the incision depth from the baseline incision depth of 1.2 m, in steps of 0.3 m. Thus, we tested eight scenarios with variable tile incision depths, the values of which are listed in Table 6 (the missing scenario at the tile incision depth of 1.5 m was found to experience problems with solver convergence). Note that the simulated values of incision depths were restricted to plausible scenarios comprising a small range of incision depths (0 to 2.7 m). This was done so as to maintain resemblance to realistic drainage network conditions in agricultural watersheds, where incision depths are generally limited to shallow depths.

Separate MODFLOW models were run for each of the generated networks. The change in the proportion of baseflow being contributed by tiles was documented using the water balance summary of each model run. The relative contribution of tiles to total outflow was

quantified in terms of a capture fraction, Q_T, that was defined as the ratio of the outflow volume captured by the tile drains to the total outflow volume. Note that in a steady state model, the total amount of outflow is a constant that equals the total amount of flow entering the aquifer. Therefore, a change in Q_T is physically equivalent to a change in the absolute outflow exiting via the tile drains. Both variables will be influenced by the same physical factors therefore an analysis of either of the two variables is justified. We chose to analyze the behavior of the capture fraction, Q_T, as a function of variable tile drainage density and incision depth. The resulting trends were reflective of the behavior of both the capture fraction as well as the discharge volume that is captured by the tile network, and were therefore interpreted keeping both variables in mind.

Thereafter, particles were uniformly released at the water table across the entire watershed and tracked using MODPATH for each simulation. MODPATH results were processed to obtain the TTD corresponding to each scenario, that were subsequently analyzed to determine the response of the groundwater travel times to changes in tile drainage density and incision depth. Furthermore, we performed a conceptual analysis of the impact that tile incision depth has on groundwater travel times. The analysis yielded results that were found to agree well with those obtained from the simulation.

5.4. Results and Discussion

5.4.1. Impact of tile drainage density on travel times

Simulations based on the thirteen alternative tile density scenarios generated distributions of groundwater travel time that were best represented by an exponential distribution characterized by varying values of the decay constant. Fig. 38 shows a comparison of the

TTDs obtained at maximum and minimum tile densities. As anticipated, increasing tile density increased the overall proportion of short transit times across the watershed. But both distributions were observed to conform to an ideal exponential distribution. Thus, variation of drainage density did not change the characteristic shape of the TTD that stayed close to an ideal exponential distribution through the entire range of drainage densities simulated. Indeed, for each scenario, the quality of fit was attested by the equality between the best-fit scale parameter and the mean of the empirical distribution for almost all the scenarios, as well as the relatively small value of the standard error (Table 5).

The strong match between the empirical distributions and an exponential was also reflected in the comparison of the values of standard deviation and coefficient of variation (Table 5). Although the standard deviation of the distributions decreased by 65%, from 53.16 years to 18.50 years, this did not result in a proportionate change in the coefficient of variation, that hovered close to the theoretical value of 1 for an ideal exponential distribution, and decreased only slightly from 1.319 to 0.914. In other words, much of the variation in travel times due to changes in tile drainage density can be ascribed to a scaling of the distribution of travel times by their mean.

Examining the statistics defining the distributions revealed similar behavior in both the median and mean travel times as shown in Table 5. Both variables were observed to decrease with increasing tile drainage densities, though the impact was observed to be stronger on the latter. Mean travel time was observed to decrease by around 50% from 40.29 to 20.23 years, while the median travel time decreased by a smaller proportion (around 33%) from 22.98 to 15.35 years. This difference in the two trends can be ascribed to the positive skew of the travel time distribution. In other words, the sharper reaction observed in the mean relative to

the median of the travel times indicates that the tail-end long transit times of the positively skewed distribution decreases significantly in response to an increase in the drainage density of the tile network. This impact was also demonstrated in the dramatic decrease in the maximum travel time from a value greater than 750 years for the lowest drainage density to around 250 years for the higher drainage density scenarios.

Thus, the overall travel times across the watershed were observed to respond strongly to alterations in tile drainage. However, their pace of decrease due to increasing tile drainage density was observed to vary sharply over the simulated density range. Initially, as drainage density was increased, the travel times were observed to decrease at a rapid pace. But the impact was observed to diminish as drainage densities were increased further. An analysis of the variation in the mean travel time showed that initial increases in tile drainage density, from 0 to 0.0015 m^{-1}, decreased the mean from 40.29 to 24.52 years, a change of 15.77 years. Further increase in the drainage density by 0.0023 m^{-1} (from 0.0015 to 0.0038 m^{-1}) decreased the mean travel time by 4.29 years only (from 24.52 to 20.23 years). A decrease of 4.29 years accounts for only 21.4% of the total decrease in mean travel time simulated by the model (from 40.29 to 20.23 years), even though it corresponds to more than 60% of the total simulated increase in drainage density.

This motivated a deeper analysis of the trend in the mean travel time (Fig. 39). We found that at small tile drainage densities, there was a rapid decrease in the mean travel time as tile drainage density was increased. Beyond a certain density range there was a definitive slow down in the rate of change in the mean travel time. The variation of the mean travel time with respect to drainage density was best fit by a decaying exponential curve ($R^2 = 0.9663$). This suggests that the range of the groundwater travel times in the watershed are restricted to

a range that is determined by an initial maximum value and a lower bound, that it approaches asymptotically as tile density is increased further and further.

The inverse of the best-fit decay constant constituted a characteristic tile drainage density parameter for the watershed that was found to equal 0.00104 m^{-1}. Physically, this parameter demonstrates that the marginal impact of increasing tile lengths on the distribution of travel times diminishes dramatically beyond a certain characteristic value of tile drainage density. The value of this characteristic tile density beyond which groundwater travel times are less sensitive to variation in drainage densities will be unique to every watershed, and will depend on specific attributes of the watershed that are yet unknown, and subject to further examination.

The form of the best-fit curve also suggested that at very high tile densities the mean travel time starts to asymptote to a constant value that was found to be 19.2 years for the simulated flow system. Physically, this indicates that beyond a certain point additional tile length is simply ineffective in capturing more particles and decreasing travel times further. In other words, tiles placed at a fixed (typically, shallow) incision depth cannot reduce travel time below a certain lower bound, no matter how high their density. This is because increasing drainage density causes the water table levels to decline. Once the water table falls to a level below the elevation of the tile drain, the latter becomes ineffective in capturing more flow. Note that these results are in the specific context of steady-state travel times. It is likely that transient travel times will continue to capture transient flow, and therefore be impacted by increasing tile densities to a greater extent.

In light of the abovementioned physical reason that causes the watershed mean travel time to approach a finite lower bound, we might anticipate the existence of a correlation

between groundwater travel times and the amount of inflow that is captured by the tile drains. This possible relationship is explored in a later section. Furthermore, the link between the specified elevation or incision depth of the tile drain and the point beyond which the drain fails to intercept the water table, suggests that the values of the lower asymptote of mean travel time, and in fact the mean travel times at each drainage density, should vary systematically with incision depth. The relation between travel times and tile incision depth was investigated further, the results of which are also presented in a later section.

5.4.2. Impact of tile drainage density on tile contribution to baseflow

The relative contribution of tiles to total outflow was quantified in terms of a capture fraction, Q_T, that was defined as the ratio of the outflow volume captured by the tile drains to the total outflow volume. Fig. 40 shows the trend in Q_T as a function of drainage density.

Interpreting in terms of both the outflow volumes and capture fraction, we observed that increasing the drainage density in the system increased the volume and proportion of flow exiting through the tile drains. The fraction of flow captured by the tiles was found to rise from by 35.8%. But this increase was nonlinear, with initial incremental increase in tile length capturing inflow at a significant pace. Further increases in tile density lead to a decrease in the efficacy of the drainage network to capture more inflow. Indeed, an initial increasing in the drainage density by 0.0015 m^{-1} was observed to increase the baseflow by 26.5%. However, a subsequent increase of 0.0023 m^{-1}, accounting for more than 60% of the total simulated range of drainage density density, caused a further increase in the baseflow contribution of tiles by only 9.3%, that was around one-fourth or 25% of the total simulated increase (from 0 to 35.8%).

Thus, the marginal impact of tile drainage density on the baseflow contribution of tiles fell dramatically as drainage density was increased. Indeed, the plateau in the trend at the higher end of tile densities suggested that beyond a certain range of drainage densities, further additions to the tile length were ineffective and were not able to capture further inflow. Note that these results have been obtained for the case of steady state flow; it is likely that increased drainage densities would continue to capture an increasing amount of the transient component of total inflow.

The nonlinear trend was best described by an exponential best-fit curve ($R^2 = 0.9841$), that approached saturation as drainage density was further increased. Thus, much like groundwater travel times in the watershed, the fraction of outflow captured by the tile drains was confined to a finite range of values lying between zero (no contribution to total outflow at zero drainage density) and a maximum upper bound of 37.27%. The system approached this upper bound asymptotically as the simulated drainage network was represented by the higher end values of drainage density.

The underlying physical causes creating this trend are the same as those influencing the nonlinear variation in groundwater travel times as a function of tile drainage density. In other words, as discussed in the previous section, watershed travel times approach a finite lower bound asymptotically due to the fact that beyond a certain value of drainage density, the water table falls to such an extent that it becomes lower than the local elevation of the tile drain. The same phenomenon is manifest through the plateau in the fraction of outflow that is captured by the tile drains. Additional tile lengths are ineffective in capturing greater amounts of total outflow once the steady-state water table levels drop below the elevation of

the tile drain. This leads to saturation in the fraction of outflow that is captured by the tile drainage network.

The inverse of the best-fit decay constant constituted another characteristic drainage density parameter for the watershed that equaled 0.00119 m^{-1}. Thus, similar to the case of watershed travel times, this parameter will depend on specific physical properties of the watershed. Their identity and the functional relation between them and the characteristic density parameter need to be explored further.

5.4.3. Relation between travel times and tile contribution to baseflow

It is interesting to note the high degree of similarity in the trends and exponential best-fit curves of both the watershed mean travel time and the tile contribution to baseflow as functions of variation in the tile drainage density. Comparison of Fig. 39 and Fig. 40 suggests that one is a near perfect mirror image of the other (reflected about the X axis). This suggests the existence of an inverse relation between the two variables. In other words, changes in watershed travel times due to variation in tile drainage density are evidenced by a corresponding change in the contribution of tile drains to total outflow, as long as other basin parameters maintain constant values.

Furthermore, the characteristic drainage density parameters defining the behavior of watershed travel times and tile contribution to baseflow were also observed to be very similar in magnitude (0.00104 m^{-1} and 0.00119 m^{-1}, respectively). The close match between the respective decay constants of the best-fit exponential curves suggested the existence of an approximate linear correlation between the mean travel time and Q_T, as demonstrated in Fig. 41. The linear best-fit trendline (R^2 = 0.9834) was found to have a slope of -0.52, and a y-intercept with value 38.46 (the units of both parameters was years). The clustering of data

points as they approached the higher end of the range of Q_T values, and the lower end of the range of mean travel time values, represented the higher end drainage density scenarios when both variables started tending towards their respective upper and lower bounds asymptotically. Thus, the theoretical extrapolation of the trendline beyond this range would not be realized in reality. In other words, the plot of the mean travel time versus the inflow captured by the tile drains would systematically converge to a single point defined by non-zero coordinates in the phase space of travel time versus Q_T. The location of the point of convergence shall vary based on other catchment parameters, such as tile incision depth, intrinsic aquifer parameters, groundwater recharge to the aquifer, etc. To determine these, the nature of this relation needs to be examined in the context of a variety of watersheds.

5.4.4. Impact of tile incision depth on travel times

As discussed earlier, the failure of increasing tile density to impact watershed travel times, in terms of both the shape and the mean of the travel time distribution, was deduced to reflect the circumstance of water table levels dropping below the incision depth of the tile drainage network. Thus, an increase in the tile incision depth would allow for the tile network to intercept the water table at greater depths, and therefore continue to lower the mean travel time for a wider range of drainage densities. This suggests that an increase in the tile incision depth is expected to impact the travel times associated with each drainage density. To quantify the relation between watershed travel times and tile incision depth, we simulated alternative scenarios of variable incision depths, while holding the drainage density constant at an arbitrary value of 0.0038 m^{-1}.

Overall, travel times were observed to decrease with increasing tile incision depths. The travel time distributions generated by each scenario were observed to match an exponential

distribution characterized by different values of the decay constant. The values of the best-fit scale parameters and their standard errors are listed in Table 6. Fig. 42 shows a comparison of the travel time distribution obtained at minimum and maximum tile incision depths. Similar to the case of drainage density variation, increasing incision depths increased the proportion of short transit times, while maintaining the characteristic shape of the exponential distribution. This was reflected in the equality between the best-fit scale parameters and the mean of the empirical distributions obtained for all simulated scenarios (Table 6).

Moreover, the coefficient of variation was observed to stay relatively constant (ranging from 0.917 to 0.930) and almost equal to unity, the coefficient of variation for the ideal exponential distribution. This indicates that the exponential distribution is a robust representation of the distribution of groundwater travel times in a watershed relative to a wide variety of tile drainage density and incision depth values.

A deeper analysis of the representative statistics of the distributions revealed interesting features of the comparison between the impacts of tile drainage density and incision depth on groundwater travel times. With increasing incision depths, the mean and median travel times were observed to decrease at a uniform rate. Mean travel time decreased by 3.49 years (a decrease of 16%), while the median travel time decreased by 2.79 years (a decrease of 17%). This shows that unlike the case of drainage density variation, tile incision depths have a comparable impact on both the mean and median travel times. This implies that the positively skewed long transit times scale in proportion to the rest of the travel time distribution. This in turn would give rise to comparable rates of decrease in the mean and median of the distribution. The observed variation in the maximum travel times reinforced

this conclusion. Compared to the dramatic decrease of maximum travel time observed in the case of variable tile density, increasing tile incision depth did not change the maximum travel time as dramatically. Almost all the values were observed to be close to 250 years, and decrease moderately with increasing incision depths, spanning a range of around 50 years.

We examined the trend in the mean travel time in greater detail. As discussed earlier, increasing the tile incision depth resulted in an overall decrease in watershed travel times, which was also reflected in the trend of the mean travel time (Fig. 43). Physically, this can be understood to occur due to an overall increase in hydraulic head gradients as the tile drains become engraved deeper into the watershed landscape. However, the nearly exact linearity of the decreasing trend ($R^2 = 0.9999$) that was observed was unanticipated. The best-fit linear trendline was observed to have a slope of 1.45 years/meter, and a y-intercept of 21.96 years. We analyzed this trend conceptually and obtained interesting results that are presented in the next section.

5.4.5. Conceptual analysis of relation between tile incision depth and travel times

A conceptual analysis of the travel time along a typical flow line from a topographic high (such as an upland position) to a tile drain located at a lower elevation was performed to demonstrate the linear relation between tile incision depth and the average travel time along the flow line, and to evaluate the possible factors that determine the parameters (slope and intercept) of the linear equation.

Fig. 44 shows a pictorial representation of the cross section along such a flow line from source to sink. The source is located in a topographic high where the water table is at an elevation of “D” meters relative to the datum that is fixed at the land surface elevation where the tile drain is located. The tile is incised by a depth of “Δ” meters relative to the land

surface elevation. The horizontal distance between the source and the sink is given by "X" meters. Note that for the unconfined aquifer at the Walnut Creek watershed, the horizontal dimensions (~100-1000 m) are much greater than its vertical dimensions (~10 m). Also, the tile incision depths are very small (less than 3 meters) relative to the overall basin relief (~50 m). Therefore,

$X >> D >> \Delta$

The travel time of a representative flow line along the water table, T, will be given by the formula,

$$T = \frac{L}{v} \tag{1}$$

where "L" (in m) is the total flow path length from source to sink, and "v" (m/yr) is the average velocity along it. As a first-order approximation, L can be represented by the straight line distance along the water table from the source to the sink. This approximation is valid particularly for systems where undulations in the water table introduced due to local gradients are smaller than the overall watershed-scale gradient. Using this approximation, we can express "L" in terms of "X", "D", and "Δ" as,

$$L = \sqrt{X^2 + (D + \Delta)^2} \tag{2}$$

Using Darcy's law, the average flow velocity "v" can be expressed as,

$$v = \frac{Ki}{n_e} \tag{3}$$

where K is the hydraulic conductivity (m/yr), "i" is the hydraulic gradient along the length of the representative flow path, and n_e is the effective porosity. For the given flow line running along the water table, the hydraulic head difference from the source to sink is determined by

the elevation difference between the two locations, which is given by (D+Δ). This head difference occurs over a length "L" meters. Thus, "i" can be expressed as,

$$i = \frac{D + \Delta}{L} \tag{4}$$

Using equations 1-4, we are able to express the travel time, T, as follows:

$$T = \frac{n_e}{K}\left(\frac{L^2}{D+\Delta}\right) = \frac{n_e}{K}\left\{\left(\frac{X^2}{D+\Delta}\right) + \left(D+\Delta\right)\right\} \tag{5}$$

Equation 5 above can be re-written as,

$$T = \frac{n_e}{K}\left\{\frac{X^2}{D} * \left(1+\frac{\Delta}{D}\right)^{-1} + \left(D+\Delta\right)\right\} \tag{6}$$

Since Δ << D, we can expand the first term in the brackets in equation 6 using the Taylor series expansion about Δ/D = 0, as follows:

$$\left(1+\frac{\Delta}{D}\right)^{-1} \simeq 1 - \frac{\Delta}{D} + \left(\frac{\Delta}{D}\right)^2 ... \tag{7}$$

Since Δ/D << 1, the expression on the left-hand side in equation 7 will be dominated by the lower order terms in the expansion. Retaining the first two terms (the zero-th and first order terms) in the above equation, we can simplify equation 6. After collecting terms of equal power in Δ, equation 6 simplifies to,

$$T = \frac{n_e}{K}\left(\frac{X^2}{D} + D\right) - \frac{n_e \Delta}{K}\left(\frac{X^2}{D^2} - 1\right) \tag{8}$$

This shows that the first-order approximation of the relation between the travel time along a representative flow line, T, and tile incision depth, Δ, is indeed linear. The slope, M (in units of yr/m), and y-intercept, C (yr) are therefore given as,

$$M = -\frac{n_e}{K}\left(\frac{X^2}{D^2} - 1\right) \tag{9}$$

and,

$$C = \frac{n_e}{K}\left(\frac{X^2}{D} + D\right) \tag{10}$$

As a reality check, we compared the simulated values of M and C (-1.45 yr/m and 21.96 yr, respectively) with those obtained using a set of representative values for the parameters included in equations 9 and 10. For the Walnut Creek watershed, the estimated values of the parameters were as follows:

X ~ 300 m, D ~ 10 m, ne ~ 0.3, and K ~ 0.48 m/day or 175 m/yr

Substituting these values in equations 9 and 10 produced a slope and y-intercept with values -1.54 yr/m and 15.45 yr, respectively. Both values were reasonably close to those simulated. The computed slope differed from the simulated value by only 6%, while the computed y-intercept differed from the simulated value by 30%. This agreement is particularly significant given that the formula was derived from basic principles, with much simplification in the geometry of the flow system, and the values used to compute the slope and y-intercept were only estimated averages.

The linear dependence of watershed travel times on tile incision depth was thus established via simulation and theory, for small values of incision depth.

5.4.6. Impact of tile incision depth on tile contribution to baseflow

We quantified the impact of tile incision depth on baseflow in terms of the fraction of outflow captured by the tiles, Q_T. Fig. 45 shows the dependence of Q_T on tile incision depth.

The tile contribution to baseflow was observed to increase with increasing tile incision depth. The trend was best represented by a linear trendline in the simulated range of incision depths ($R^2 = 0.9822$), with a slope and y-intercept value of 10.45 m^{-1} and 24.88%, respectively. Note that the y-intercept value will not be physically realized since tile contribution to baseflow will fall to 0 as incision depth becomes smaller.

The increasing trend in tile contribution to baseflow can be understood conceptually in terms of the active tile length and hydraulic gradients. Deeper tiles intercept a greater proportion of the water table that increases the total quantity of outflow captured by the tiles. Moreover, deeper incision depths also increase the hydraulic gradients that are directed towards them, which by Darcy's law increases the flux entering the tiles. Therefore, both factors will contribute to an increase in the total quantity of flow leaving through the tile drains as tile incision depth is increased.

Note that the increase in hydraulic gradients due to an increase in incision depth causes the decrease in groundwater travel times. Therefore, like in the case of drainage density variation, we observe tile incision depth to impact travel times and tile contribution to baseflow on the basis of the same physical factors. Indeed, in both scenarios of increasing tile drainage density and incision depths, increase in tile contribution to baseflow seems to implicitly indicate a decrease in the corresponding groundwater travel times, and vice versa. Moreover, the similar functional form of the trends in both variables when varied relative to both independent variables – exponential trends with respect to changing tile drainage density, and linear trends with respect to change in tile incision depth, suggests the two variables are inversely related in a number of scenarios where one tile network parameter (such as tile density or incision depth) is varied while the other parameters are held constant.

The inverse relation between the two dependent variables for the case of variable incision depths is shown in Fig. 46. Comparison of figures 41 and 46 shows that the trends are similar, although in the case of Fig. 46, the best-fit slope is significantly flatter (a magnitude of 0.14 years, versus 0.52 years, obtained for Fig. 41). This indicates that variation in tile incision depth has a greater impact on the tile contribution to baseflow, than it does on groundwater travel times. Indeed, increasing incision depth caused the tile contribution to baseflow to change by 24.5% (from 29.94% to 54.44%), but change mean travel time by 16% only (from 21.54 to 18.05 years). This can be deduced to arise from the fact that the even though both groundwater travel times and tile outflow volumes are affected by the increasing hydraulic gradients created by deeper tile incision depths, the increase in tile outflow is caused by the additional effect of deeper tiles intercepting a larger extent of the water table. This latter effect will increase the total number of particles reaching the tiles, but not necessarily the *distribution* of travel times. The distribution of travel times is normalized to 1 particle, hence not impacted by larger particle numbers. Thus, variations in tile incision depths are likely to have a stronger impact on tile discharge volumes than groundwater travel times.

On the other hand, as shown earlier, tile drainage density variation caused the mean travel time to decrease by 50% (from 40.29 to 20.23 years), while tile contribution to baseflow changed by 35.8% (from 0 to 35.8%). Thus, variation in tile drainage density impacted groundwater travel times more strongly than the volume of tile outflow. This can be understood as follows: increasing drainage density increases the spatial variability observed in water table elevations, and therefore increases the hydraulic gradients. By Darcy's law, an increase in the water table gradients increases the flow velocities and decreases the travel

times associated with that flow. The same increase in hydraulic gradients and flow velocities also causes tile discharge volumes to increase. However, the decrease in travel times is caused by the additional effect of decreasing flow path lengths, as the sink network branches out deeper into the watershed. The decrease in flow path lengths will decrease travel times, but not necessarily impact the total *quantity* of flow reaching the tile drains. Thus, variations in tile drainage density are likely to have a stronger impact on groundwater travel times than tile discharge volumes.

In light of the above results we see that subsurface tile network is likely to have a great impact on the hydrology of a watershed. But the impact may vary, based on (1) the specific aspect of the tile network being considered (drainage density or incision depth), and (2) the specific hydrologic variable of interest (for example, groundwater travel times versus tile discharge volumes). But there are certain qualitative commonalities observed in the dependencies that are discussed below.

Comparing the change in mean travel time caused by increasing tile drainage density and incision depth showed that both variables decreased the mean travel time by 50% and 16%, respectively. Increase in tile drainage density and incision depth also increased the tile contribution to baseflow by 35.8% and 24.5%, respectively. Thus, both tile drainage density and incision depth have the same qualitative impact on the groundwater hydrology of the watershed, as expressed in terms of travel times and the baseflow contribution of tiles. This result is highly significant in light of the water quality issues affecting many watersheds across the country. Specifically, in the interest of reducing nitrate loads, we observe the decrease in tile outflow volumes produced by decreasing tile incision depths might be offset by an increase in the outflow volume produced by increasing the tile drainage density or the

tile spacing at that shallower depth. This procedure is likely to allow the natural processes of soil denitrification to act on shallow depths of the water table that were previously quickly drained by the deeper drainage network. This is likely to decrease the nitrate losses, and thereby improve stream water quality. However, the higher proportion of shallow flow now contributing to the streamflow due to increase in drainage density at shallower incision depths might offset this water quality improvement. Thus, extensions to tile drainage networks must be conducted with caution, after careful consideration of all affected parameters and the consequent costs and benefits.

5.5. Conclusion

We examined the impact of tile drainage on the groundwater hydrology of a watershed. This was done by simulating the impact of tile drainage density and incision depth on the groundwater travel times and baseflow at a representative watershed using a two dimensional, steady state groundwater flow model. We observed both tile drainage density and incision depth to have a significant impact on both the mean travel time and tile contribution to baseflow. An increase in either of the two independent variables caused groundwater travel times to decrease, and the fraction of outflow captured by tiles to increase. We found the trends of both hydrologic variables to be exponential relative to the tile drainage density, and linear relative to the tile incision depth, over the simulated range of drainage density and incision depth values. The similarity of trends in both hydrologic variables indicated a correlation between the two that was found to be approximately linear. The trend is the mean travel time as a function of tile incision depth was analyzed using a

conceptual model, and the results obtained were found to compare well with the simulated results.

A qualitative comparison of the relative influences of tile drainage density and incision depths on groundwater travel times and baseflow volumes revealed further insights. Increases in both tile drainage density and incision depth had the same qualitative impact on groundwater travel times (that were observed to decrease), and tile outflow volumes (that were observed to increase). This indicates that a change in one network parameter can be offset by a change in the other parameter. Thus, for best drainage management practices, the paired combination of the two tile network parameters of drainage density (or drain spacing) and depth can be optimized as a whole. This would, for example, be beneficial to minimize nitrate losses in the watershed and improve surface water quality.

Moreover, incorporating reference to the specific hydrologic criterion that the watershed manager seeks to achieve in the optimal analysis is likely to benefit. This is concluded based on our qualitative findings that the impact of the tile network was significantly different based on the specific type of hydrologic variable being considered. Tile drainage density was observed to impact groundwater travel times more significantly than the volume of tile discharge. On the other hand, incision depth was observed to have a stronger impact on the tile discharge volume than groundwater travel times. Thus, a complete analysis of the hydrologic impact of the tile drainage network in a watershed may require an examination of the unique relationship between the particular tile network control parameter being considered with the specific dependent hydrologic variables of concern.

References

Blann, K.L., Anderson, J.L., Sands, G.R., Vondracek, B., 2009. Effects of agricultural drainage on aquatic ecosystems: a review. Critical Reviews in Environmental Science and Technology, 39(11): 909-1001.

Bricker, S.B., Clement, C.G., Pirhalla, D.E., Orlando, S.P., Farrow, D.R.G., 1999. National estuarine eutrophication assessment: Effects of nutrient enrichment in the nation's estuaries. NOAA, National Ocean Service, Special Projects Office and the National Centers for Coastal Ocean Science, Silver Spring, MD, pp. 71.

Burchell, M.R., Skaggs, R.W., Chescheir, G.M., Gilliam, J.W., Arnold, L.A., 2003. Shallow subsurface drains to reduce nitrate losses from drained agricultural lands. Paper no. 03-2320, ASAE Annual Int'l Mtg., Las Vegas, NV.

Carpenter, S.R. et al., 1998. Nonpoint pollution of surface waters with phosphorus and nitrogen. Ecological Applications, 8(3): 559-568.

Davis, D.M., Gowda, P.H., Mulla, D.J., Randall, G.W., 2000. Modeling nitrate nitrogen leaching in response to nitrogen fertilizer rate and tile drain depth or spacing for southern Minnesota, USA. Journal of Environmental Quality, 29(5): 1568-1581.

Eidem, J.M., Simpkins, W.W., Burkart, M.R., 1999. Geology, groundwater flow, and water quality in the Walnut Creek watershed. Journal of Environmental Quality, 28(1): 60-69.

Goswami, D., Kalita, P.K., 2009. Simulation of base-flow and tile-flow for storm events in a subsurface drained watershed. Biosystems Engineering, 102(2): 227-235.

Green, C.H., Haney, R., 2005. Grassed waterways. SERA-17 (http://www.sera17.ext.vt.edu/SERA_17_Publications.htm).

Hallberg, G.R., 1987. Nitrates in ground water in Iowa. In: D'Itri, F.M., Wolfson, L.G. (Eds.), Rural ground water contamination. Lewis, Chelsea, MI, pp. 23-68.

Harbaugh, A.W., Banta, E.R., Hill, M.C., McDonald, M.G., 2000. MODFLOW-2000, the U.S. Geological Survey modular ground-water model -- User guide to modularization concepts and the Ground-water flow process: U.S. Geological Survey Open-File Report 00-92. Reston, VA, pp. 121.

Helmke, M.F., Simpkins, W.W., Horton, R., 2005. Fracture-controlled nitrate and atrazine transport in four Iowa till units. Journal of Environmental Quality, 34(1): 227-236.

Jindal, P., 2010. A study of the groundwater travel time distribution at a rural watershed in Iowa: A systems theory approach to groundwater flow analysis, Ph.D. thesis, Iowa State University, Ames, IA, 202 pp.

Kladivko, E.J. et al., 2004. Nitrate leaching to subsurface drains as affected by drain spacing and changes in crop production system. Journal of Environmental Quality, 33(5): 1803-1813.

Meals, D.W., Dressing, S.A., Davenport, T.E., 2010. Lag time in water quality response to best management practices: A review. Journal of Environmental Quality, 39(1): 85-96.

Molenat, J., Davy, P., Gascuel-Odoux, C., Durand, P., 2000. Spectral and cross-spectral analysis of three hydrological systems. Physics and Chemistry of the Earth Part B-Hydrology Oceans and Atmosphere, 25(4): 391-397.

Nangia, V., Gowda, P.H., Mulla, D.J., Sands, G.R., 2010. Modeling impacts of tile drain spacing and depth on nitrate-nitrogen losses. Vadose Zone Journal, 9(1): 61-72.

NRCS, 2004. How to design, construct, seed and maintain small grassed waterways: Iowa Job Sheet, National Resources Conservation Service. In: Service, N.R.C. (Ed.), Des Moines, IA.

Pollock, D.W., 1994. User's guide for MODPATH/MODPATH-PLOT, version 3: A particle tracking post-processing package for MODFLOW, the U.S. Geological Survey finite-difference ground-water flow model: U.S. Geological Survey Open-File Report 94-464, Reston, VA, pp. 237.

Prior, J.C., 1991. Landforms of Iowa. University of Iowa Press, Iowa City, IA.

Rabalais, N.N., 1998. Oxygen depletion in coastal waters. National Oceanic and Atmospheric Administration's State of the Coast Report, Silver Spring, MD: NOAA, pp. 52.

Randall, G.W., Goss, M.J., 2001. Nitrate losses to surface water through subsurface, tile drainage. In: Follett, R.F., Hatfield, J.L. (Eds.), Nitrogen in the Environment: Sources, Problems, and Management. Elsevier, New York, pp. 95-122.

Rovey II, C.W., 1998. Digital simulation of the scale effect in hydraulic conductivity. Hydrogeology Journal, 6(2): 216-225.

Schilling, K., Zhang, Y.K., 2004. Baseflow contribution to nitrate-nitrogen export from a large, agricultural watershed, USA. Journal of Hydrology, 295(1-4): 305-316.

Schilling, K.E., 2002. Chemical transport from paired agricultural and restored prairie watersheds. Journal of Environmental Quality, 31(4): 1184-1193.

Schilling, K.E., 2009. Investigating local variation in groundwater recharge along a topographic gradient, Walnut Creek, Iowa, USA. Hydrogeology Journal, 17(2): 397-407.

Schilling, K.E., Helmers, M., 2008. Effects of subsurface drainage tiles on streamflow in Iowa agricultural watersheds: Exploratory hydrograph analysis. Hydrological Processes, 22(23): 4497-4506.

Schilling, K.E., Hubbard, T., Luzier, J., Spooner, J., 2006. Walnut Creek watershed restoration and water quality monitoring project: final report. Iowa Department of Natural Resources, Geological Survey Bureau Technical Information Series 49, Iowa City, IA, pp. 124.

Schilling, K.E., Jacobson, P., 2008. Groundwater nutrient concentrations near an incised midwestern stream: effects of floodplain lithology and land management. Biogeochemistry, 87(2): 199-216.

Schilling, K.E., Libra, R.D., 2003. Increased baseflow in Iowa over the second half of the 20th century. Journal of the American Water Resources Association, 39(4): 851-860.

Schilling, K.E., Wolter, C.F., 2000. Application of GPS and GIS to map channel features in Walnut Creek, Iowa. Journal of the American Water Resources Association, 36(6): 1423-1434.

Schilling, K.E., Wolter, C.F., 2001. Contribution of base flow to nonpoint source pollution loads in an agricultural watershed. Ground Water, 39(1): 49-58.

Schilling, K.E., Zhang, Y.K., Drobney, P., 2004. Water table fluctuations near an incised stream, Walnut Creek, Iowa. Journal of Hydrology, 286(1-4): 236-248.

Schulze-Makuch, D., Cherkauer, D.S., 1998. Variations in hydraulic conductivity with scale of measurement during aquifer tests in heterogeneous, porous carbonate rocks. Hydrogeology Journal, 6(2): 204-215.

Skaggs, R.W., Chescheir, G.M., 2003. Effects of subsurface drain depth on nitrogen losses from drained lands. Transactions of the ASAE, 46(2): 237-244.

Stone, R., McKague, K., 2009. Grassed waterways: Ontario Ministry of Agriculture, Food and Rural Affairs Factsheet 09-021.

Tomer, M.D., Meek, D.W., Jaynes, D.B., Hatfield, J.L., 2003. Evaluation of nitrate nitrogen fluxes from a tile-drained watershed in central Iowa. Journal of Environmental Quality, 32(2): 642-653.

Weisbrod, T.S., 2005. Modeling the influence of land use on shallow groundwater flow and nitrate transport, Neal Smith National Wildlife Refuge, Jasper county, Iowa, M.S. thesis, University of Iowa, Iowa City, IA, 136 pp.

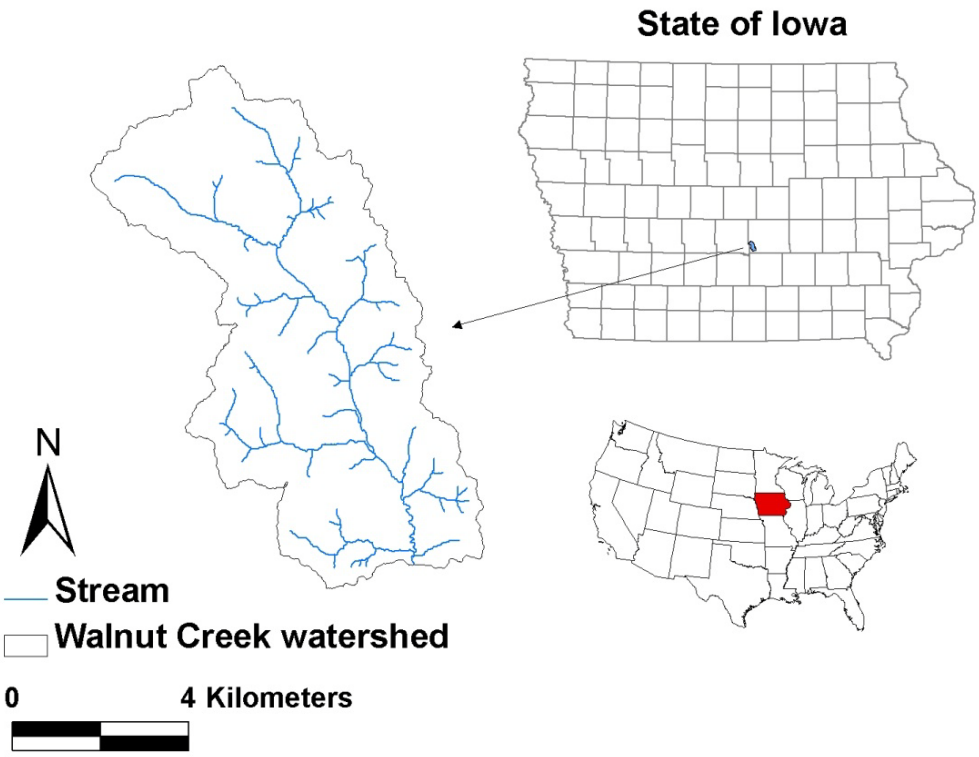

Fig. 35. Site location

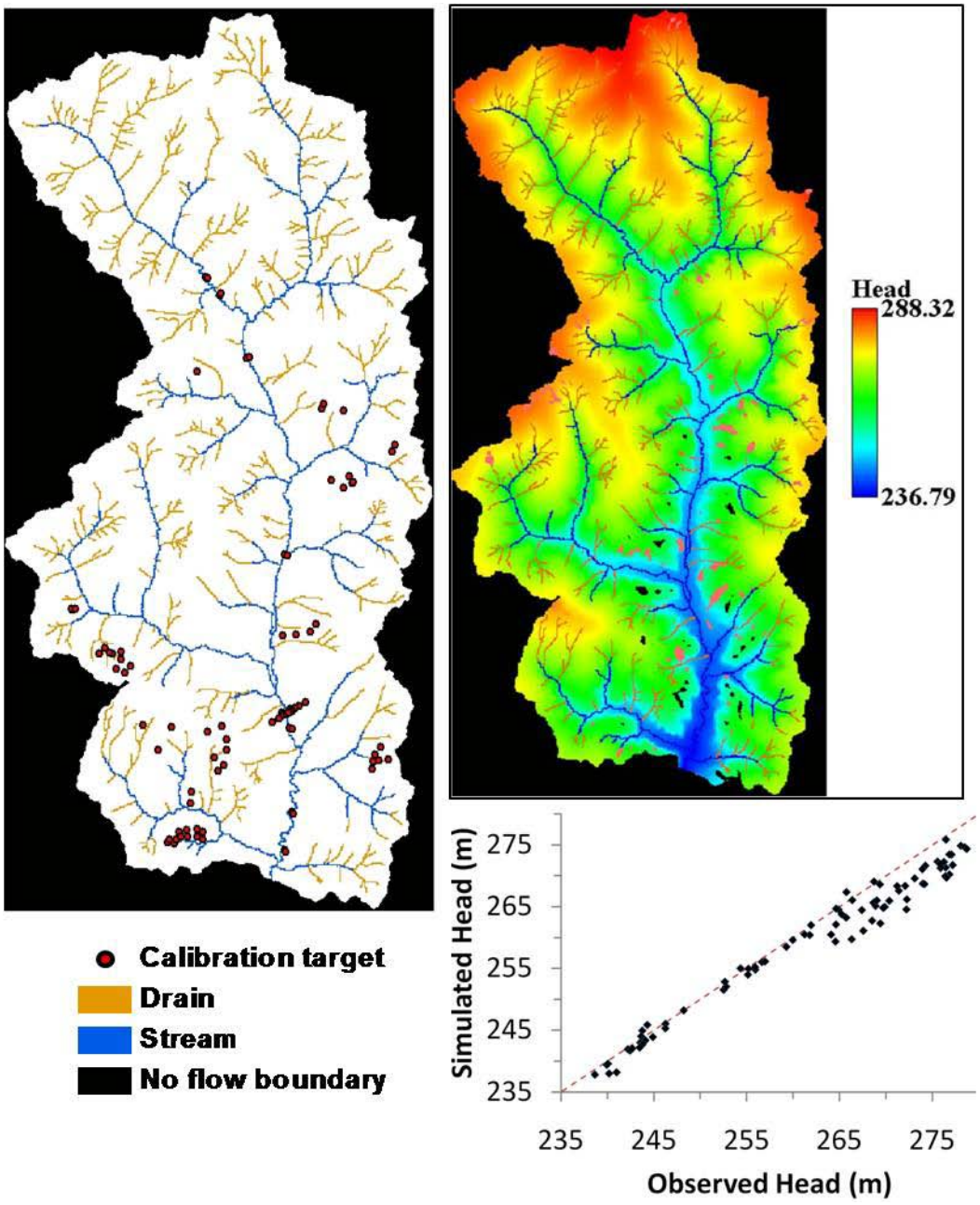

Fig. 36. MODFLOW model: boundary conditions and calibration target locations (left), distribution of hydraulic head (in meters, red and black spots represent stray flooded and dry cells, respectively) (top right); and final calibration plot (bottom right).

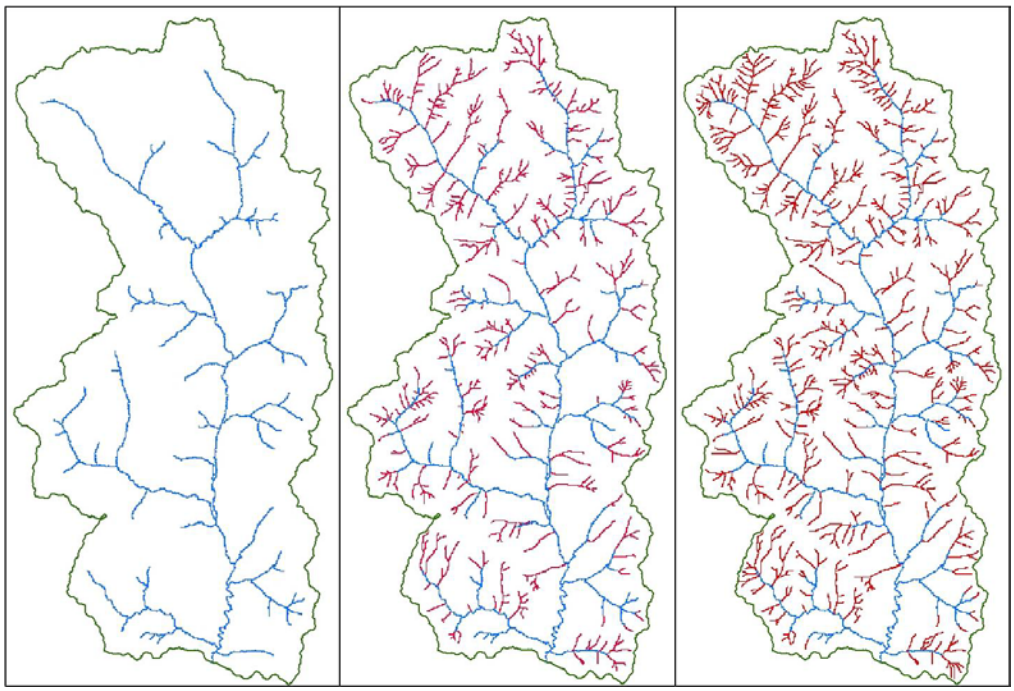

Fig. 37. Simulated tile drainage densities (in red) were gradually varied from 0 (on left) to 0.0038 m^{-1} (right). Baseline tile density of the calibrated model (at 0.0027 m^{-1}) is included for reference (center). Stream network is shown in blue.

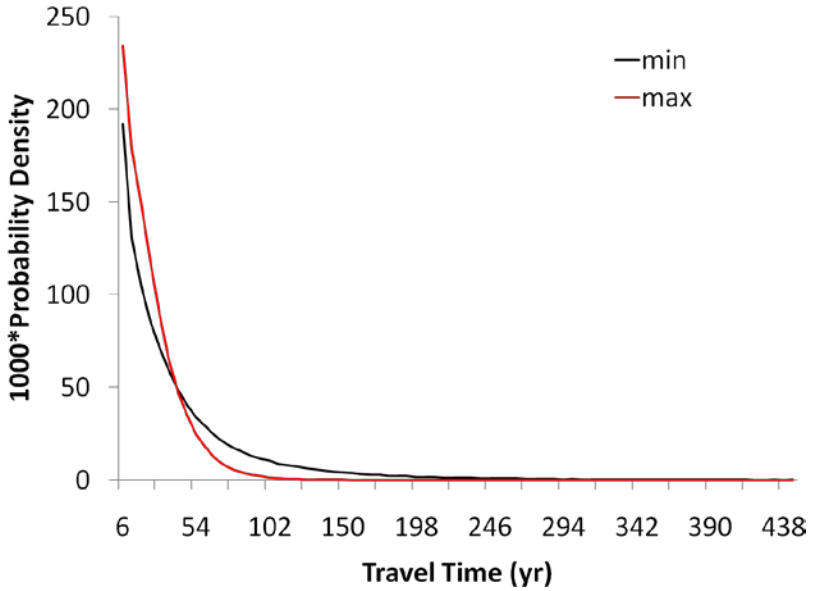

Fig. 38. Travel time distributions for minimum ("min", 0 m^{-1}) and maximum ("max", 0.0038 m^{-1}) tile drainage densities. Tile incision depth was constant (1.2 m). Both distributions were best represented by an exponential distribution. Distributions are normalized to 1000 particles each.

Table 5. Summary of the characteristic travel times and best-fit parameters associated with the travel time distributions obtained for variable tile drainage density scenarios. Tile incision depth was kept constant (1.2 m). (*) denotes the calibrated baseline drainage density. Std dev and CV denote the standard deviation and coefficient of variation, respectively.

Tile drainage density (10^{-3} m^{-1})	Mean (yr)	Median (yr)	Maximum (yr)	Minimum (yr)	Std dev (yr)	CV	Best fit parameters	
							Scale parameter (yr)	Standard error (yr)
0	40.29	22.98	890.82	0.06	53.16	1.319	40.29	0.11
0.11	35.26	21.47	631.62	0.08	42.45	1.204	35.26	0.10
0.20	33.22	20.79	583.05	0.09	39.16	1.179	33.22	0.09
0.37	30.64	19.96	496.85	0.09	34.15	1.114	30.64	0.09
0.72	27.28	18.58	452.07	0.09	29.40	1.077	27.28	0.08
1.13	25.87	17.93	406.12	0.09	27.21	1.052	25.87	0.07
1.49	24.52	17.05	613.27	0.09	25.99	1.060	24.52	0.07
1.87	24.21	16.85	440.38	0.09	25.67	1.060	23.96	0.07
2.31	20.87	15.71	224.34	0.12	19.20	0.920	20.87	0.06
2.67*	20.51	15.55	226.75	0.12	18.69	0.911	20.51	0.06
3.08	20.36	15.47	260.37	0.12	18.55	0.911	20.36	0.06
3.46	20.27	15.40	261.30	0.12	18.47	0.912	20.27	0.06
3.77	20.23	15.35	391.06	0.12	18.50	0.914	20.23	0.06

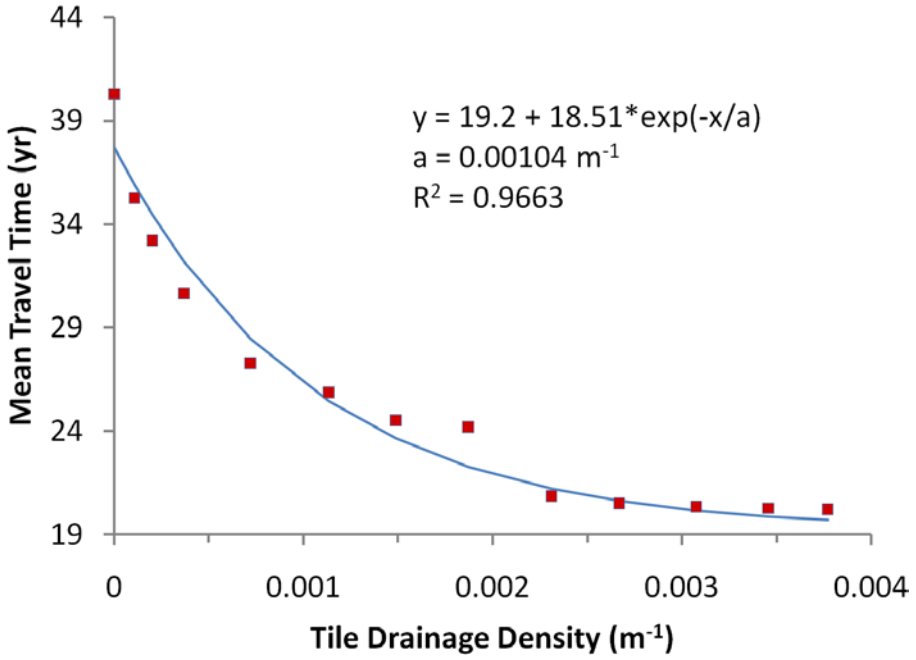

Fig. 39. Impact of drainage density on watershed mean travel time. The trend was best fit to a decaying exponential curve, that was parameterized by 3 best-fit parameters.

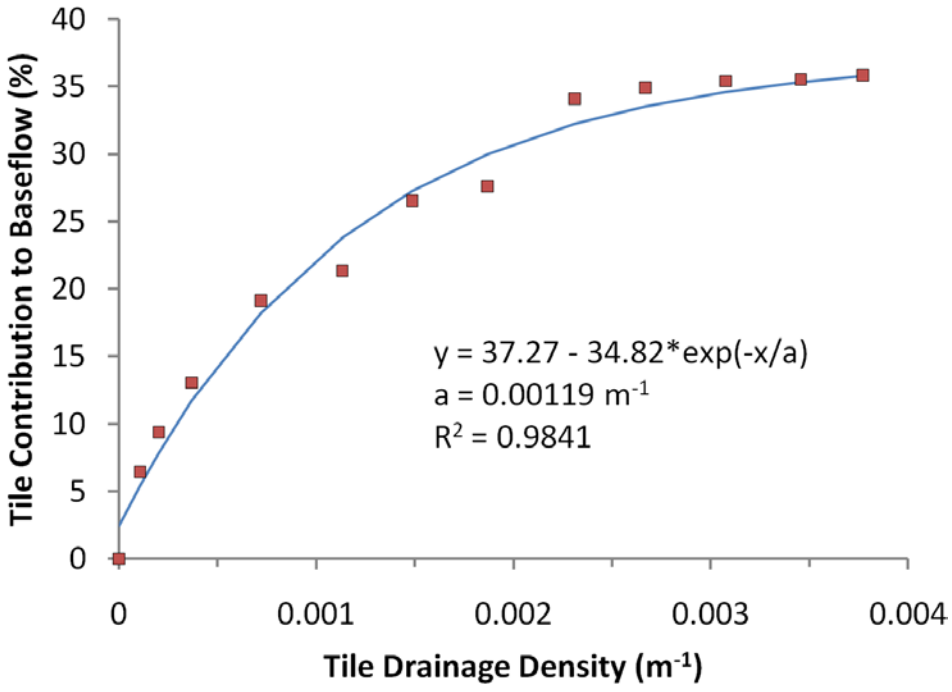

Fig. 40. Dependence of the fractional contribution of tile drains to total outflow (expressed in %) on tile drainage density. The trend was best fit to an exponential curve that was parameterized by 3 best-fit parameters.

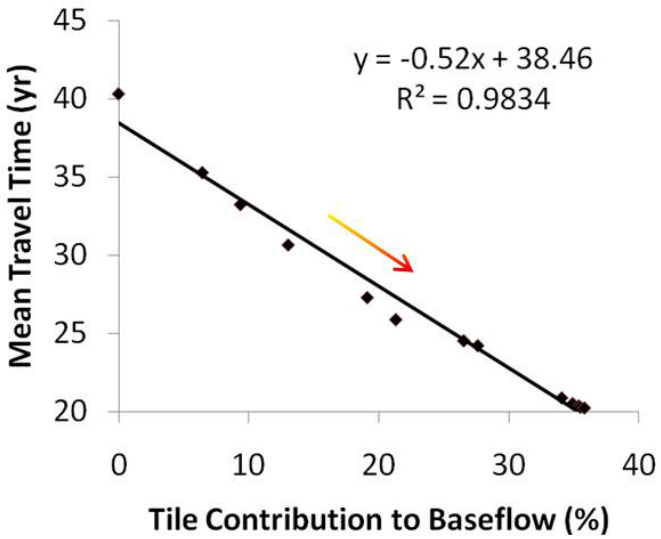

Fig. 41. The relation between the mean travel time and tile contribution to baseflow (%) simulated by varying tile drainage density. Tile incision depth was constant (at 1.2 m). Arrow points in the direction of increasing drainage density. At high drainage densities, the flow system converged to a single point represented by the lower and upper bounds of mean travel time and tile contribution to baseflow shown in Figs. 39 and 40, respectively.

Table 6. Summary of the characteristic travel times and best-fit parameters for travel time distributions obtained for alternative tile incision depths. Drainage density was constant (0.0038 m^{-1}). (*) denotes the baseline incision depth. Std dev, CV, Scale par and Std err denote the standard deviation, coefficient of variation, scale parameter, and standard error, respectively.

Tile incision depth (m)	Mean (yr)	Median (yr)	Maximum (yr)	Minimum (yr)	Std dev (yr)	CV	Best fit parameters	
							Scale par (yr)	Std err (yr)
0.3	21.54	16.33	271.6	0.12	19.75	0.917	21.54	0.06
0.6	21.09	16.02	234.11	0.12	19.27	0.914	21.09	0.06
0.9	20.65	15.69	224.18	0.12	18.84	0.912	20.65	0.06
1.2*	20.23	15.35	391.06	0.12	18.50	0.914	20.23	0.06
1.8	19.35	14.67	279.32	0.12	17.7	0.915	19.35	0.06
2.1	18.92	14.31	228.98	0.12	17.37	0.918	18.92	0.05
2.4	18.46	13.91	230.6	0.12	17.04	0.923	18.46	0.05
2.7	18.05	13.54	245.95	0.12	16.79	0.930	18.05	0.05

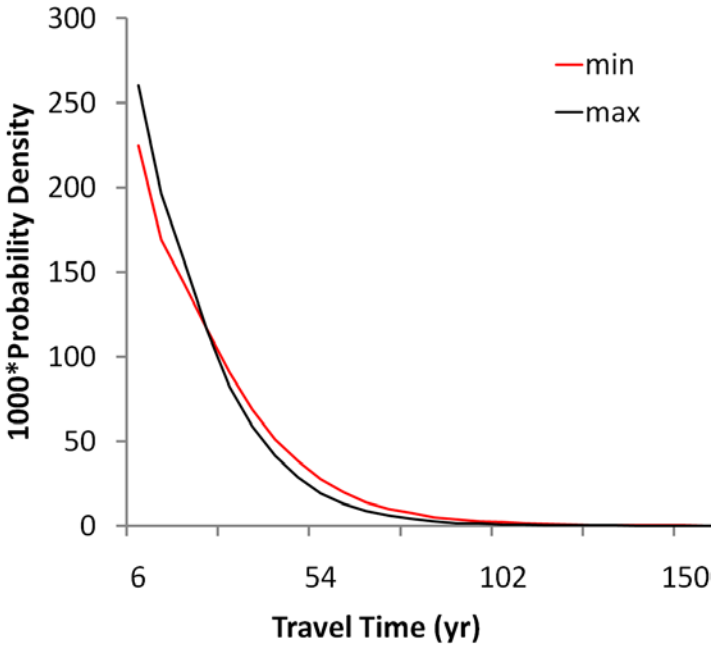

Fig. 42. Travel time distributions for minimum ("min", 0.3 m) and maximum ("max", 2.7 m) tile incision depths. Tile drainage density was held constant (0.0038 m^{-1}). Both distributions were best fit by an exponential distribution. Distributions are normalized to 1000 particles each.

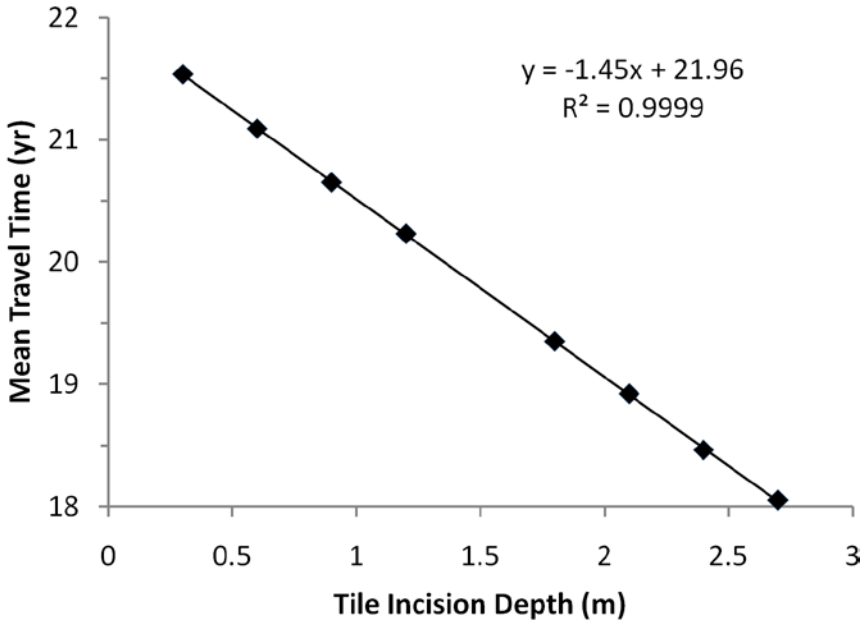

Fig. 43. Variation of the watershed mean travel time with respect to tile incision depth. Drainage density was held constant at 0.0038 m^{-1}. The trend was extremely close to linear, as demonstrated by the excellent agreement between the simulated observations and the best-fit linear trendline.

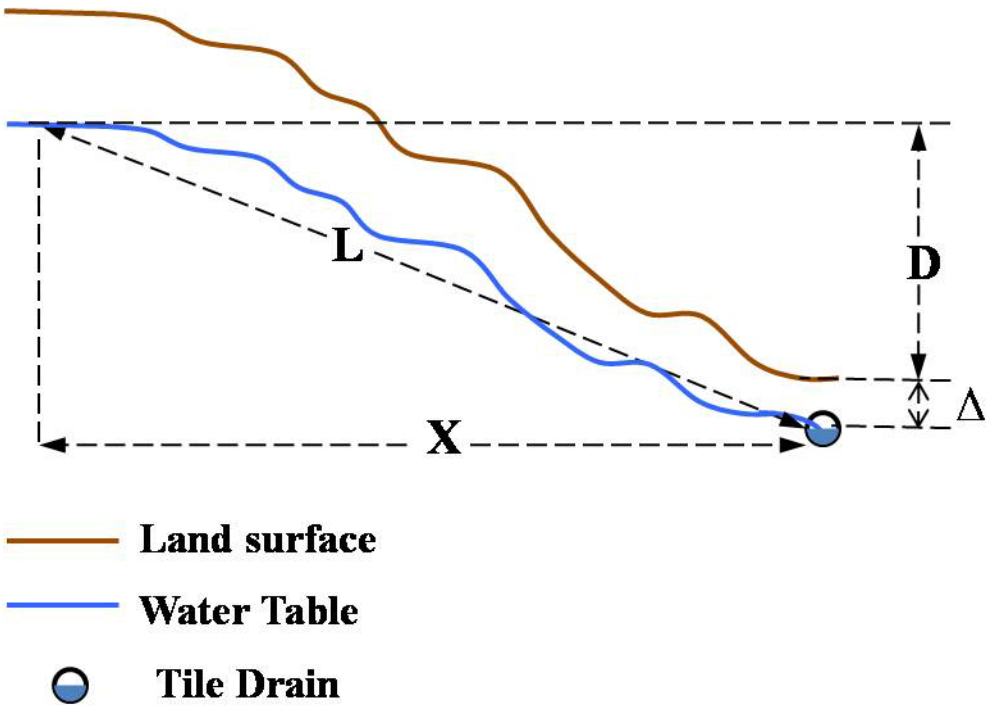

Fig. 44. Cross section along a representative flow line shown from its source to the tile sink where it ends. The tile drain is incised by a depth Δ with respect to the land surface.

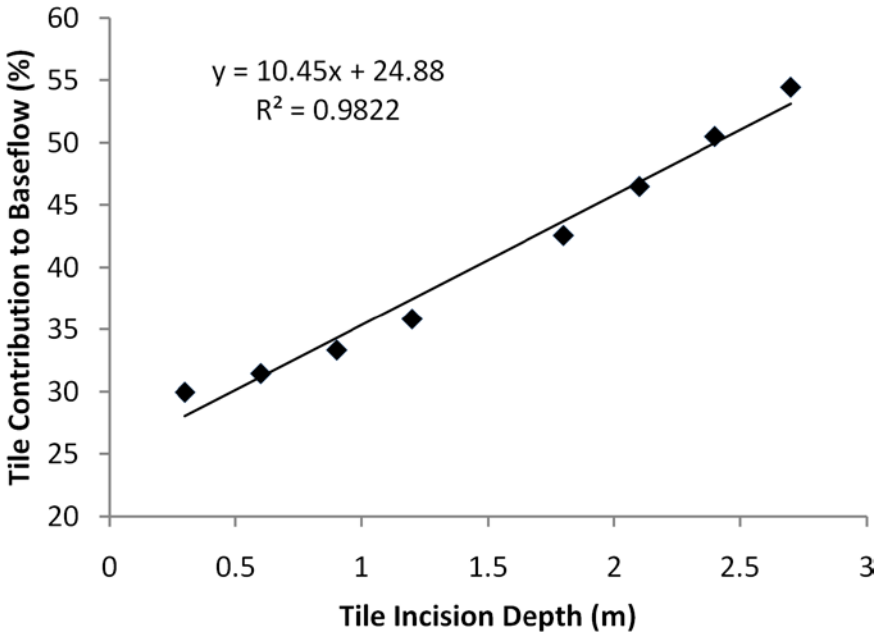

Fig. 45. Dependence of the fractional contribution of tile drains to total outflow (expressed in %) on tile incision depth. Drainage density was held constant at 0.0038 m^{-1}. The trend was observed to be near linear.

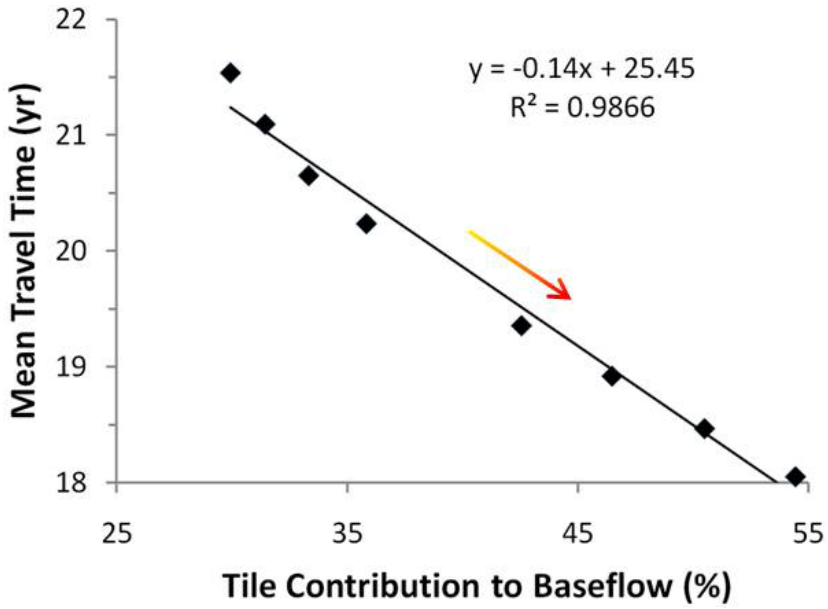

Fig. 46. The relation between the watershed mean travel time and fractional contribution of tile drains to total baseflow (expressed in %) simulated by varying tile incision depths. Drainage density held constant (at 0.0038 m^{-1}). Arrow points in the direction of increasing tile incision depth. Similar to Fig. 5, the relation was approximated by a linear trendline, though the values of the best-fit slope and intercept were different.

VI. General conclusions

6.1. Conclusions

This dissertation explored the application of the travel time distribution formulation in the context of groundwater-surface water interaction at the watershed scale in a tile-drained, agricultural landscape. Through the medium of a distributed hydrologic modeling, we constructed the two dimensional, steady state groundwater flow model of the shallow, unconfined loess-alluvial aquifer at the Walnut Creek watershed, Iowa using MODFLOW. We then coupled the groundwater flow model to particle tracking analysis using MODPATH and generated the groundwater travel time distribution of the watershed. The distribution was characterized by an exponential decay with a mean travel time of 20.51 years. Thus, we found that the time scales over which one can expect to observe the surface water response to distributed, watershed-wide changes implemented at the land surface to be of the order of two decades.

Furthermore, we examined the impact of various control variables on this distribution. The first variable we considered was the degree of uncertainty introduced due to model selection. We compared three modeling approaches that span the range of model complexity. The simplest approach was represented by the analytic model, while the GIS and MODFLOW models represented intermediate and high complexity range of models, respectively. The excellent match between the travel time distributions obtained from three completely different modeling frameworks suggests that all three approaches produce similar results. All distributions were characterized by an exponential decay. The analytic distribution travel times, represented by a mean travel time of 16.22 years, were slightly

lower than the corresponding MODFLOW and GIS simulated values, represented by mean travel times 20.51 and 19.61 years, respectively.

An analysis of the MODFLOW and GIS flow path length and velocity distributions suggested the agreement between their travel time distributions to be a consequence of higher values of flow velocity in the GIS model compensating high values of flow path length computed by GIS. The agreement broke down at model cell resolution that was demonstrated in the mismatch between their spatial distributions of travel times. Moreover, the GIS model was specifically observed to break down in the floodplain landscape position, when the land surface fails to reflect the downward convergence of water table flow lines towards the deeply incised stream channel.

Therefore, we infer that the impact of model selection on the overall groundwater travel time distribution of the watershed may not be significant, and simpler schemes may produce similar results as a distributed hydrologic model. But when the project goals necessitate a localized, spatially explicit evaluation of groundwater travel times, then model selection may exercise significant influence on the resulting distribution.

Thereafter, an examination of the sensitivity of the groundwater travel time distribution to various control variables was conducted. We focused on the control variables of flow depth, tile drainage density and incision depth, and net aquifer recharge.

We found that depth of flow had a significant impact on groundwater travel times, in terms of the shape and representative statistics of the distribution. Using a MODPATH model parameter, namely the “sink strength threshold”, as a surrogate for flow depth, we found that the travel time distribution shape and mean varied from an exponential distribution with a mean of 20.51 years, at a representative shallow flow depth of 3.55 m, to a gamma

distribution with a mean of 40.20 years, at a greater depth of 10.81 m. The structure of the effective sink network was also significantly impacted by variations in depth of flow.

We observed tile drainage density to have a significant impact on groundwater travel times with the mean travel time of the distribution decreasing from 40.29 to 20.23 years as drainage density increased from 0 to 0.0038 m^{-1}, though the marginal impact was observed to diminish at higher tile drainage densities. The diminishing trend was observed to correspond with a similar trend in the tile contribution to baseflow that was observed to approach an upper bound asymptotically.

On the other hand, we observed tile incision depth to have a relatively small impact on groundwater travel times. Increasing tile incision depth from 0.3 m to 2.7 m decreased mean travel time by 3.49 years only, from 21.54 to 18.05 years. This is because increasing incision depth, not only increases hydraulic gradients and consequently flow velocities, but it also increases groundwater flow path lengths. In our system, the latter variable (flow length) tempered the impact of the former variable (hydraulic gradients), though the former was still dominant. A conceptual analysis confirmed the simulated linear trend of mean travel time with respective to variation in tile incision depth.

Lastly, we observed the impact of net aquifer recharge on groundwater travel times to vary based on landscape position within the watershed. The results, presented in the appendix, showed that increasing recharge in the uplands to have the greatest impact on the mean groundwater travel time of the watershed (that decreased by 9.2 years), while variations in recharge in the floodplain had a relatively insignificant impact (causing a decrease of only 0.56 years). The impact correlated with the impact on average water table level that was found to be impacted most by increasing recharge in the uplands (increasing

by 1.21 m), and least by a similar increase in the floodplain (changing by 0.12 m only). The side slopes had an intermediate impact on both the mean travel time and average water table level, that varied by 5.43 years and 0.98 m, respectively. These results have the potential to be examined further.

6.2. Recommendations for future work

As mentioned above, the impact of recharge on the distribution of groundwater travel times has a potential to produce further insights into the groundwater flow system. Besides this topic, a deeper examination of the link between depth of flow and travel times is recommended. Specifically, the coincidence of the depth when the trend in the length ratio of the effective sink network switched from increasing to decreasing, with the depth at which the travel time distribution switched from an exponential to a gamma distribution is highly suggestive of some unknown and interesting correlations. Furthermore, the suggestive link between groundwater mean travel time and tile contribution to baseflow can be examined further, for instance, in the context of different flow depths and recharge scenarios. Finally, the impact of scale (in terms of watershed size) and stream network shape on the comparison of the three modeling approaches promises to be an interesting study, since the analytic distribution incorporates no explicit reference to watershed size or the stream network characteristics.

VII. Appendix : Impact of aquifer recharge on groundwater travel times

Total annual recharge was varied over a range of ± 20 mm about the calibrated, baseline value of 120 mm. Three sets of hypothetical scenarios were produced. For each set, the variation was localized to a specific landscape position, namely, the uplands, side slopes, or floodplain. The individual recharge at each landscape position was varied in steps of 10 mm, such that the total equivalent recharge varied from 100 to 140 mm (approximately). Thus, the maximum quantity of recharge water added or subtracted was the nearly same for each set of scenarios. Overall, groundwater travel times were observed to decrease with increasing recharge. However, the magnitude of the decrease in travel times was strongly dependent on landscape position. We observed the variation of recharge in the uplands to cause a maximum change in the watershed-wide mean travel time. Variation of recharge in the floodplain caused a minimal change in the mean travel time, while recharge variations in the side slopes caused an intermediate degree of change in the mean travel time (Table 7, Fig 47).

This decrease was caused by increasing water table levels on the upgradient sections of the flowlines, while the water table levels in the downgradient sections were primarily determined by the constant stream stage. Hence, to gain further insight into the effect of spatially variable recharge on travel times, we examined the trends in the average water table elevation as a function of recharge variations at each landscape position. As anticipated, increasing recharge increased the water levels in the aquifer in all 3 sets of scenarios, but the degree of change varied widely. Recharge variation in the uplands and the side slopes had a much greater impact on water table levels compared to variations in the floodplain. The total extent of change in the water table level was observed to be highest for the recharge

variations in the uplands, and decrease systematically as the simulated variations were performed further downgradient (Table 7, Fig. 48).

This is most likely because an increase in the recharge at the end of a flowline, when it is nearing a fixed head sink (the stream sink in the floodplain), will only serve to increase the volume of flow to the sink, without significantly impacting the hydraulic heads along the flowline. Thus, an increase in the floodplain recharge causes a very small increase in the average watershed-wide water table levels. This causes the flow path lengths, hydraulic gradients, and consequently travel times, to be only minimally impacted.

Thus, the sensitivity of groundwater travel times to the control variable aquifer recharge is dependent on the location where the change occurs. The further downgradient this location is, the smaller is the impact it has on water table elevations, which in turn leads to a smaller impact on groundwater travel times.

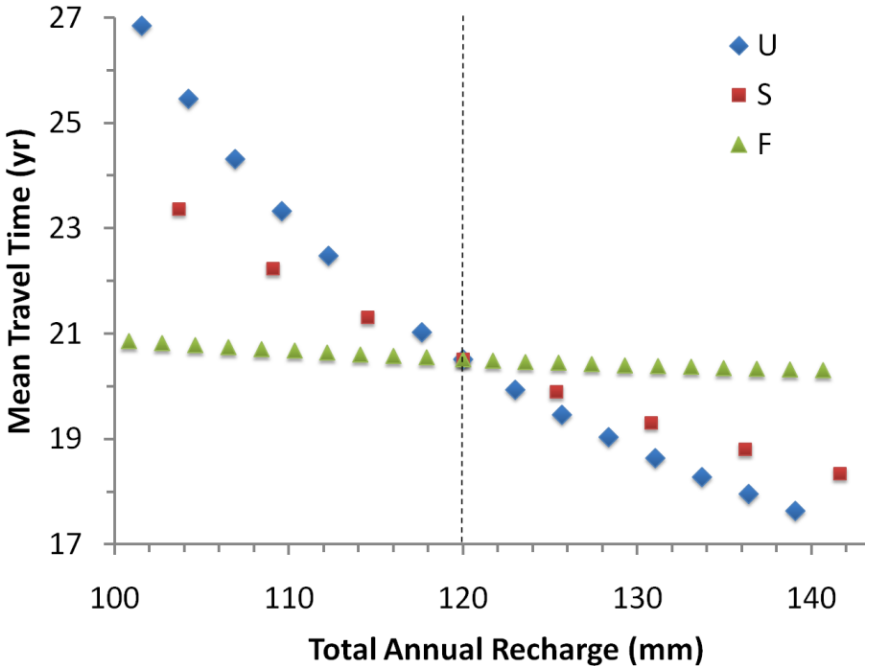

Fig. 47. Impact of recharge variation in the uplands (U), side slopes (S), and floodplain (F) on the groundwater mean travel time of the watershed

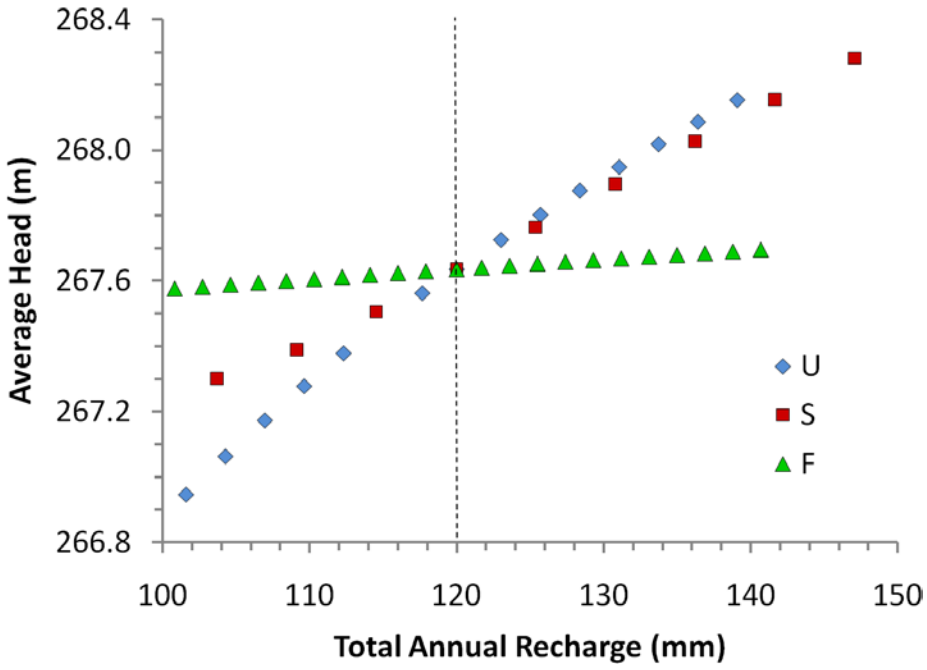

Fig. 48. Impact of recharge variation in the uplands (U), side slopes (S), and floodplain (F) on the watershed-wide average water table elevation

Table 7. Total change in mean travel time (ΔT) and mean water table elevation (Δh) due to change in total aquifer recharge (ΔR) at each landscape position

Landscape position	ΔR (mm/yr)	ΔT (yr)	Δh (m)
Upland	37.52	9.20	1.21
Side slope	43.38	5.43	0.98
Floodplain	39.84	0.56	0.12

Acknowledgements

Reaching the culmination of my graduate study would not have been possible without the goodwill and guidance of certain members of this community. I am deeply indebted to many people, both at Iowa State University and the University of Iowa.

First and foremost, I am most grateful to Dr. Takle for his unconditional and enthusiastic support and advice throughout the course of this study. Right from the start, Dr. Takle, Cathy, Manoj and Phil encouraged me to seek my own direction. Their genuine concern for the student's welfare has been appreciated very much.

This work would have never materialized had it not been for the sincere consideration of certain people at UI. I am deeply grateful to Keith, Nandita, and Calvin. Their tremendous guidance and unfailing help to an "outsider", at every stage – from start to finish, was valued very much. I committed a lot of mistakes in the process, got caught in many bouts of anxiety and worry, but their exemplary patience, sense of balance, and clear focus, always brought me back on track. Many of the lessons learned shall be carried forth through life.

I was indeed fortunate to have had the opportunity to share research ideas with faculty and students at another campus, namely, Indiana University, Bloomington. Discussions with Dr. Haitjema and Daniel Abrams were immensely helpful, and indeed, were the catalyst behind the second paper. I am extremely grateful to them for their time and interest, which encouraged me to pursue that particular direction.

There are many other people whose support and kind guidance at different points in my study have brought me to this point. I first wish to thank Drs. Franz and Helmers, who were always very welcoming when I approached them with a question that was confounding me.

Many thanks also to Dr. Dixon and Dennis Lock at the department of statistics for their guidance in the statistical analysis. A special thanks to the people who helped me at different points in time with the nuts and bolts of the process – Charles Sauer, Jess Robinson, Mike Long, Robin McNeely, Todd Campbell, Dr. Harding, and Dr. Simpkins, for introducing me to groundwater hydrology and MODFLOW. I am also very grateful to my committee members, especially Drs. Tomer and Kling, for their acceptance and support, without which I would not have reached this point. Among fellow students, from past and present, I wish to acknowledge the support and help that I received from Natalia Loukinova, Min Wang, Susy Ankerstjerne, and Evan Christianson, at different points in my graduate study here.

There are many, many more people whom I wish to convey my heartfelt gratitude to. But words would not suffice. May my gratitude to them, and to all introduced above, reflect in my actions at every step.

References

Anderson, M.P., Woessner, W.W., 1992. Applied groundwater flow modeling: Simulation of flow and advective transport. Academic Press, San Diego, CA, 381 pp.

Ballaron, P.B., 1998. Use of a field drain and an artificial wetland to minimize groundwater contamination from an agricultural site. Publication no. 197. In: Commission, S.R.B. (Ed.), Harrisburg, PA.

Bouwer, H., Rice, R.C., 1976. A slug test for determining hydraulic conductivity of unconfined aquifers with completely or partially penetrating wells. Water Resources Research, 12(3): 423-428.

Burkart, M.R., James, D.E., 1999. Agricultural-nitrogen contributions to hypoxia in the Gulf of Mexico. Journal of Environmental Quality, 28(3): 850-859.

Burns, D. et al., 2005. Effects of suburban development on runoff generation in the Croton River basin, New York, USA. Journal of Hydrology, 311(1-4): 266-281.

Burns, D.A. et al., 1998. Base cation concentrations in subsurface flow from a forested hillslope: The role of flushing frequency. Water Resources Research, 34(12): 3535-3544.

Burns, D.A. et al., 2003. The geochemical evolution of riparian ground water in a forested Piedmont catchment. Ground Water, 41(7): 913-925.

Buxton, H.T., Reilly, T.E., Pollock, D.W., Smolensky, D.A., 1991. Particle tracking analysis of recharge areas on Long Island, New York. Ground Water, 29(1): 63-71.

Christianson, E.G., 2008. A hydrogeologic investigation of Ada Hayden Lake in Ames, Iowa, M.S. thesis, Iowa State University, Ames, IA, 208 pp.

Clarke, J.S., West, 1998. Simulation of ground-water flow and stream-aquifer relations in the vicinity of the Savannah River Site, Georgia and South Carolina, predevelopment through 1992: U.S. Geological Survey Water-Resources Investigations Report 98-4062, Reston, VA, pp. 135.

Daniel, W.W., 1978. Applied nonparametric statistics. Houghton Mifflin Company, Boston, MA.

Dinçer, T., Payne, B.R., Florkowski, T., Martinec, J., Tongiorgi, E., 1970. Snowmelt runoff from measurements of tritium and oxygen-18. Water Resources Research, 6(1): 110-124.

Goolsby, D.A., Battaglin, W.A., 2000. Nitrogen in the Mississippi basin-Estimating sources and predicting flux to the Gulf of Mexico: U.S. Geological Survey Fact Sheet 135-00, Reston, VA, pp. 6.

Goswami, D., Kalita, P.K., 2009. Simulation of base-flow and tile-flow for storm events in a subsurface drained watershed. Biosystems Engineering, 102(2): 227-235.

Green, C.H., Haney, R., 2005. Grassed waterways. SERA-17 (http://www.sera17.ext.vt.edu/SERA_17_Publications.htm).

Haitjema, H.M., 1995. On the residence time distribution in idealized groundwatersheds. Journal of Hydrology, 172(1-4): 127-146.

Hallberg, G.R., 1987. Nitrates in ground water in Iowa. In: D'Itri, F.M., Wolfson, L.G. (Eds.), Rural ground water contamination. Lewis, Chelsea, MI, pp. 23-68.

Harbaugh, A.W., Banta, E.R., Hill, M.C., McDonald, M.G., 2000. MODFLOW-2000, the U.S. Geological Survey modular ground-water model -- User guide to modularization concepts and the Ground-water flow process: U.S. Geological Survey Open-File Report 00-92. Reston, VA, pp. 121.

Harvey, J.W., Bencala, K.E., 1993. The effect of streambed topography on surface-subsurface water exchange in mountain catchments. Water Resources Research, 29(1): 89-98.

Helmke, M.F., Simpkins, W.W., Horton, R., 2005. Fracture-controlled nitrate and atrazine transport in four Iowa till units. Journal of Environmental Quality, 34(1): 227-236.

Hollander, M., Wolfe, D.A., 1999. Nonparametric statistical methods. Wiley-Interscience.

Hvorslev, M.J., 1951. Time lag and soil permeability in groundwater observations, *Bull. 36*, U.S. Army Corps of Eng., Drainageways Experiment Station, Vicksburg, MS.

Kollet, S.J., Maxwell, R.M., 2008. Demonstrating fractal scaling of baseflow residence time distributions using a fully-coupled groundwater and land surface model. Geophysical Research Letters, 35(7).

Long, A.J., Derickson, R.G., 1999. Linear systems analysis in a karst aquifer. Journal of Hydrology, 219(3-4): 206-217.

Maloszewski, P., Zuber, A., 1982. Determining the turnover time of groundwater systems with the aid of environmental tracers. 1. Models and their applicability. Journal of Hydrology, 57(3-4): 207-231.

Maloszewski, P., Zuber, A., 1993. Principles and practice of calibration and validation of mathematical models for the interpretation of environmental tracer data in aquifers. Advances in Water Resources, 16(3): 173-190.

McGuire, K.J., McDonnell, J.J., 2006. A review and evaluation of catchment transit time modeling. Journal of Hydrology, 330(3-4): 543-563.

Meals, D.W., Dressing, S.A., Davenport, T.E., 2010. Lag time in water quality response to best management practices: A review. Journal of Environmental Quality, 39(1): 85-96.

Molenat, J., Gascuel-Odoux, C., 2002. Modelling flow and nitrate transport in groundwater for the prediction of water travel times and of consequences of land use evolution on water quality. Hydrological Processes, 16(2): 479-492.

Mook, W.G., Groenweld, D.J., Brouwn, A.E., van Ganwijk, A.J., 1974. Analysis of a runoff hydrograph by means of natural oxygen-18. In: Isotope techniques in groundwater hydrology, Proceedings of an international symposium. IAEA, Vienna, pp. 145-155.

Niemi, A.J., 1978. Residence time distribution of variable flow processes. International journal of applied radiation and isotopes, 28: 855-860.

NRCS, 2004. How to design, construct, seed and maintain small grassed waterways: Iowa Job Sheet, National Resources Conservation Service. In: Service, N.R.C. (Ed.), Des Moines, IA.

Ozyurt, N.N., 2008. Residence time distribution in the Kirkgoz karst springs (Antalya-Turkey) as a tool for contamination vulnerability assessment. Environmental Geology, 53(7): 1571-1583.

Pijanowski, B., Ray, D.K., Kendall, A.D., Duckles, J.M., Hyndman, D.W., 2007. Using backcast land-use change and groundwater travel-time models to generate land-use legacy maps for watershed management. Ecology and Society, 12(2).

Pollock, D.W., 1994. User's guide for MODPATH/MODPATH-PLOT, version 3: A particle tracking post-processing package for MODFLOW, the U.S. Geological Survey finite-difference ground-water flow model: U.S. Geological Survey Open-File Report 94-464, Reston, VA, pp. 237.

Prior, J.C., 1991. Landforms of Iowa. University of Iowa Press, Iowa City, IA.

Quinn, J.J., Tomasko, D., Kuiper, J.A., 2006. Modeling complex flow in a karst aquifer. Sedimentary Geology, 184(3-4): 343-351.

Rabalais, N.N., Turner, R.E., Scavia, D., 2002. Beyond science into policy: Gulf of Mexico hypoxia and the Mississippi river. Bioscience, 52(2): 129-142.

Reilly, T.E., Plummer, L.N., Phillips, P.J., Busenberg, E., 1994. The use of simulation and multiple environmental tracers to quantify groundwater flow in a shallow aquifer. Water Resources Research, 30(2): 421-433.

Riva, M., Guadagnini, L., Guadagnini, A., Ptak, T., Martac, E., 2006. Probabilistic study of well capture zones distribution at the Lauswiesen field site. Journal of Contaminant Hydrology, 88(1-2): 92-118.

Rovey II, C.W., 1998. Digital simulation of the scale effect in hydraulic conductivity. Hydrogeology Journal, 6(2): 216-225.

Schilling, K.E., 2002. Chemical transport from paired agricultural and restored prairie watersheds. Journal of Environmental Quality, 31(4): 1184-1193.

Schilling, K.E., 2009. Investigating local variation in groundwater recharge along a topographic gradient, Walnut Creek, Iowa, USA. Hydrogeology Journal, 17(2): 397-407.

Schilling, K.E., Hubbard, T., Luzier, J., Spooner, J., 2006a. Walnut Creek watershed restoration and water quality monitoring project: final report. Iowa Department of Natural Resources, Geological Survey Bureau Technical Information Series 49, Iowa City, IA, pp. 124.

Schilling, K.E., Jacobson, P., 2008. Groundwater nutrient concentrations near an incised midwestern stream: effects of floodplain lithology and land management. Biogeochemistry, 87(2): 199-216.

Schilling, K.E., Li, Z.W., Zhang, Y.K., 2006b. Groundwater - surface water interaction in the riparian zone-of an incised channel, Walnut Creek, Iowa. Journal of Hydrology, 327(1-2): 140-150.

Schilling, K.E., Spooner, J., 2006. Effects of watershed-scale land use change on stream nitrate concentrations. Journal of Environmental Quality, 35(6): 2132-2145.

Schilling, K.E., Thompson, C.A., 1999. Walnut Creek nonpoint source monitoring project, Jasper county, Iowa: Water years 1995-1997. Iowa Department of Natural Resources, Geological Survey Bureau Technical Information Series 39, Iowa City, IA, pp. 169.

Schilling, K.E. et al., 2007. Hydrogeologic controls on nitrate transport in a small agricultural catchment, Iowa. Journal of Geophysical Research-Biogeosciences, 112(G3).

Schilling, K.E., Wolter, C.F., 2000. Application of GPS and GIS to map channel features in Walnut Creek, Iowa. Journal of the American Water Resources Association, 36(6): 1423-1434.

Schilling, K.E., Wolter, C.F., 2001. Contribution of base flow to nonpoint source pollution loads in an agricultural watershed. Ground Water, 39(1): 49-58.

Schilling, K.E., Wolter, C.F., 2007. A GIS-based groundwater travel time model to evaluate stream nitrate concentration reductions from land use change. Environmental Geology, 53: 433-443.

Schilling, K.E., Zhang, Y.K., Drobney, P., 2004. Water table fluctuations near an incised stream, Walnut Creek, Iowa. Journal of Hydrology, 286(1-4): 236-248.

Schulze-Makuch, D., Cherkauer, D.S., 1998. Variations in hydraulic conductivity with scale of measurement during aquifer tests in heterogeneous, porous carbonate rocks. Hydrogeology Journal, 6(2): 204-215.

Schwientek, M., Maloszewski, P., Einsiedl, F., 2009. Effect of the unsaturated zone thickness on the distribution of water mean transit times in a porous aquifer. Journal of Hydrology, 373(3-4): 516-526.

Sivapalan, M., 2003. Process complexity at hillslope scale, process simplicity at the watershed scale: is there a connection? Hydrological Processes, 17(5): 1037-1041.

Stone, R., McKague, K., 2009. Grassed waterways: Ontario Ministry of Agriculture, Food and Rural Affairs Factsheet 09-021.

Turner, J. et al., 2006. Future trends in transport and fate of diffuse contaminants in catchments, with special emphasis on stable isotope applications. Hydrological Processes, 20(1): 205-213.

Valett, H.M. et al., 1997. Hydrologic influences on groundwater surface water ecotones: Heterogeneity in nutrient composition and retention. Journal of the North American Benthological Society, 16(1): 239-247.

Wayland, K.G., Hyndman, D.W., Boutt, D., Pijanowski, B.C., Long, D.T., 2002. Modelling the impact of historical land uses on surface-water quality using groundwater flow and solute-transport models. Lakes & Reservoirs: Research and Management, 7: 189-199.

Weisbrod, T.S., 2005. Modeling the influence of land use on shallow groundwater flow and nitrate transport, Neal Smith National Wildlife Refuge, Jasper county, Iowa, M.S. thesis, University of Iowa, Iowa City, IA, 136 pp.

Winter, T.C., Rosenberry, D.O., LaBaugh, J.W., 2003. Where does the ground water in small watersheds come from? Ground Water, 41(7): 989-1000.

Wondzell, S.M., Gooseff, M.N., McGlynn, B.L., 2007. Flow velocity and the hydrologic behavior of streams during baseflow. Geophysical Research Letters, 34(24).

Wriedt, G., Rode, M., 2006. Modelling nitrate transport and turnover in a lowland catchment system. Journal of Hydrology, 328(1-2): 157-176.

Wroblicky, G.J., Campana, M.E., Valett, H.M., Dahm, C.N., 1998. Seasonal variation in surface-subsurface water exchange and lateral hyporheic area of two stream-aquifer systems. Water Resources Research, 34(3): 317-328.

Yurtsever, Y., 1983. Models for tracer data analysis. In: Guidebook on nuclear techniques in hydrology. IAEA, Vienna, pp. 381-402.

Zheng, C., Wang, P.P., 1999. MT3DMS: A modular three-dimensional multispecies transport model for simulation of advection, dispersion, and chemical reactions of contaminants in groundwater systems: Documentation and user's guide. Contract Report SERDP-99-1 : U.S. Army Engineer Research and Development Center, Vicksburg, MS.